Sulfur based Composite Cathode Materials for Rechargeable Lithium Batteries

by

Yongguang Zhang

A thesis
presented to the University of Waterloo
in fulfillment of the
thesis requirement for the degree of
Doctor of Philosophy
in
Chemical Engineering

Waterloo, Ontario, Canada, 2013

AUTHOR'S DECLARATION

I hereby declare that I am the sole author of this thesis. This is a true copy of the thesis, including any required final revisions, as accepted by my examiners.

I understand that my thesis may be made electronically available to the public.

Abstract

Lithium-ion batteries are leading the path for the power sources for various portable applications, such as laptops and cellular phones, which is due to their relatively high energy density, stable and long cycle life. However, the cost, safety and toxicity issues are restricting the wider application of early generations of lithium-ion batteries. Recently, cheaper and less toxic cathode materials, such as $LiFePO_4$ and a wide range of derivatives of $LiMn_2O_4$, have been successfully developed and commercialized. Furthermore, cathode material candidates, such as $LiCoPO_4$, which present a high redox potential at approximately 4.8 V versus Li^+/Li, have received attention and are being investigated. However, the theoretical capacity of all of these materials is below 170 mAh g^{-1}, which cannot fully satisfy the requirements of large scale applications, such as hybrid electric vehicles and electric vehicles. Therefore, alternative high energy density and inexpensive cathode materials are needed to make lithium batteries more practical and economically feasible.

Elemental sulfur has a theoretical specific capacity of 1672 mAh g^{-1}, which is higher than that of any other known cathode materials for lithium batteries. Sulfur is of abundance in nature (e.g., sulfur is produced as a by-product of oil extraction, and hundreds of millions of tons have been accumulated at the oil extraction sites) and low cost, and this makes it very promising for the next generation of cathode materials for rechargeable batteries. Despite the mentioned advantages, there are several challenges to make the sulfur cathode suitable for battery use, and the following are the main: (i) sulfur has low conductivity, which leads to low sulfur utilization and poor rate capability in the cathode; (ii) multistep electrochemical reduction processes generate various forms of soluble intermediate lithium polysulfides, which dissolve in the electrolyte, induce the so-called shuttle effect, and cause irreversible loss of sulfur active material over repeat cycles; (iii) volume change of sulfur upon cycling leads to its mechanical rupture and, consequently, rapid degradation of the electrochemical performance.

A variety of strategies have been developed to improve the discharge capacity, cyclability, and Coulombic efficiency of the sulfur cathode in Li/S batteries. Among those techniques, preparation of sulfur/carbon and sulfur/conductive polymer composites has

received considerable attention. Conductive carbon and polymer additives enhance the electrochemical connectivity between active material particles, thereby enhancing the utilization of sulfur and the reversibility of the system, i.e., improving the cell capacity and cyclability. Incorporation of conductive polymers into the sulfur composites provides a barrier to the diffusion of polysulfides, thus providing noticeable improvement in cyclability and hence electrochemical performance.

Among the possible conductive polymers, polypyrrole (PPy) is one of the most promising candidates to prepare electrochemically active sulfur composites because PPy has a high electrical conductivity and a wide electrochemical stability window (0-5 V *vs* Li/Li^+). In the first part of this thesis, the preparation of a novel nanostructured S/PPy based composites and investigation of their physical and electrochemical properties as a cathode for lithium secondary batteries are reported. An S/PPy composite with highly developed branched structure was obtained by a one-step ball-milling process without heat-treatment. The material exhibited a high initial discharge capacity of 1320 mAh g^{-1} at a current density of 100 mA g^{-1} (0.06 C) and retained about 500 mAh g^{-1} after 40 cycles. Alternatively, *in situ* polymerization of the pyrrole monomer on the surface of nano-sulfur particles afforded a core-shell structure composite in which sulfur is a core and PPy is a shell. The composite showed an initial discharge capacity of 1199 mAh g^{-1} at 0.2 C with capacity retention of 913 mAh g^{-1} after 50 cycles, and of 437 mAh g^{-1} at 2.5 C. Further improvement of the electrochemical performance was achieved by introducing multi-walled carbon nanotubes (MWNT), which provide a much more effective path for the electron transport, into the S/PPy composite. A novel S/PPy/MWNT ternary composite with a core-shell nano-tubular structure was developed using a two-step preparation method (*in situ* polymerization of pyrrole on the MWNT surface followed by mixing of the binary composite with nano-sulfur particles). This ternary composite cathode sustained 961 mAh g^{-1} of reversible specific discharge capacity after 40 cycles at 0.1 C, and 523 mAh g^{-1} after 40 cycles at 0.5 C. Yet another structure was prepared exploring the large surface area, superior electronic conductivity, and high mechanical flexibility graphene nanosheet (GNS). By taking advantage of both capillary force driven self-assembly of polypyrrole on graphene

nanosheets and adhesion ability of polypyrrole to sulfur, an S/PPy/GNS composite with a dual-layered structure was developed. A very high initial discharge capacity of 1416 mAh g^{-1} and retained a 642 mAh g^{-1} reversible capacity after 40 cycles at 0.1 C rate. The electrochemical properties of the graphene loaded composite cathode represent a significant improvement in comparison to that exhibited by both the binary S/PPy and the MWCNT containing ternary composites.

In the second part of this thesis, polyacrylonitrile (PAN) was investigated as a candidate to composite with sulfur to prepare high performance cathodes for Li/S battery. Unlike polypyrrole, which, in addition of being a conductive matrix, works as physical barrier for blocking polysulfides, PAN could react with sulfur to form inter- and/or intra-chain disulfide bonds, chemically confining sulfur and polysulfides. In the preliminary tests, PAN was ballmilled with an excess of elemental sulfur and the resulting mixture was heated at temperatures varying from 300^{o}C to 350°C. During this step some H_2S gas was released as a result of the formation of rings with a conjugated π-system between sulfur and polymer backbone. These cyclic structures could 'trap' some of the soluble reaction products, improving the utilization of sulfur, as it was observed experimentally: the resulting S/PAN composite demonstrated a high sulfur utilization, large initial capacity, and high Coulombic efficiency. However, the poor electronic conductivity of the S/PAN binary composite compromises the rate capability and sulfur utilization at high C-rates. These issues were addressed by doping the composite with small amounts of components that positively affected the conductivity and reactivity of the cathode. $Mg_{0.6}Ni_{0.4}O$ prepared by self-propagating high temperature synthesis was used as an additive in the S/PAN composite cathode and considerably improved its morphology stability, chemical uniformity, and electrochemical performance. The nanostructured composite containing $Mg_{0.6}Ni_{0.4}O$ exhibited less sulfur agglomeration upon cycling, enhanced cathode utilization, improved rate capability, and superior reversibility, with a second cycle discharge capacity of over 1200 mAh g^{-1}, which was retained for over 100 cycles. Alternatively, graphene was used as conductive additive to form an S/PAN/Graphene composite with a well-connected conductive network structure. This ternary composite was prepared by ballmilling followed

by low temperature heat treatment. The resulting material exhibited significantly improved rate capability and cycling performance delivering a discharge capacity of 1293 mAh g^{-1} in the second cycle at 0.1 C. Even at up to 4 C, the cell still achieved a high discharge capacity of 762 mAh g^{-1}.

Different approaches for the optimization of sulfur-based composite cathodes are described in this thesis. Experimental results indicate that the proposed methods constitute an important contribution in the development of the high capacity cathode for rechargeable Li/S battery technology. Furthermore, the innovative concept of sulfur/conductive polymer/conductive carbon ternary composites developed in this work could be used to prepare many other analogous composites, such as sulfur/polyaniline/carbon nanotube or sulfur/polythiophene/graphene, which could also lead to the development of new sulfur-based composites for high energy density applications. In particular, exploration of alternative polymeric matrices with high sulfur absorption ability is of importance for the attainment of composites that possess higher loading of sulfur, to increase the specific energy density of the cathode. Note that the material preparation techniques described here have the advantage of being reproducible, simple and inexpensive, compared with most procedures reported in the literature.

Acknowledgements

First and foremost, I would like to express my sincere gratitude to my supervisor, Professor Pu Chen, for his constant support, motivation and his guidance. Without him, I would have been lost in the research work, and his erudition and enthusiasm will inspire me to continue the exploration of the nature and science. Special thanks are extended to Positec and the China Scholarship Council for the financial support.

Hearty thanks to all of the members of the energy and integrative research group, past and present. All the group members were always ready to help in any part of the project. I am so grateful that I learned the most valuable experimental skills from Dr. Zhumabay Bakenov. I would appreciate nice collaboration with Dr. Denise Gosselink and Aishuak Konarov. During my PhD study, I have received great help from the following undergraduate research assistants: Kyung Eun Kate Sun, Muhammad Malik, Hayden Greentree Soboleski, Zhi Li, Cong Ding, Matthew Li, Josua Markus, Takayuki Fukada, Caroline Kim, Giwon Seo, Mubashir Mir.

I am thankful to my family for supporting me during my study period. Special thanks go to my true love, Yan Zhao, for her unlimited love and constant patience. Special thanks also go to my parents for endless support and love. Without them, none of my achievements would be possible. The thesis is dedicated to all of them.

Dedication

Dedicated to My Parents and Wife

Table of Contents

List of Figures

List of Tables

List of Abbreviations

NMP: 1-methyl-2-pyrrolidinone

CTAB: Cetyltrimethylammonium bromide

LiTFSI: Lithium bistrifluoromethanesulfonamide

$LiPF_6$: Lithium hexafluorophosphate

EC: Ethylene carbonate

DMC: Dimethylcarbonate

DEC: diethyl carbonate

PAN: Polyacrylonitrile

PVdF: Polyvinylidene fluoride

TEGDME: Tetraethylene glycol dimethyl ether

FTIR: Fourier Transform Infrared Spectroscopy

XRD: X-ray diffraction

BET: Brunauer-Emmet-Teller

CV: Cyclic voltammetry

AIS: AC impedance spectroscopy

EDS: Energy Dispersive Spectroscopy

FESEM: Field emission scanning electron microscopy

HRTEM: High resolution transmission electron microscopy

TEM: Transmission electron microscopy

Chapter 1
Introduction and Motivation

1.1 Overview

The establishment of alternative energy sources is vital for the existence and sustainable development of our modern society. Currently, most of mankind energy demands have been met by the use of fossil fuels. However, the limited amount of fossil fuels global reserves, which may last for only a few more decades, and the environmental impact of burning these fuels call for the development of cleaner and renewable energy sources, such as wind and solar **[1,2]**. Nevertheless, due to their energy input/output intermittent character, these technologies require reliable, low cost and environmentally friendly, large scale energy storage systems [**3,4]**. Lithium-ion batteries (LIBs) are among the most promising candidate for such applications. However, the available LIBs cathode materials, such as those based on transition metal oxides and phosphates, have an inherent theoretical capacity limit of 300 mAh g^{-1}, and maximum usable capacity of only 210 mAh g^{-1} **[5-8]**. As a result, the storage capacity of the LIBs cells is severely compromised.

Elemental sulfur (S) is a more attractive cathode candidate due to its low cost, environmental friendliness, and highest theoretical capacity (1672 mAh g^{-1}) and theoretical specific energy density (2600 Wh kg^{-1}) among known cathode materials **[9]**, which is far greater than that of current lithium-ion cells as shown in **Fig. 1.1 [10]**.

The common Li/S battery architecture is comprised of a sulfur cathode and a lithium metal anode isolated by separator soaked with organic electrolyte as shown in **Fig. 1.2 [10]**.

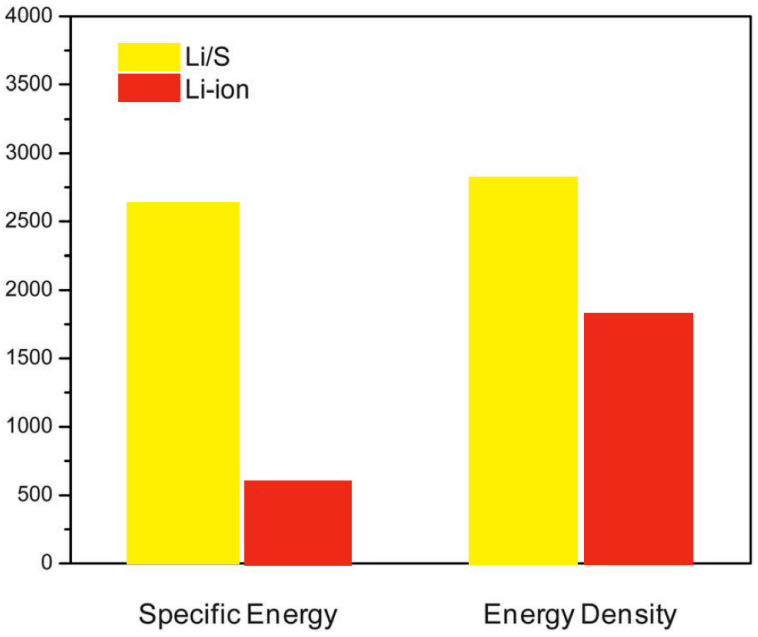

Fig 1.1 Comparison of theoretical specific energy and energy density of the lithium/sulfur cell with those of current lithium-ion cells. Adapted from **Ref. 10** with permission from The Royal Society of Chemistry.

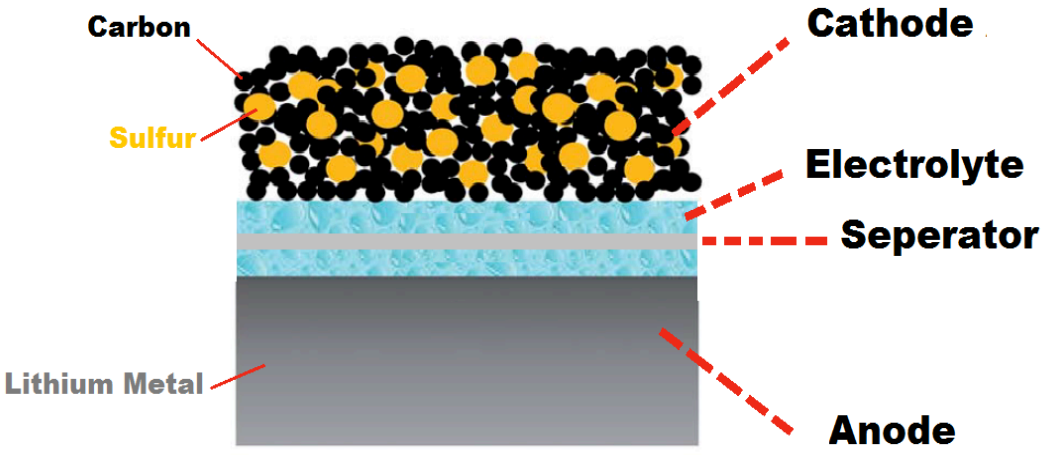

Fig 1.2 Schematic diagrams of the starting configurations of lithium/sulfur cells. Adapted from **Ref. 10** with permission from The Royal Society of Chemistry.

During discharge, elemental sulfur in the solid phase ($S_{8(s)}$) from the cathode is first dissolved into the electrolyte as ($S_{8(l)}$) which is then reduced to sulfide ions with progressively lower states of oxidation according to the following electrochemical reactions **[11]** (also see the **Fig. 1.3 [12]**):

$$\frac{1}{2}S_{8(l)} + e^- \underset{c}{\overset{d}{\rightleftarrows}} \frac{1}{2}S_8^{2-}$$

$$\frac{3}{2}S_8^{2-} + e^- \underset{c}{\overset{d}{\rightleftarrows}} 2S_6^{2-}$$

$$S_6^{2-} + e^- \underset{c}{\overset{d}{\rightleftarrows}} \frac{3}{2}S_4^{2-}$$

$$\frac{1}{2}S_4^{2-} + e^- \underset{c}{\overset{d}{\rightleftarrows}} S_2^{2-}$$

$$\frac{1}{2}S_2^{2-} + e^- \underset{c}{\overset{d}{\rightleftarrows}} S^{2-}$$

In spite of the obvious advantages of energy density and cost, many challenges still preclude the commercialization of the Li/S battery. These include low discharge capacity, poor cyclability, and low Coulombic efficiency which result from the cathode insulating nature of S, large volume changes during lithium reaction processes, and the solubility of polysulfides, as charge-discharge reaction products, into the liquid electrolytes. A variety of strategies have been employed to improve the performance of the sulfur cathode in Li/S batteries. Among them, preparation of sulfur/carbon and sulfur/conductive polymer composites have received considerable attention and recent results show that the sulfur carbon composites benefit from their hierarchical design (**Fig. 1.4 [13]**). Microporous carbon spheres **[14]**, spherical ordered mesoporous carbon nanoparticles **[15]**, porous hollow carbon **[16]**, graphene oxide sheets **[17],** porous carbon nanofibers **[18]**, and hollow carbon

nanofibers **[19]** have been developed to encapsulate sulfur **[13]**.

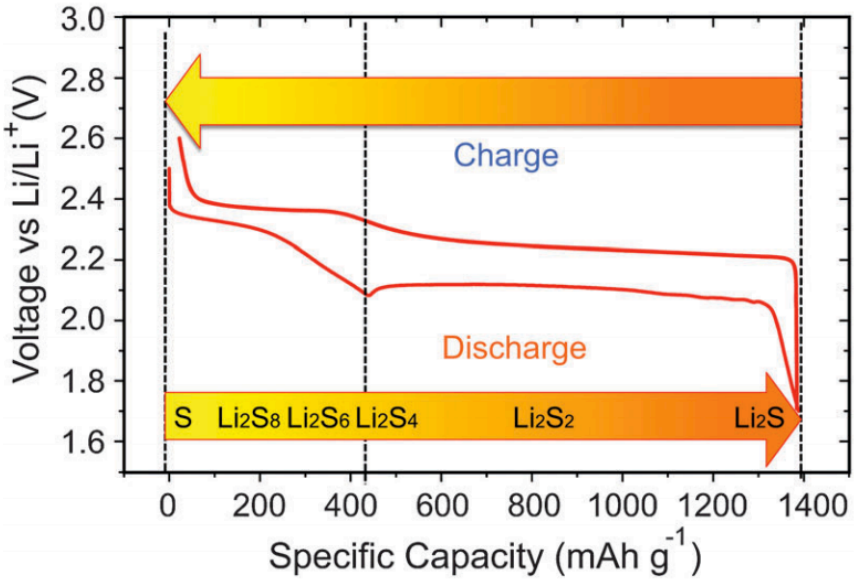

Fig 1.3 The voltage profile and chemistry of sulfur cathode in the organic electrolyte. Reproduced from **Ref. 12** with permission from The Royal Society of Chemistry.

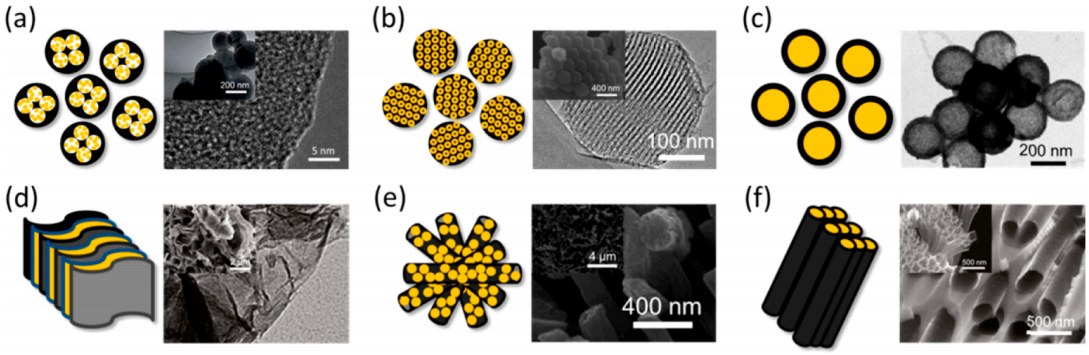

Fig 1.4 Hierarchical designs of carbon-based sulfur composites: (a) microporous carbon spheres, (b) spherical ordered mesoporous carbon nanoparticles, (c) porous hollow carbon, (d) graphene oxide sheets, (e) porous carbon nanofibers, and (f) hollow carbon nanofibers to encapsulate sulfur. Reprinted with permission from **Ref. 13**. Copyright (2013) American Chemical Society.

Alternatively, polymers can play a significant role in rechargeable Li/S batteries. Incorporation of conductive polymers into the sulfur composites provides a barrier to the diffusion of polysulfides, thus imparting noticeable improvement in the cyclability and hence electrochemical performance.

In this research, polypyrrole (PPy) and polyacrylonitrile (PAN) were evaluated as conductive matrices and/or barrier for blocking polysulfides to improve the electrochemical performance of Li/S batteries. A diverse array of synthesis methods was evaluated for morphology control and material architectural design. The preparation techniques employed have the advantage of being reproducible, simple and inexpensive, compared with most procedures reported in the literature.

Although conductive polymers provide a pathway for electron transport, their electronic conductivity is much lower than carbonaceous materials, jeopardizing their ability of being the sole electron conductor within the sulfur electrode. Hence, an innovative concept of sulfur/conductive polymer/conductive carbon ternary composites was developed in this work. Experimental results indicate that the proposed methods constitute an important contribution in the development of the high capacity cathode for rechargeable Li/S battery technology.

1.2 Research Objectives

The goal of this research was to develop novel sulfur based composites cathodes to improve specific energy/power, obtain good efficiencies and enhance cycling stability as steps toward high-performance lithium/sulfur cells. To achieve this goal, a few strategies to improve the electrochemical performance of Li/S batteries were surveyed exploring the use of conductive polymers as a conductive matrix or barrier for blocking polysulfides. The

specific objectives of this research study are:

1) Design and tune the structure and morphology of polymer materials to retain the polysulfides and maximize sulfur loading, while increasing the utilization of sulfur and improving energy density;

2) Explore nanoscale coatings on sulfur electrodes to retain polysulfides inside the electrode while still providing good pathways for electrons and lithium ions;

3) Develop sulfur/conductive polymer/conductive carbon ternary composites, favoring both cyclability and rate capability;

4) Optimize the material preparation techniques to obtain a reproducible, simple and inexpensive synthesis procedure;

5) Investigate the capacity fading mechanisms of sulfur cathode using microscopic imaging characterization to gain new insights into rational design of better electrodes.

1.3 Outline of the Thesis

This thesis consists of chapters as follows:

Chapter 1 gives the overview of the thesis, including introduction and fundamentals of the Li/S batteries. The main objectives of the research are also listed in this chapter.

Chapter 2 reviews the available literature about the operation principle, the latest developments, and new opportunities of Li/S batteries.

In Chapter 3, the preparation of S/PPy binary composite is investigated. Firstly, a novel branched structural S/PPy composite are prepared *via* simple one-step ballmilling without heat-treatment, and electrochemical properties as a cathode for lithium secondary batteries are studied. To further improve the electrochemical performance, 3D current collector is

employed into Li/S batteries containing branched structure S/PPy composite. Results indicate that carbon fiber cloth is as a very promising, effective, and inexpensive current collector for Li/S batteries. Furthermore, another strategy to synthesize a core-shell structure of sulfur within PPy is discussed. And its physical and electrochemical properties as a cathode for lithium secondary batteries are measured.

In Chapter 4, to further improve conductive of S/PPy based composite, we develop S/PPy/conductive carbon ternary composite. Firstly, multi-walled carbon nanotube is introduced into S/PPy composite and a novel S/PPy/MWNT ternary composite with a core-shell nano-tubular structure is prepared by a two-step method, and its physical and electrochemical properties as a cathode for Li/S batteries are investigated. Secondly, graphene is employed into S/PPy composite and S/PPy/GNS composite with dual-layered structure is prepared. And its physical and electrochemical properties as a cathode for Li/S batteries are investigated.

From Chapter 5 to Chapter 6, PAN based sulfur composite are studied.

Chapter 5 reports on the preparation of nanosized $Mg_{0.6}Ni_{0.4}O$ *via* a self-propagating high temperature synthesis (SHS) method and its effect on the electrochemical performance of the S/PAN/$Mg_{0.6}Ni_{0.4}O$ ternary composite cathode.

In chapter 6, graphene is evaluated as a conductive additive to form a ternary S/PAN/graphene with a well-connected conductive network structure. The S/PAN/graphene composite was prepared by simple ball milling followed by low temperature heat treatment.

Finally, Chapter 7 gives the conclusions of this thesis and recommendations for future work.

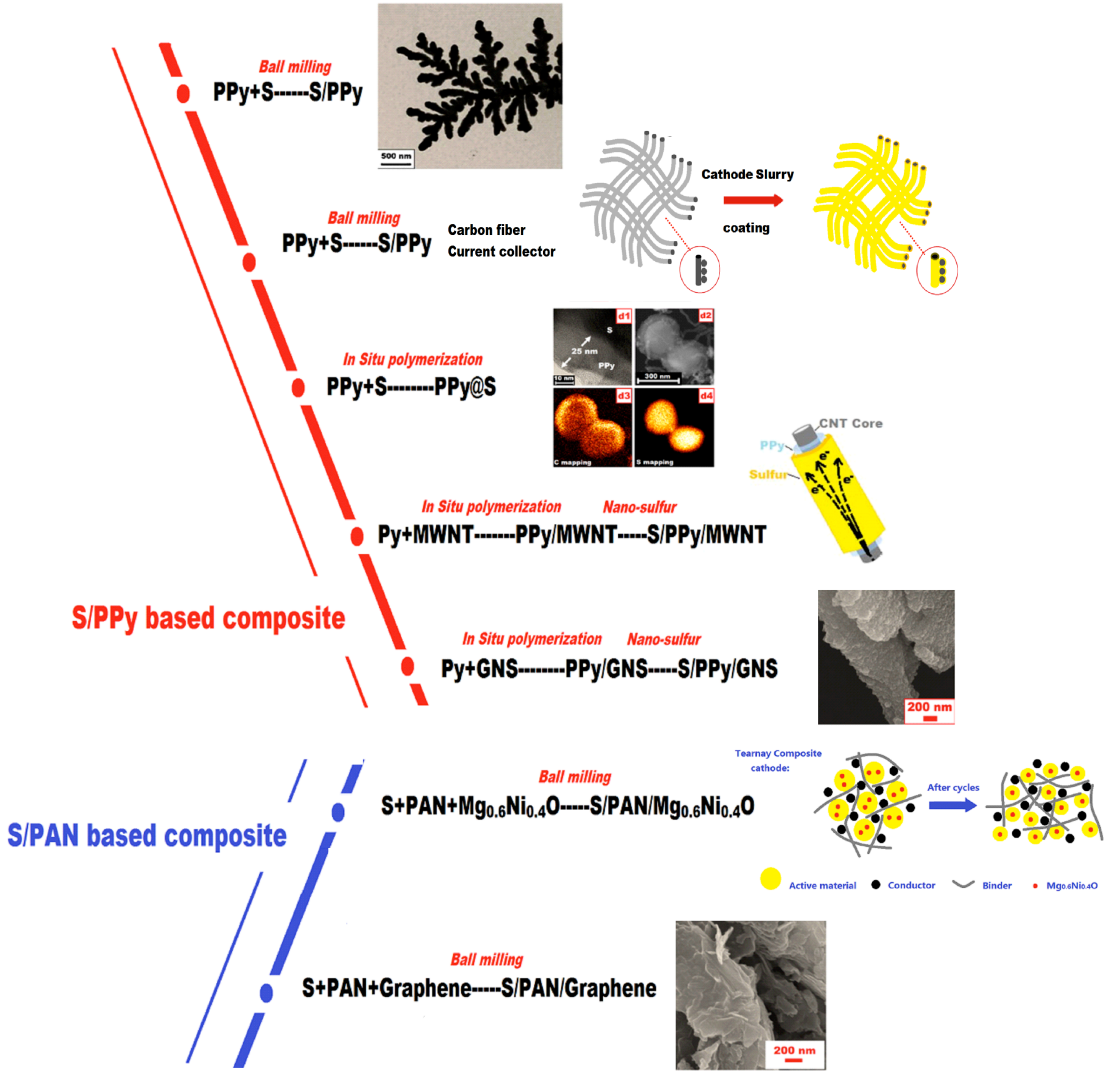

Fig 1.5 The sketch of the thesis.

Chapter 2
Background and Literature

2.1 General Introduction of Lithium Sulfur batteries

The lithium-ion rechargeable batteries have been widely used in the portable electronic devices such as laptops, cameras and cell phones **[1-4]**. The rapid growth of electric vehicles has been requiring the development of next generation batteries with high specific capacity and energy density. Lithium/Sulfur (Li/S) cell is one of the most promising candidates for a storage device due to:

(1) Low cost and abundant resources of sulfur;

(2) Non-poisonous and environment friendly;

(3) Wide temperature range of operation;

(4) Intrinsic protection mechanism from over charge, providing safety;

(5) Possibility of long cycling **[5]**.

Furthermore, the Li/S battery yields a high theoretical specific capacity of 1675 mAh g^{-1} and theoretical specific energy of 2500 Wh kg^{-1} (or 2800 Wh L^{-1}) on a weight or volume basis respectively **[6]**, based on the Li/S redox couple, $S + 2Li^+ + 2e^- \leftrightarrow Li_2S$ on the assumption of the complete reaction of lithium with sulfur to Li_2S. It differs from conventional lithium batteries. For example, the specific capacities of $LiMn_2O_4$, $LiCoO_2$ and $LiNiO_2$ are 126, 149 and 180 mAh g^{-1}, respectively **[7]**, whose values are limited by the extent of lithium intercalation into transition metal oxides **[8]**, reversible uptake of Li ions and electrons in a solid with minimal change to the structure. Typically, a lithium transition-metal oxide or phosphate is used as a positive electrode that re-intercalates Li^+ at a high

potential with respect to the carbon negative electrode **[9]**. The high capacity and recharge ability of sulfur can be achieved from the electrochemical cleavage and reformation of a sulfur-sulfur bond in cathode **[9]**.

The discharge process of the Li/S battery proceeds in two steps **[10]**: first, the transformation of sulfur to lithium polysulfides (Li_2S_n, $2<n<8$) and followed by the transformation of lithium polysulfides to lithium sulfide (Li_2S) **[11-13]**. The lithium polysulfides, which are formed during the first discharge step of Li/S battery, are dissolved into the electrolyte, which causes the irreversible loss of the sulfur active materials **[13-18]**. According to Nimon and co-workers **[19]**, when polysulfides were dissolved into an electrolyte, they also diffused into the lithium anode and reacted with the lithium to reduce the cycling efficiency. Thus, the cyclic behavior of the Li/S battery becomes very poor mainly due to the polysulfides dissolution into the electrolyte. Besides, the low electrical conductivity of sulfur (5×10^{-30} S cm^{-1}) and the volume expansion of sulfur during cycling greatly limits the cycle life of the sulfur cathode and impedes the widespread practical applications of rechargeable lithium sulfur batteries **[20]**. To overcome these shortcomings, various strategies have been explored, including fabrication of carbon/sulfur composites, preparation of conductive polymer/sulfur composites, and the optimization of the organic electrolyte.

2.2 Fabrication of Carbon/Sulfur Composites

Recently, porous carbon materials have been proven to be effective and facile candidates in improving the conductivity of sulfur and restraining the diffusion of lithium polysulfides because of their excellent conductivity, large surface area, and strong adsorption property.

Various carbon/sulfur composites utilizing active carbon, mesoporous carbon, carbon nanofiber or nanotube, microporous carbon sphere, and graphene, have been fabricated.

In Wang *et al*'s research **[21]**, the cathode material composites were prepared with a structure of elemental sulfur embedded and trapped in nano-pores and micro-pores of active carbon to overcome the loss of the active mass in the cathode, which showed good cycle ability in rechargeable lithium cell based on gel electrolyte. The reversible capacity of the composite was about 440 mAh g^{-1} and the utilization of sulfur during cycling approached 90%.

Mesoporous carbon was reported **[22]** that it was used in industry as an adsorbing material because of their high surface area. Furthermore, mesoporous carbon had good electrical conductivity. According to Liang *et al* **[23]**, a soft-template synthesis method was applied to produce sulfur/carbon composite cathode for Li/S rechargeable batteries. This method was first introduced by Liang *et al* **[24-27]** to synthesize mesoporous carbon. After activating mesoporous carbon using potassium hydroxide (KOH), the carbon obtained a hierarchical structure with a bimodal pore size (micropore and mesopore). The bimodal pores played important roles during electrochemical reaction: micropores trapped sulfur particles to give high electrical conductivity and to prevent the particles from escaping from cathode and macropores allowed a large number of lithium ions to transport between anode and cathode, which leaded to high ionic conductivity. As a result, initial discharge capacity reached 1584 mAh g^{-1}; this value was greater than the literature value of 1155 mAh g^{-1}.

Wang *et al* **[28]** reported that sulfur-mesoporous carbon composite was prepared by heating a mixture of elemental sulfur and synthesized mesoporous carbon. A novel

electrolyte was prepared by dissolving lithium bistrifluoromethane-sulfonimidate (LiTFSI) in the synthesized ionic liquid consisting of 1-ethyl-3-methylimidazo-lium bis(trifluoromethylsulfonyl)imide (EMITFSI) at a concentration of 1 mol L^{-1}. This composite was tested in both the ionic liquid and the organic solvent electrolytes. And the composite using ionic liquid electrolyte showed better results in the capacity and cyclic stability than that of the conventional organic solvent electrolyte of 1 mol L^{-1} LiTFSI-PEGDME.

CMK-3, the most well-known member of the mesoporous carbon family, was studied as CMK-3/S composite in the Li/S battery **[9]**. It was found that the sulfur was homogeneously distributed in the framework of the mesoporous carbon, which allowed ingress of electrolyte within the structure. The empty volume within the pores was also available to accommodate the uptake of Li ions, due to the lower density of Li_2S compared to the sulfur. The insulating sulfur only occupied the empty channels in the mesoporous carbon and did not block the electrical current transporting paths **[9]**. To further reduce the dissolution of the polysulfide into the electrolyte, the polymer, polyethylene glycol (PEG) chains of varying molecular weight, was coated on the external surface of the composite (CMK-3/S), helped retard diffusion of polysulfide out of the cathode structure. It was found that the cycling stability was improved. The initial discharge capacity was increased to 1320 mAh g^{-1}, but no fading was observed in the second 10 cycles and the capacity was stabilized at 1100 mAh g^{-1} on cycling.

Choi *et al* **[29]** presented that carbon nanofiber (CNF) with an average diameter of 150 nm was added into the cathode to improve cyclic ability. Cathode, with CNF using PEO and

PVDF as the binders, showed better cycle property than the one without CNF, which was due to the suppression of agglomeration of sulfur or lithium sulfide.

Sulfur encapsulated in porous carbon nanofibers was synthesized via electro-spinning, carbonization and solution-based chemical reaction-deposition method **[30]**. The chemical reaction deposition strategy provided intimate contact between the S and the CNFs. This would not necessarily be the case for other reported methods, such as ball milling and thermal treatment. These novel CNF/S nanocomposites with various S loadings showed high reversible capacity, good discharge capacity retention and enhanced rate capability when they were used as cathodes in rechargeable Li/S cells, which could attribute the good electrochemical performance to the high electrical conductivity and the extremely high surface area of the CNFs that homogeneously disperse and immobilize S on their porous structures, alleviating the polysulfide shuttle phenomenon.

In Han *et al*'s research **[31]**, multi-walled carbon nanotubes (MWNT), prepared by thermal chemical vapor deposition, were used as an inactive additive material for elemental sulfur cathodes for Li/S rechargeable batteries. The assembly of the relatively long and thin MWNT could generate 3-D network structures, which was favorable to the retention of soluble polysulfides on cathode, sulfur utilization and cyclic ability of the sulfur batteries.

A hierarchical S/MWNT nanomicrosphere with a high power and energy density as well as an excellent cycle life was introduced in Zheng *et al*'s work **[32]**. Sulfur was uniformly coated on the surface of functional MWNT, which served as a carbon matrix, to form a typical nanoscale core-shell structure with a sulfur layer of thickness 10-20 nm. Then the nanoscale sulfur intermediate composite was ball-milled to form interwoven and porous

sphere architecture with large pores (around 1 mm to 5 mm). Different from most sulfur/carbon materials with micropore and mesopore structure, the micrometre scale S/MWNT nanomicrosphere with a large pore structure could also exhibit high sulfur utilization and cycle retention.

To enhance the long stability of sulfur cathode for a high energy Li/S battery system, a sulfur/carbon sphere composite was prepared by encapsulating sulfur into micropores of carbon spheres by thermal treatment of a mixture of sublimed sulfur and carbon spheres **[33]**. The elemental sulfur existed as a highly dispersed state inside the micropores of carbon spheres with a large surface area and a narrow pore distribution. It is demonstrated from galvanostatic discharge-charge process, cyclic voltammetry (CV) and electrochemical impedance spectra (EIS) that the sulfur/carbon sphere composite had a large reversible capacity and an excellent high rate discharge capability as cathode materials. It was noted that the electrochemical reaction constrained inside the micropores proposed here would be the dominant factor for the enhanced long stability of the sulfur cathode.

A novel sulfur/graphene cathode composite was synthesized that was easily scalable for large-scale production **[34]**. The use of partially oxidized graphene as both an electrical conduit for insulating sulfur and as a barrier to retard polysulfide dissolution led to an effective cathode material. This sulfur base composite was very important for realistic commercial Li-S batteries due to its extremely high sulfur content of 87 wt% and its respectable initial discharge capacity of 705 mAh g^{-1}.

Cao *et al* reported the design and synthesis of a carbon/sulfur nanocomposite coated with reduced graphene oxide (RGO) **[35]**. The obtained RGO-coated sample had a good capability

of confining the polysulfides. A thermally exfoliated graphene nanosheet (TG) with a large specific surface area, high pore volume, excellent conductivity, and broad pore distribution stacked by ultrathin graphene sheets was selected to prepare a TG-sulfur (TG-S) stack-up nanocomposite. RGO was coated on the TG-S nanocomposite through a liquid process. As prepared RGO-TG-S nanocomposite showed an outstanding high-rate performance for Li/S batteries. The carbon framework served not only as a conductive layer for encapsulating sulfur and polysulfides, but also as a nanoelectrochemical reaction chamber.

2.3 Preparation of Conductive Polymer/Sulfur Composites

Sulfur/polypyrrole (S/PPy) was synthesized via chemical polymerization using sodium *p*toluenesulphonate as the dopant, 4-styrenesulphonic sodium salt as the surfactant, and $FeCl_3$ (0.1 M) as the oxidant **[36]**. PPy nanoparticles coated on the surface of sulfur powder could trap the polysulfides. As a result, the composite showed good electrochemical properties, improvement of cyclic ability of the cell and increment of the initial discharge capacity from 1100 to 1280 mAh g^{-1} after coating with the polypyrrole.

Wire-, ribbon-, and sphere-like nanostructures of polypyrrole have been synthesized by solution chemistry methods in the presence of various surfactants (anionic, cationic, or nonionic surfactant) with various oxidizing agents (ammonium persulfate or ferric chloride), respectively **[37]**. By using cationic surfactants as soft templates, a novel nanowire of S/PPy cathode was prepared via simple heating method **[38]**. The result of the electrochemical performance of Li/S battery showed an initial discharge capacity of 1222 mAh g^{-1} with PPy as matrix and the remaining capacity of 570 mAh g^{-1} after 20 cycles.

A tubular polypyrrole fiber (T-PPy) as another type of conductive matrixes was introduced by Liang *et al* **[39]**. During the co-heating process, the capillary force allowed the sulfur to penetrate into the T-PPy matrix. The result showed that the reversible capacity of 650 mAh g^{-1} was maintained for over 80 cycles for the S/T-PPy composite with 30 wt% sulfur and initial discharge capacity was 1151.7 mAh g^{-1}. The enhanced conductivity, the favorable distribution of the nanosized sulfur in the T-PPy and the stable retention of polysulfides leaded to the improvement of the cycling stability of the sulfur based electrode.

Wang *et al* studied polyacrylonitrile (PAN) **[28]** as the reaction precursor with elemental sulfur heating at 280-300^{o}C to obtain a novel conductive S/PAN composite. The composite, with sulfur embedded in this conductive polymer matrix, was expected to hinder the sulfur and polysulfides from dissolving into the electrolyte and improve the electrochemical kinetics of the sulfur cathode. The lithium battery with S/PAN composite as the cathode active material offered high capacity density and good cycle ability. The specific capacity of the composite was up to 850 mAh g^{-1} at the first cycle. The specific capacity remained above 600 mAh g^{-1} after 50 cycles, which demonstrated high sulfur utilization and relatively stable cycle behavior.

PAN, however, showed poor electrical conductivity in the cathode, which limited the high power rate of sulfur composite materials. To solve this problem, further study **[40]** was done by using the carbon nanotube (CNT) to set up a highly conductive network in the composite. It was noted that CNT not only kept the cathode integrity and accommodated the volume change during charge/discharge processes, but also provided stable channels for electrical and ionic conduction at high power rates. By applying CNT, sulfur utilization and

cycling stability of the cathode had been significantly improved. The capacity remained 96.5% of sulfur utilization after 100 cycles. Moreover, the S/PAN/CNT composite exhibited excellent high power rate capability up to 7C (386.7 mAh g^{-1}).

Polyacrylonitrile/graphene (PAN/GNS) composites were synthesized via an in situ polymerization method **[20]**, which served as a precursor to prepare a cathode material for high-rate rechargeable Li/S batteries. It was observed from scanning electron microscopy (SEM) and transmission electron microscopy (TEM) that the PAN nanoparticles, less than 100 nm in size, were anchored on the surface of the GNS and this unique structure was maintained in the sulfur composite cathode material. The electrochemical properties of the pyrolyzed PAN-S/GNS (pPAN-S/GNS) composite cathode were evaluated by cyclic voltammograms, galvanostatic discharge/charge cycling and electrochemical impedance spectroscopy. The results showed that the pPAN-S/GNS nanocomposite, with a GNS content of 4 wt%, exhibited a reversible capacity of 700 mAh g^{-1} composite in the first cycle, corresponding to a sulfur utilization of 90%. The GNS in the composite materials worked as a 3-D nano current collector, which could act not only as an electronically conductive matrix, but also as a framework to improve the electrochemical performance.

2.4 Optimization of the Organic Electrolytes

Another strategy to improve the capacity and cyclability of Li/S batteries is the electrolyte optimization so as to reduce loss of sulfur by dissolution in the liquid electrolyte **[41-46]**. Among the possible electrolyte modifications, replacement of the common liquid organic electrolytes with polymer electrolytes has proved promising and efficient. It is

possible and convenient to group all the polymer systems into two broad categories, i.e., pure solid polymer electrolyte (SPE) and plasticized or gel polymer electrolyte systems (GPE).

The first category, pure solid polymer electrolyte, is composed of lithium salts (e.g., $LiClO_4$, $LiBF_4$, $LiPF_6$, $LiAsF_6$, $LiCF_3SO_3$, $LiN(CF_3SO_2)_2$, $LiC(CF_3SO_2)_3$) dissolved in high molecular weight polyether hosts, (e.g., PEO and PPO) which acts as solid solvents **[47]**. The ionic conduction mechanism of SPE is intimately associated with the local segmental motions of the polymer. The second category of polymer electrolyte, gel polymer electrolyte, is characterized by a higher ambient ionic conductivity but poorer mechanical properties when compared with SPE. GPE is usually obtained by incorporating a larger quantity of liquid electrolyte to a polymer matrix that is capable of forming a stable gel polymer host structure.

Polymer electrolytes have several obvious advantages over their liquid electrolyte. Among the advantages of these electrolytes, they include no internal shorting, leakage of electrolytes and no non-combustible reaction products at the electrode surface existing in the liquid electrolytes **[48-52]**. The pre-requisites for a polymer electrolyte for lithium batteries are: high ionic conductivity at ambient and subambient temperatures, good mechanical strength, appreciable transference number, thermal and electrochemical stabilities, and better compatibility with electrodes **[53-55]**. In particular, for Li/S battery, it is expected that the polymer membrane can act as a physical barrier, which can help control the dissolution of the sulfide anions from the cathode and also prevent the attack of the same anions at the anode **[56]**.

2.4.1 Dry Solid Polymer Electrolyte in Li/S Batteries

In dry solid polymer electrolytes, the polymer host itself is used as a solid solvent along with lithium salt and this does not contain any organic liquids. As a polymer host, the high molecular weight poly (ethylene oxide) (PEO)-based solid polymer electrolytes are emerging as the best candidates to be used because of their solvation power, complexion ability and ion transport mechanism directly connected with the alkaline salt (Li^+). However, the ionic conductivity of PEO-lithium salts (LiX) electrolytes at ambient temperature (10^{-7}-10^{-6} S cm^{-1}) is not high enough for most practical applications. In order to overcome this problem, consistent research efforts have been devoted to improve the ionic conductivity in PEO-LiX (X= ClO_4^-, $CF_3SO_3^-$, BF_4^-, PF_6^- etc.) solid polymer electrolytes **[54, 57]**.

In Jeon *et al*'s study **[58]**, $LiClO_4$ was chosen to dissolve in high molecular weight polymer host-PEO which acted as solid solvents. Dry polymer electrolyte made of PEO with tetra (ethylene glycol dimethyl ether) was employed into Li/S cells to study issues such as the fading capacity and low sulfur utilization. According to the change in morphologies for a composite sulfur cathode, which was obtained by scanning electron microscopy (SEM), a model for the change in morphology of the composite cathode was built as shown in **Figure 2.1**. The authors offered us a mechanism for the capacity fading was mainly due to the heterogeneity and worsening distribution of sulfur along with cycling. Some researchers have been trying to further improve the conductivity by the use of inorganic ceramic filler such as Al_2O_3, SiO_2, TiO_2 and ZrO_2 in the host polymer matrix **[59-67]**.

In Shin *et al*'s study **[68]**, $(PEO)_{10}LiCF_3SO_3$ polymer electrolyte with titanium oxide (Ti_nO_{2n-1}, n=1, 2) was introduced into Li/S system, and they not only investigated the ionic

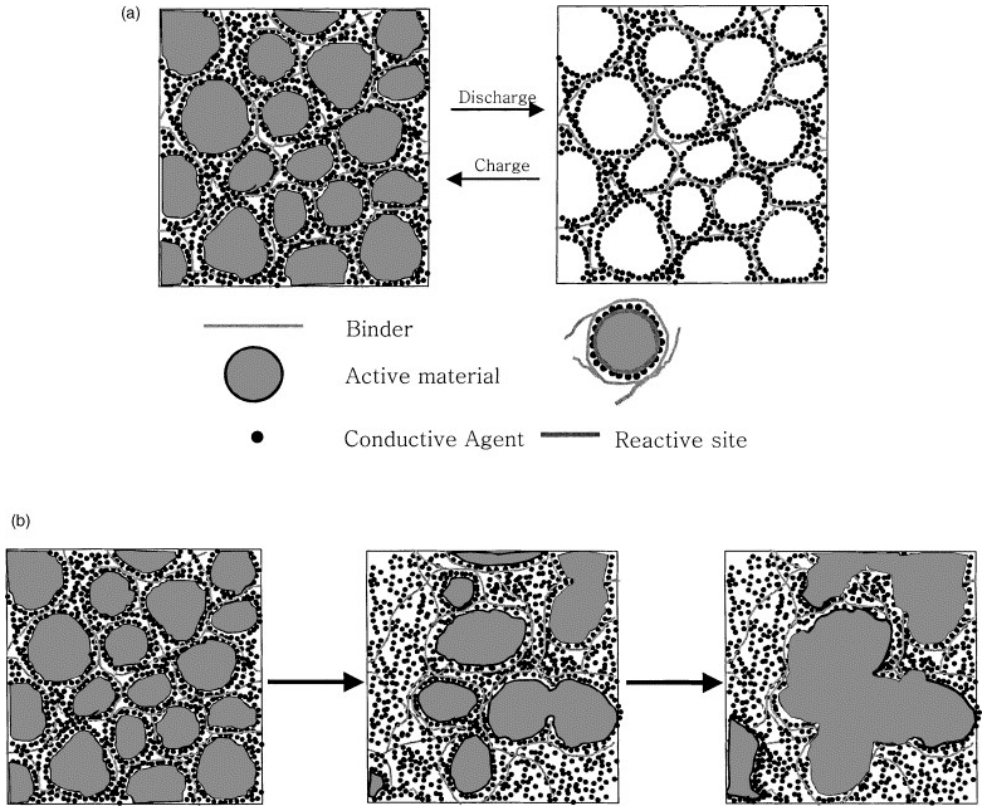

Fig 2.1 Model for morphology change of composite cathode during charge-discharge: **(a)** ideal case; **(b)** real case. Reprinted from **Ref. 58** with permission from Elsevier.

conductivity and interfacial stability of this dry polymer electrolyte but also the discharge characteristics of Li/S cells with $(PEO)_{10}LiCF_3SO_3$ polymer electrolyte. From the results of this study, titanium oxide is a good candidate as ceramic filler in $(PEO)_{10}LiCF_3SO_3$ dry polymer electrolyte. Titanium Oxide filler has a size of sub-micron and several micron consisting of various phases that were prepared by ball milling for 100 h, which were introduced into the $(PEO)_{10}LiCF_3SO_3$ polymer electrolyte. The addition of titanium oxide

containing Ti_2O_3, TiO and Ti_2O into the $(PEO)_{10}LiCF_3SO_3$ polymer electrolyte improved the ionic conductivity due to the change of -C-O-C- vibration and ionic structure of polymer electrolyte by the decrease in crystallinity of PEO polymer electrolyte, and the interface resistance between polymer electrolyte and lithium electrode was remarkably decreased by lowering the contact area between lithium and electrolyte.

In Jeong *et al*'s study **[69]**, $(PEO)_6LiBF_4$ polymer electrolyte was prepared under three different mixing conditions: stirred polymer electrolyte, ball-milled polymer electrolyte and ball-milled polymer electrolyte with 10 wt% Al_2O_3. The Li/S cell containing ball-milled $(PEO)_6LiBF_4$-Al_2O_3 polymer electrolyte delivered a high initial discharge of 1670 mAh g^{-1}, which was better than the cells with stirred $(PEO)_6LiBF_4$ polymer electrolyte or $(PEO)_6LiBF_4$ ball-milled polymer electrolyte. And also the cycle performance of Li/$(PEO)_6LiBF_4$/S cell had remarkably improved with the addition of Al_2O_3. $(PEO)_{20}Li(CF_3SO_2)_2N$-$\gamma LiAlO_2$ was prepared and introduced into Li/S battery in Wen *et al*'s study **[70]**. The all-solid-state Li/S cell with PEO based polymer electrolyte operating at 75 °C exhibited an average capacity of 290 mAh g^{-1} in 50 cycles. The cycle-stability of Li/S polymer battery could be improved by amending the method to prepare the sulfur composite cathode by blending sulfur and PEO by thermal melting at 180 °C in a sealed container. The SEM results confirmed the mechanism of capacity fading **[58]**, which suggested that the capacity of Li/S polymer battery was mostly suffered from aggregation of sulfur or lithium sulfide during cycling.

This research group did a further study to combine $(PEO)_{18}Li(CF_3SO_2)_2N$-$SiO_2$ polymer electrolyte and sulfur/mesoporous-carbon composite cathode as an all solid state polymer battery **[71]**. The conductivity of the PEO based electrolyte could reach 5×10^{-4} S cm^{-1} at

70 °C. In the sulfur cathode, mesoporous carbon sphere with the uniform channels was employed as the conductive agent, and sulfur was penetrated into those channels by a co-heating method. By this, the prepared all solid state polymer battery showed excellent cycling performance with a reversible discharge capacity of about 800 mAh g^{-1} at 70 °C after 25 cycles.

2.4.2 Gel Polymer Electrolytes in Li/S Batteries

In the point of view of dry solid polymer, the main obstacle is still the ionic conductivity, which is generally below 10^{-3} S cm^{-1} and not enough for practical application. At room temperature, the all solid state Li/S batteries usually showed poor performance. As a result, gel polymer electrolytes were developed **[72-74]**, which can be regarded as an intermediate state between typical liquid electrolytes and dry solid polymer electrolytes. In gel polymer electrolytes, the liquid component is trapped in the polymer matrix, thereby preventing leakage of liquid electrolyte. Therefore, the pore structure of the polymer membrane is the key component and is especially important for the ionic conductivity. In Li/S battery, to date, several types of polymer membranes have been developed and characterized, such as those based on poly(ethylene oxide) (PEO), poly(vinylidene fluoride) (PVDF) and poly(vinylidene fluoride)-hexafluoropropylene (PVDF-HFP).

2.4.2.1 PEO-Based Gel Polymer Electrolyte

Important progress was recently made by Scrosati and co-workers **[75]**, who built a lithium metal-free new battery version shown in **Figure 2.2**. They also renewed the electrolyte component by replacing the common liquid organic solutions with a gel-type

polymer membrane, formed by trapping ethylene carbonate/dimethylcarbonate lithium hexafluorophosphate (EC: DMC/$LiPF_6$) solution saturated with lithium sulfide in a polyethylene oxide/lithium trifluoromethanesulfonate (PEO/$LiCF_3SO_3$) polymer matrix **[76]**.

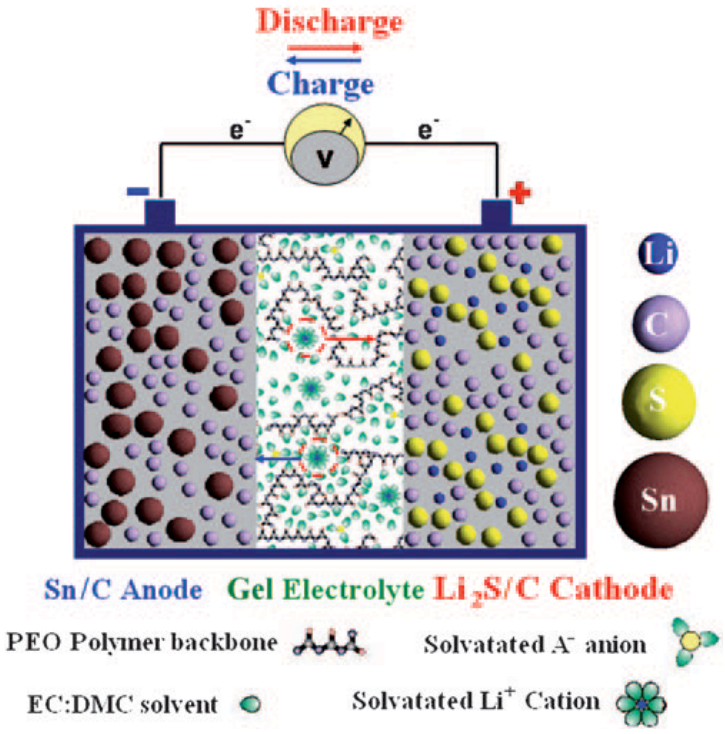

Fig 2.2 Sketch of the Sn/C/CGPE/ Li_2S/C polymer battery developed herein. The battery is formed by a Sn/C composite anode, a PEO based gel polymer electrolyte, and a Li_2S/C cathode. PEO = poly(ethylene oxide). Reprinted by permission from Wiley-VCH Verlag GmbH & Co. KGaA. from **Ref. 75**.

A dispersed zirconia ceramic filler enhanced the mechanical properties of the gel and improved liquid retention within its bulk **[77]**. Impedance studies **[78]** indicated that the resistance of the as-prepared GPE was low and stable with time with a high conductivity approaching 10^{-2} S cm^{-1} (**Figure 2.3**). With the assembly of the Sn/C anode, Li_2S/C cathode

and PEO based GPE, this polymer battery showed a high initial discharge of about 1200 mAh g^{-1} at 38 mA cm^{-2} g^{-1} (capacity calculated based on Li_2S mass only).

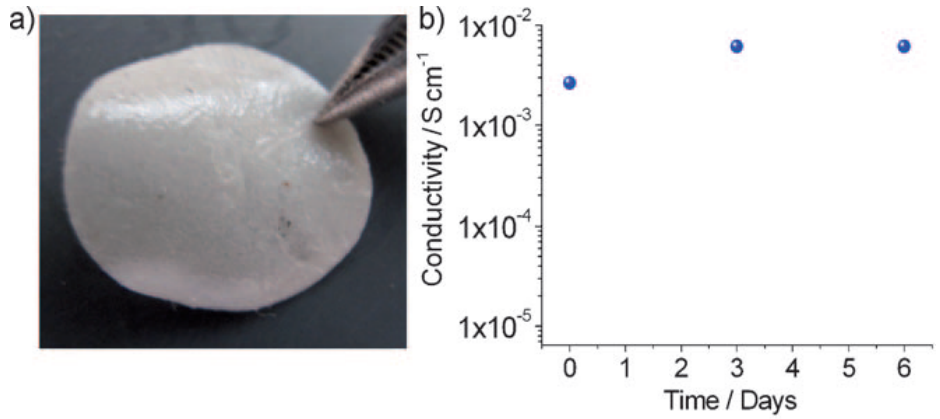

Fig 2.3 Characteristics of the PEO based gel polymer membrane to be used as electrolyte separator in the lithium-sulfur battery. a) Appearance of the membrane. b) Time evolution of the conductivity at room temperature. Reprinted by permission from Wiley-VCH Verlag GmbH & Co. KGaA. from **Ref. 75**.

2.4.2.2 PVDF Based Gel Polymer Electrolyte

Poly(vinylidene fluoride) (PVDF) has received great attention as a membrane material with regard to its outstanding properties such as high mechanical strength, thermal stability, chemical resistance, and high hydrophobicity **[79]**. By virtue of its various appealing properties, PVDF has been chosen as a suitable polymer host. PVDF-based polymer electrolytes are expected to be highly anodically stable due to the strongly electron-withdrawing functional group (–C–F). Furthermore, PVDF itself has a high dielectric constant (ε = 8.4) for a polymer, which can assist in greater ionization of lithium salts, and thus provide a high concentration of charge carriers **[80, 81]**.

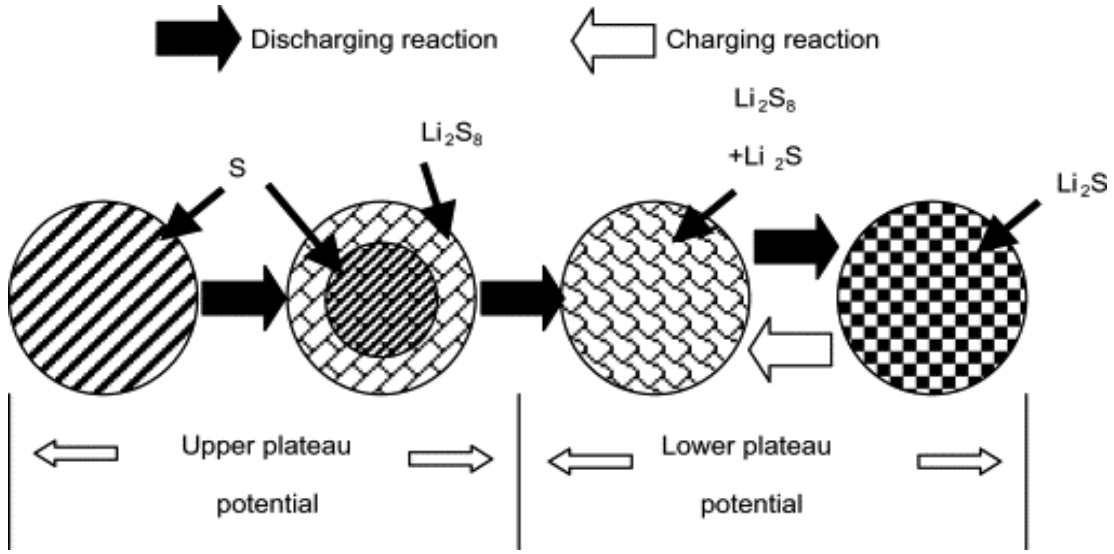

Fig 2.4 The discharge and charge reaction model of lithium/sulfur cell. Reprinted from **Ref. 82** with permission from Elsevier.

A detailed discussion regarding the discharge process of Li/PVDF/S was presented by Ryu *et al* **[82]**. The PVDF gel polymer electrolyte was prepared by $LiCF_3SO_3$ as lithium-ion resource, tetraglyme as plasticizer, and PVDF as a gelling agent in THF solvent in Ar atmosphere. A freestanding PVDF electrolyte film was obtained after the solvent was evaporated at room temperature. By using PVDF polymer electrolyte, the Li/S cell had two plateaus-like potential regions and a discharge capacity of 1268 mAh g^{-1} at the first discharge. The discharge capacity decreased to 1028 mAh g^{-1} and the upper plateau region disappeared after second discharge. From XRD and DSC results of the sulfur electrode, a model was built as shown in **Figure 2.4** to suggest that elemental sulfur disappeared and changed into Li_2S_n ($n > 4$) at the upper plateau region and Li_2S was formed at the low plateau region.

2.4.2.3 PVDF-HFP Based Gel Polymer Electrolyte

Poly(vinylidene fluoride)-hexafluoropropylene (PVDF-HFP) has drawn the attention of many researchers due to its appealing properties. The high dielectric constant of $\varepsilon = 8.4$ facilitates for higher concentration of charge carriers, and it also comprises of both amorphous and crystalline phase; the amorphous phase of the polymer helps for higher ionic conduction, whereas the crystalline phase acts as a mechanical support for the polymer electrolyte **[83-85]**.

Shin *et al* **[86]** reported the preparation and performance of PVDF-HFP gel electrolyte in Li/S batteries. The PVDF-HFP gel polymer electrolyte with tetra ethylene glycol dimethylether (TEGDME) as a plasticizer, $LiCF_3SO_3$, $LiBF_4$ and $LiPF_6$ as lithium salt and acetone as solvent was prepared by solvent casting of slurry that mixed PVDF-HFP copolymer with acetone and salt using a ball-milling technique. This polymer electrolyte showed high mechanical property and good ionic conductivity (4.99×10^{-4} S cm^{-1} at room temperature). As ball-milled gel polymer electrolytes were introduced into Li/S cells with sulfur as cathode and lithium as the anode. The first specific discharge capacities with discharge rate of 0.14 mA cm^{-2} at room temperature were about 575 and 765 mAh g^{-1}. The melting temperature of crystalline PVDF-HFP was found to decrease, which may be due to the decrease of crystallinity by scission of the polymer chain during ball milling. Therefore, it was concluded that the ball-milling technique could be a very promising preparative technique for the preparation of slurry for polymer electrolytes.

In Wang *et al*'s study **[21, 28]**, a gel polymer electrolyte was formed by trapping a liquid electrolyte of PC-EC-DEC (1:4:5 v/v) containing 1 M $LiPF_6$ in a dry PVDF-HFP/SiO_2

polymer matrix. And this dry PVDF-HFP/SiO_2 film with abundant pore structure was prepared by phase separation methods. The ionic conductivity of resulting gel polymer electrolyte was about 1.2×10^{-3} S cm^{-1} at room temperature. This gel polymer electrolyte was introduced into the cells with sulfur/active carbon composite cathode and sulfur/polyacrylonitrile (S/PAN) composite, respectively. The cell with S/PAN composite cathode exhibited a specific capacity up to 850 mAh g^{-1} in the initial and remained above 600mAh g^{-1} after 50 cycles. With elemental sulfur incorporated in porous carbon, S/C composite exhibited reversible capacity of 440 mAh g^{-1} at current density of 0.3 mA cm^{-2}.

Chapter 3
The Preparation of Sulfur/Polypyrrole Binary Composite Cathode for Li/S Batteries

3.1 One-Step Synthesis of Branched Sulfur/Polypyrrole Nanocomposite Cathode for Li/S Batteries

3.1.1 Introduction

Polypyrrole (PPy) is a conductive polymer with conductivity from a few mS cm^{-1} to 1-100 S cm^{-1} (depending on its morphology and the synthesis technique) and high absorption ability; it has been used in Li/S batteries. It was shown that along with the conductivity improvement, the PPy acts as a distribution agent favouring homogeneous sulfur distribution in the composite. Liang *et al*. **[1]** reported that S penetrates into the tubular PPy fibers by the capillary forces during a co-heating process. The composite containing 30 wt% S retained a specific capacity of around 650 mAh g^{-1} over 80 cycles. Although the combination of S with PPy showed great improvement in electrochemical performance in comparison with S powder, the heat treatment step in these studies makes the process more complicated, time and energy consuming. Moreover, S was evaporated and lost during the heat treatment steps. Therefore, the development of novel techniques to prepare S/PPy composites without heat treatment is useful.

In this part, we study the preparation of a novel branched, nanostructured S/PPy composite via a single-step ball-milling, without heat treatment, and investigate its physical and electrochemical properties as a cathode for lithium secondary batteries.

3.1.2 Experimental

Polypyrrole was synthesized as described in Wu *et al*'s work **[2]**. 12.4 g CTAB was dissolved in 0.75 L deionized water, and then 0.015 L of Py was added into the CTAB solution, stirred for 3 h. Subsequently, 0.045 L aqueous solution of 5.1 g ammonium persulfate was added, as an oxidizing agent, to initiate the polymerization, and the solution was stirred for 24 h. All synthesis procedures were carried out in a temperature range between 0-5 °C. The final precipitate of PPy was separated via filtration, thoroughly washed with deionized water and ethanol, and then vacuum dried overnight at 70 °C. To make S/PPy composite, PPy was mixed with S in the weight ratio PPy:S = 1:2, by ball-milling for 3 h at 600 rpm.

The chemical transformation of the composite during the preparation process was investigated by Fourier Transform Infrared Spectroscopy (FTIR, 520, Nicolet). The crystalline phases of the sample were determined by X-ray diffraction (XRD, D8 Discover, Bruker) equipped with Cu-Kα radiation. The composite surface morphology was examined by field emission scanning electron microscopy (FE-SEM, Leo-1530, Zeiss). The interior structure of S/PPy composite was observed using transmission electron microscopy (TEM, CM10, Philips) at 60 kV and high resolution transmission electron microscopy (HRTEM, FEI TITAN 80-300) equipped with Energy Dispersive Spectroscopy (EDS). The PPy nanowires diameter distribution, the calculation of the geometric mean diameter $d_{g,p}$ and the geometric standard deviation σ_g were done via a random sampling of nanowires from the FE-SEM images. The specific surface area was determined by the Brunauer-Emmet-Teller

method (BET, ASAP 2020, Micromeritics). The S content in S/PPy composite was determined using chemical analysis (CHNS, Vario Micro Cube, Elementar).

The electrochemical performance of S/PPy composite samples was investigated using coin-type cells (CR2032). The cell was composed of lithium metal anode and S/PPy cathode separated by a microporous polypropylene separator soaked in 1 mol L^{-1} solution of LiTFSI in TEGDME electrolyte. The composite cathode was prepared by mixing 80 wt% S/PPy, 10 wt% PVdF as a binder and 10 wt% acetylene black conducting agent in NMP. The sulfur cathode, with a weight ratio S:AB:PVdF = 6:3:1, and the PPy cathode with the composition PPy:AB:PVdF = 6:3:1 were also prepared in the same way as the S/PPy composite cathode. The resultant slurry in NMP was spread onto a circular piece of nickel foam with 1 cm in diameter. After drying in a vacuum oven for 12 h at 60 ^{o}C, the cathode was pressed at 8 MPa by a hydraulic press in order to achieve good contact between the active material and nickel foam. The electrodes were prepared to make their weight and thickness the same by precise weighing, pressing and controlling its geometry. The coin cells were assembled in a Braun glove box filled with high purity argon. The cells were tested galvanostatically between 1 and 3 V *vs*. Li^{+}/Li electrode at a current density of 100 mA g^{-1}. Applied currents and specific capacities were calculated on the basis of the weight of S in the cathode.

CV was conducted between 1 and 3 V *vs*. Li^{+}/Li at a scanning rate of 0.1 mV s^{-1}. The frequency of AC impedance was varied from 1 MHz to 1 Hz with applied voltage amplitude of 10 mV. All electrochemical measurements were performed at room temperature.

3.1.3 Results and discussion

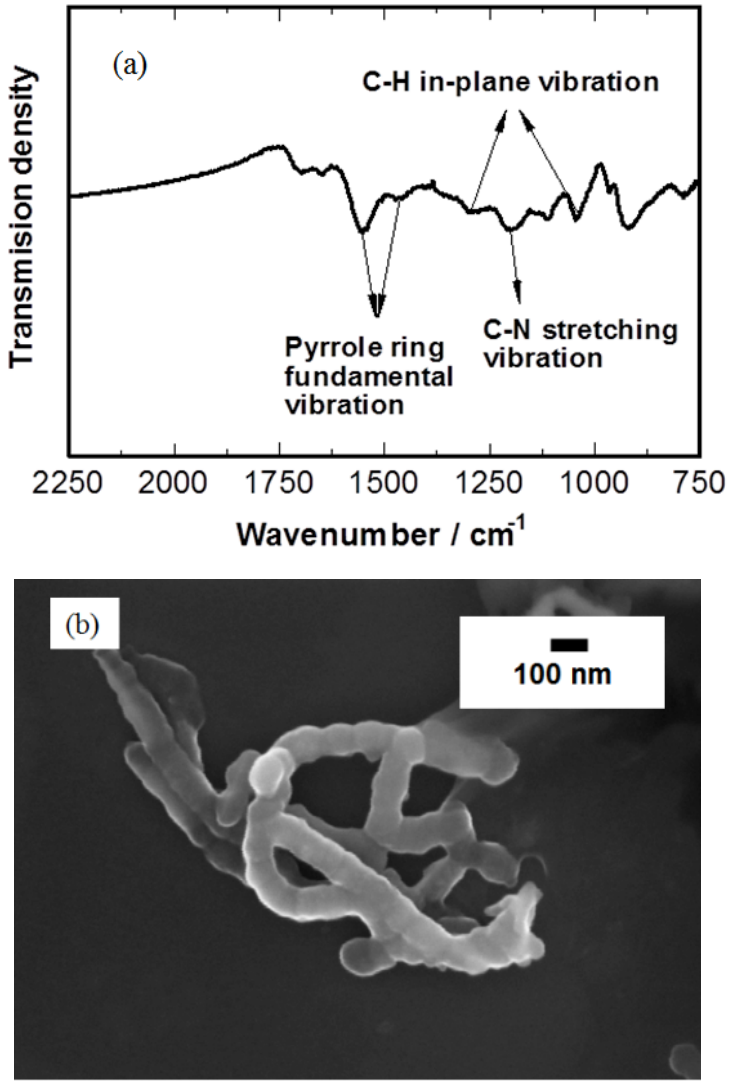

Fig 3.1 (a) FTIR spectrum and (b) SEM image of PPy as prepared sample.

From the FTIR spectra of prepared PPy shown in **Fig. 3.1a**, it could be seen that the characteristic bands of the PPy was consistent with the literature data [**1, 3-5**]. The pyrrole ring fundamental vibrations are at 1545 cm^{-1} and 1458 cm^{-1}, the =C-H in-plane vibrations are

at 1291 cm^{-1} and 1043 cm^{-1}, and the C-N stretching vibration is at 1175 cm^{-1}. Therefore, it could be concluded that the PPy structure could be successfully obtained via the chemical polymerization method. The morphology of this material was observed by SEM as given in **Fig. 3.1b**. One can see that in presence of CTAB, polypyrrole was formed as the separated nanowires. It was reported that CTAB could form rod-like micelles when organic nanoparticles solubilize into their hydrocarbon core [**6**]; these rods further direct the fibers growth like a template. It can be seen from **Fig. 3.1b** that PPy nanowires prepared in the present study are less than 100 nm in diameter. **Fig. 3.2a** presents the PPy nanowires diameter distribution obtained from the SEM observation data [**7**]. PPy nanowires have uniform diameter distribution with a geometric mean diameter of $d_{g,\,p}$ = 81.3 nm and a geometric standard deviation of σ_g = 1.33.

The XRD patterns of pure S, pure PPy and S/PPy composite are shown in **Fig. 3.2b**. One can see that while PPy was amorphous, the XRD patterns of the S used in this work exhibited *Fddd* orthorhombic structure for elemental sulfur. In comparison with S, the S/PPy composite showed sharp peaks of S with reduced peak intensity. On the other hand, no peak shift could be observed, which could be an indication of the absence of phase transformations due to ballmilling, and the sulfur crystal structure remained in the S/PPy composite. However, the XRD peak intensity reduction may indicate partial absorption of melted sulfur, during ball-milling, into the porous structure of PPy, since ball-milling generates heat and the temperature increase over the melting point of sulfur.

In this work, the conductive S/PPy composite was obtained via one-step high speed ballmilling of the mixture of sulfur and PPy, and no additional heat treatment was applied in

the preparation process. Chemical analysis has shown that the sulfur content in the S/PPy composite was about 65 wt%, i.e. there is no significant sulfur loss when the composite was prepared by the current method.

Fig. 3.3 shows HRTEM images of as prepared PPy. At a higher magnification (**Fig. 3.3a**), no obvious lattice fringes can be observed, and PPy has the amorphous structure, which is consistent with XRD results. The EDS carbon mapping of PPy (**Fig. 3.3c** and **3.3d**) shows homogeneous carbon distribution.

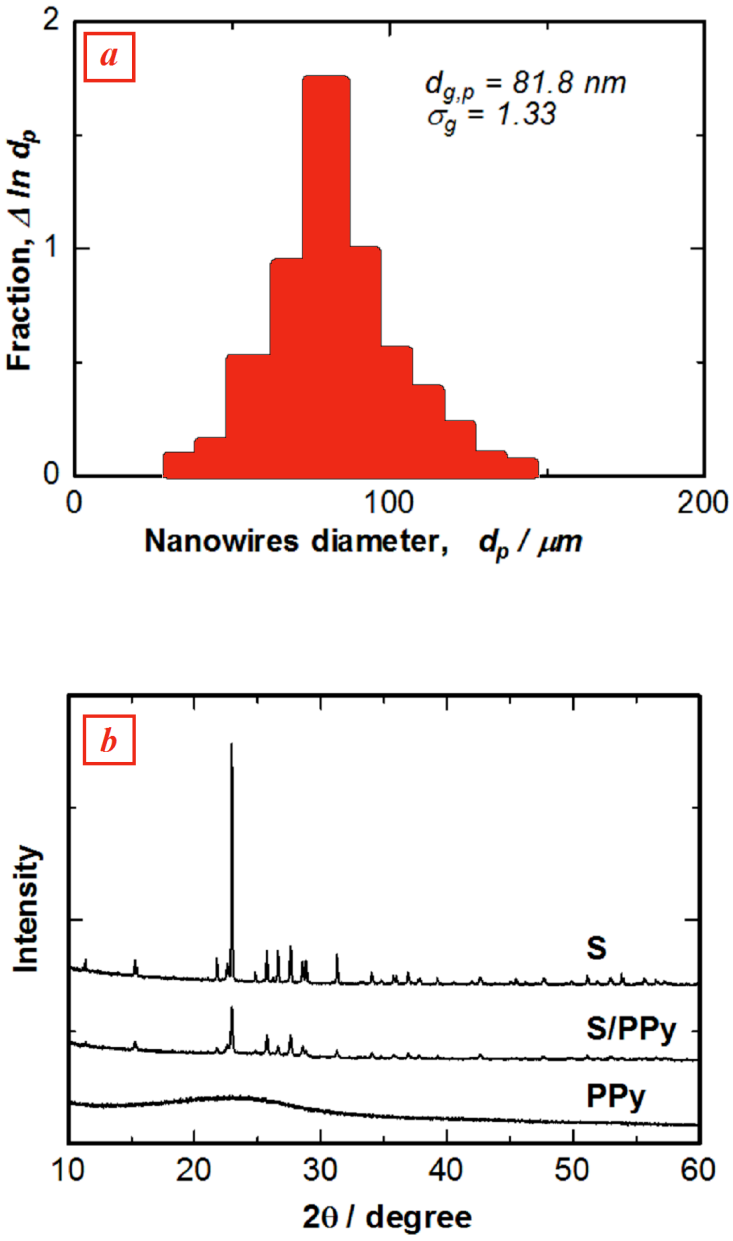

Fig 3.2 (a) Distribution of the diameters of PPy nanowires prepared in this work; (b) XRD patterns of S, PPy and S/PPy composite samples.

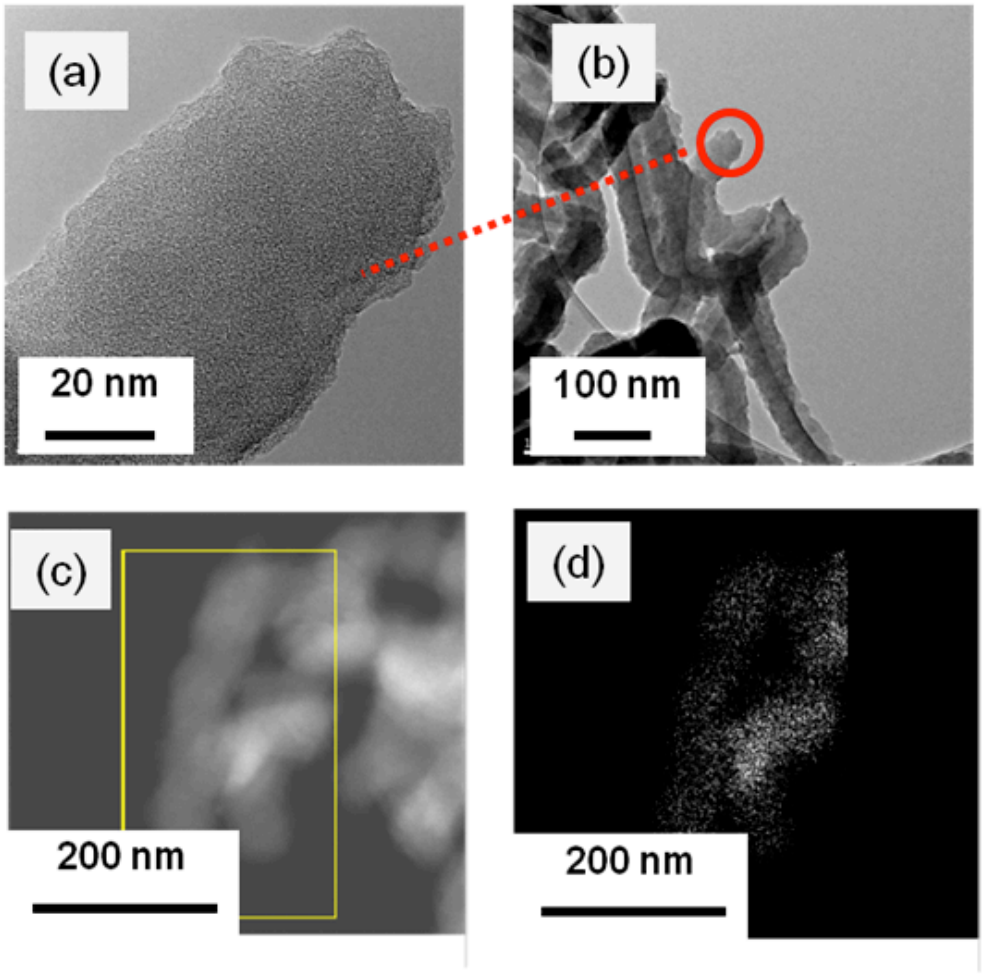

Fig 3.3 HRTEM images of PPy samples at different magnifications and EDS mapping showing distribution of carbon.

The TEM data presented in **Fig. 3.4a** shows that the S/PPy composite prepared via the present technique has a well-developed branched structure. HRTEM (**Fig. 3.4b**) of S/PPy composite shows the crystal lattice strips in the outer part of the composites nanostructure with a measured neighboring interlayer distance of 0.38 nm, which corresponds to the (2, 2, 2) crystal plane of S. This suggestion is in good agreement with the XRD results that the S/PPy composite remained the well-distinguished peaks of S. The inner part of the S/PPy composite

is less crystalline (**Fig. 3.4d**) which is due to the amorphous PPy nanowires. **Fig. 3.4e-3.4g** presents the EDS mapping of the S/PPy composite. One can see that sulfur is homogeneously distributed over the PPy nanowired substrate. This well-developed branched structure of S/PPy with homogeneous distribution of sulfur in it enhances the contact of sulfur to conductive PPy, which is very important for the electrochemical performance of the composite cathode material. Specific surface area of the as-prepared PPy was 129.8 m^2 g^{-1} with the pore volume of 0.55 cm^3 g^{-1}. After mixing with sulfur, the specific surface area of S/PPy was only 4.4 m^2 g^{-1} with the pore volume of 0.052 cm^3 g^{-1}. This remarkable specific surface area and pore size reduction could be mainly due to deposition of a large amount of sulfur into the pores and surface of PPy. The formation of the S/PPy composite with homogeneous sulfur deposition on the conductive PPy surface may drastically improve the conductivity of the composite cathode **[5]**, which is important for the sulfur utilization and increase of the sulfur cathode capacity. Furthermore, the branched nanostructure of S/PPy could accommodate the volume change of the composite during charge and discharge **[8]** and improve the cyclability of the composite cathode.

A high S content cathode is desirable to construct a high energy density battery. Exclusion of the heat treatment from the synthetic route for S/PPy composite along with saving energy and simplifying the preparation process prevents the sulfur loss due to its sublimation. This also prevents the generation of toxic volatile sulfur compounds at high temperature conditions; therefore, the preparation technique developed in this work could be more preferable than the conventional prolonged multi-step and high temperature techniques of preparation of conductive S-containing composites.

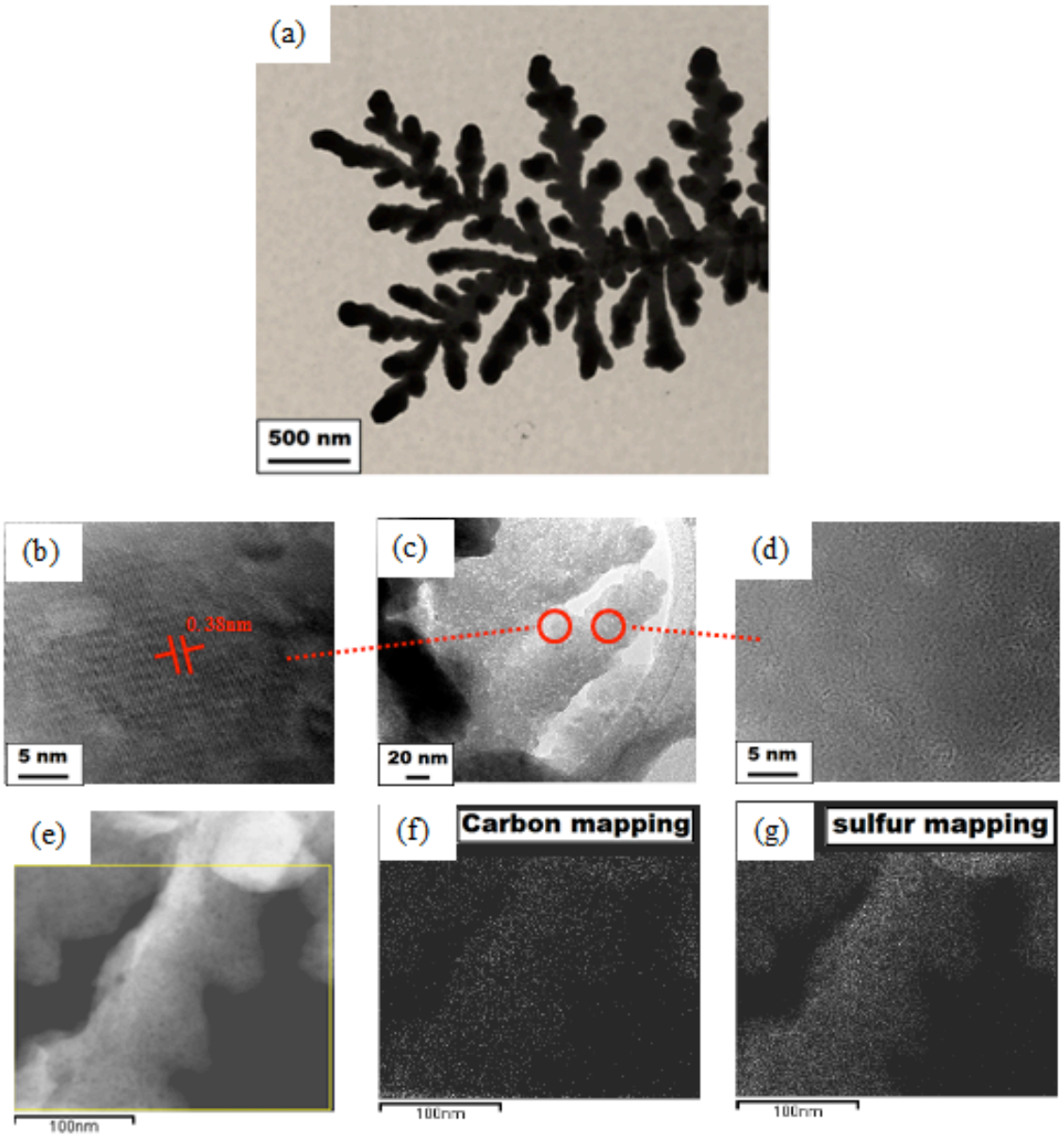

Fig 3.4 TEM and HRTEM images of S/PPy composite at different magnifications and EDS mapping showing the distribution of the elements C and S.

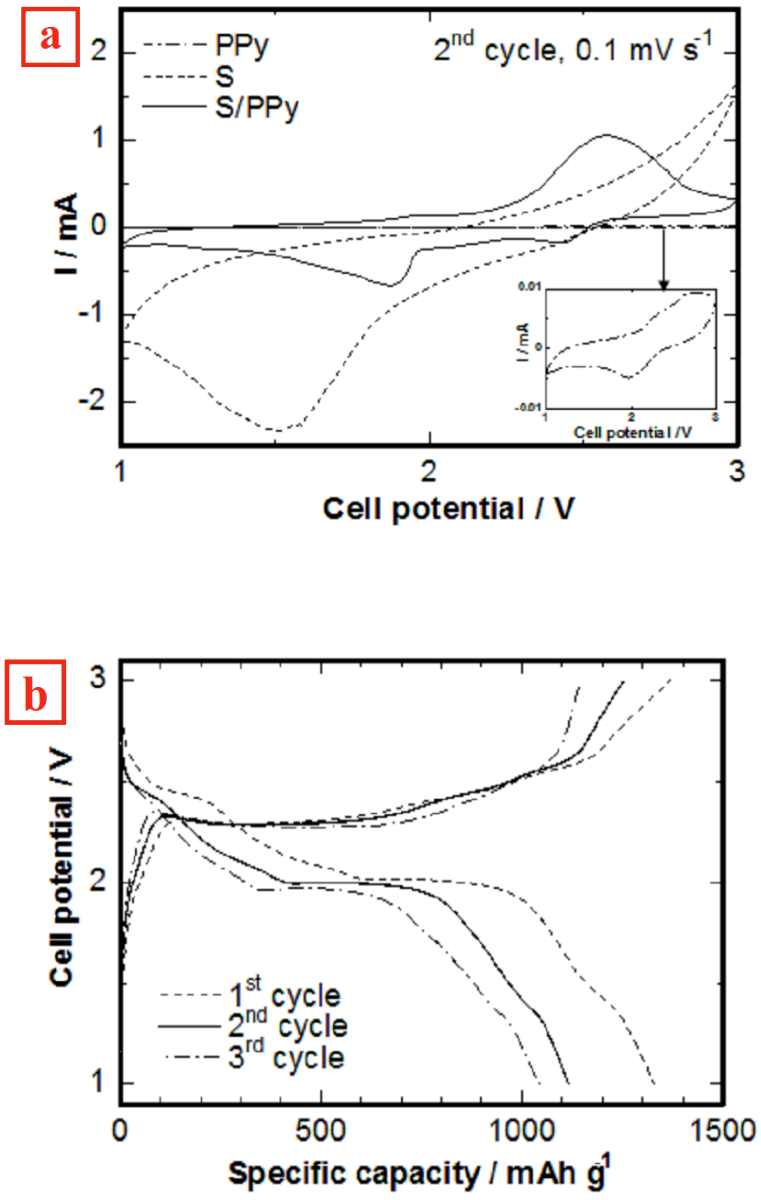

Fig 3.5 (a) CV profiles of lithium cells with S, PPy and S/PPy composite cathodes. The potential sweep rate is 0.1 mV S^{-1}; **(b)** Charge/discharge profiles of lithium cell with S/PPy composite cathode at a current density of 100 mA g^{-1}.

The CV curves are shown in **Fig. 3.5a** for S, PPy, and S/PPy composite, used as a cathode active material in the lithium half-cell. One can see that for pure S cathodes, one broad reduction peak was observed about 1.5 V *vs.* Li^+/Li, and the electrochemical processes are slow and poorly reversible. It can also be seen that PPy is electrochemically inactive at the studied potentials region and there are no noticeable electrochemical processes observed. In the case of the S/PPy composite cathode, two pairs of complex reversible redox peaks were observed around 2 and 2.5 V, which is possible due to the multi-step electrochemical reactions of S with Li^+ **[9,10]**. The CV data reveals that PPy improves the electrochemical kinetics of S. The initial profiles of galvanostatic charge-discharge tests of the S/PPy cathode are shown in **Fig. 3.5b**. It can be seen that two main plateaus appear in the potential profiles, which could be attributed to two main electrochemical reactions taking place at sulfur cathode upon cycling in Li/S battery. The results are in good agreement with the CV data. The first electrochemical reaction is presented by a short discharge plateau about 2.5 V and related to the formation of higher-order lithium polysulfides (Li_2S_n, $n \geq 4$), which are soluble in the liquid electrolyte **[9-11]**. The following prolonged plateau around 2.0 V in the discharge profiles reflects the following electrochemical transition of the polysulfides to lithium sulfide Li_2S, and this reaction kinetics is slower than that of the polysulfide formation [**9-12**]. It could be seen that while the 2 V discharge plateaus had no remarkable difference between the first and third cycles, the higher voltage plateau diminishes and almost disappears after a few cycles. This could be due to the activation of the composite cathode upon initial cycles, and achieving a steady state for the polysulfide formation. It can be seen

here that a discharge capacity of 1050 mAh g^{-1} was obtained at the third cycle, the 2.4 V plateau is short, and the system's discharge capacity mainly depends on the 2 V plateau.

The S/PPy composite cathode cyclability was remarkably enhanced compared with that of the S cathode as shown in **Fig. 3.6a**. The discharge capacity of the S/PPy composite has been stabilized after 25 cycles at about 600 mAh g^{-1} and a discharge capacity of 500 mAh g^{-1} was retained after 40 cycles. In contrast, the discharge capacity of the S cathode drastically decreased with cycling. The cell with pure sulfur cathode had a discharge capacity of only about 110 mAh g^{-1} at the 40^{th} cycle. The improvement of the cycle life could be attributed to the electronic conductivity enhancement of the S/PPy cathode, the ability to accommodate the large volume of S on PPy branched structure, and the absorption of polysulfides into the pores of PPy. In contrast, the pure S cathode exhibited much poorer cyclability. This cathode exhibited very low discharge capacity due to high resistance of sulfur, which lowers the sulfur utilization. The poor cyclability of the S cathode could be attributed to the mechanical destruction of the cathode caused by the inherent periodic volume expansion/shrinkage upon cycling. The sulfur shuttle mechanism **[13]** is a typical phenomenon in lithium-sulfur batteries, resulting in imperfect charging and decrease of discharge capacity, which leads to a low Coulombic efficiency of the cell. **Fig. 3.6b** presents the Coulombic efficiency vs. cycle number for the S/PPy lithium cell. The cells exhibited a high Coulombic efficiency of 97% at the initial cycle. However, the Coulombic efficiency decreases to 89% in the second cycle and 80% in the 5th cycle. In the first cycle, the sulfur still evenly distributed on the surface of branched PPy, and this provides a high level of the cathode reversibility because of good electronic conductivity. However, as described in the previous paragraph, both the sulfur

shuttle/dissolution and the sulfur particle agglomeration could result in the reversible capacity loss. Therefore, the Coulombic efficiency of the battery gradually reduces for several consequent cycles. Further cycling leads to the Coulombic efficiency increase, which could be due to the good contact of the remaining S with porous PPy network, allowing improved reversibility of the system. The Coulombic efficiency reaches 96% after around 40 cycles, i.e., the shuttle mechanism effect is reduced upon prolonged cycling. Therefore the capacity fading of S/PPy composite cathode upon prolonged cycling could be mostly due to the sulfur particles agglomeration and to the lesser extent from the shuttle effect.

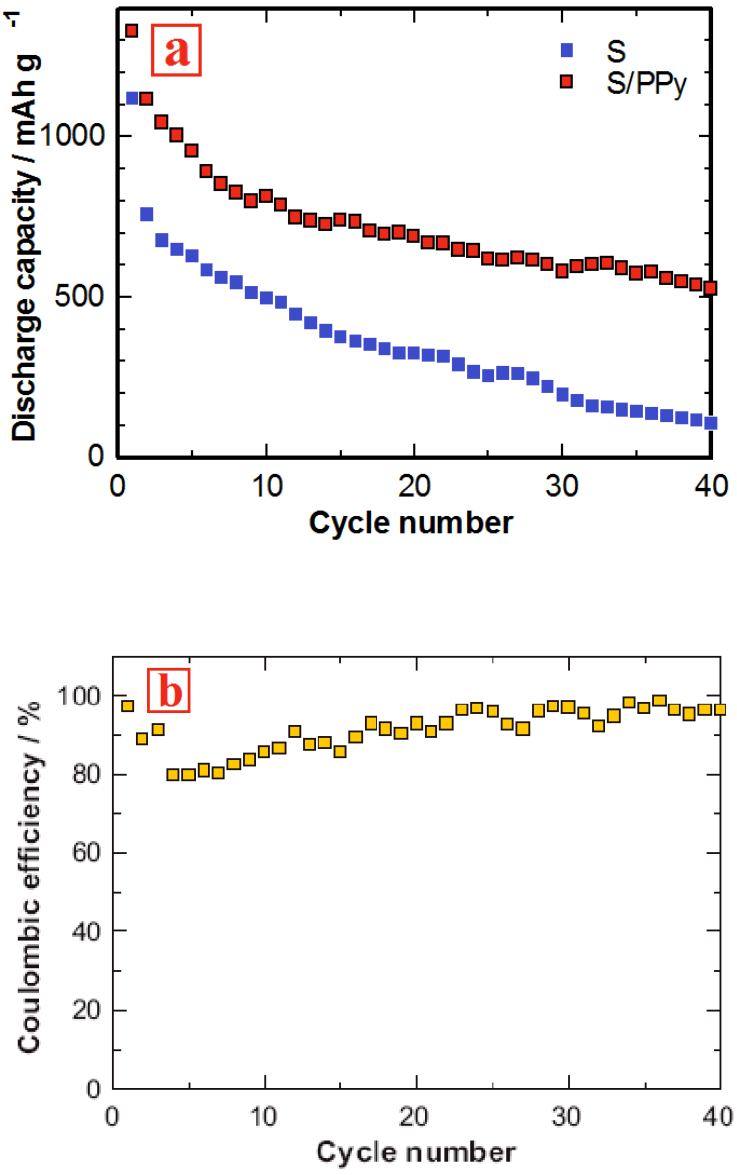

Fig 3.6 (a) Cycle performance of lithium cells with S and S/PPy composite cathodes at a current density of 100 mA g^{-1}; **(b)** Coulombic efficiency of lithium cells with S/PPy composite cathodes vs. cycle number at a current density of 100 mA g^{-1}.

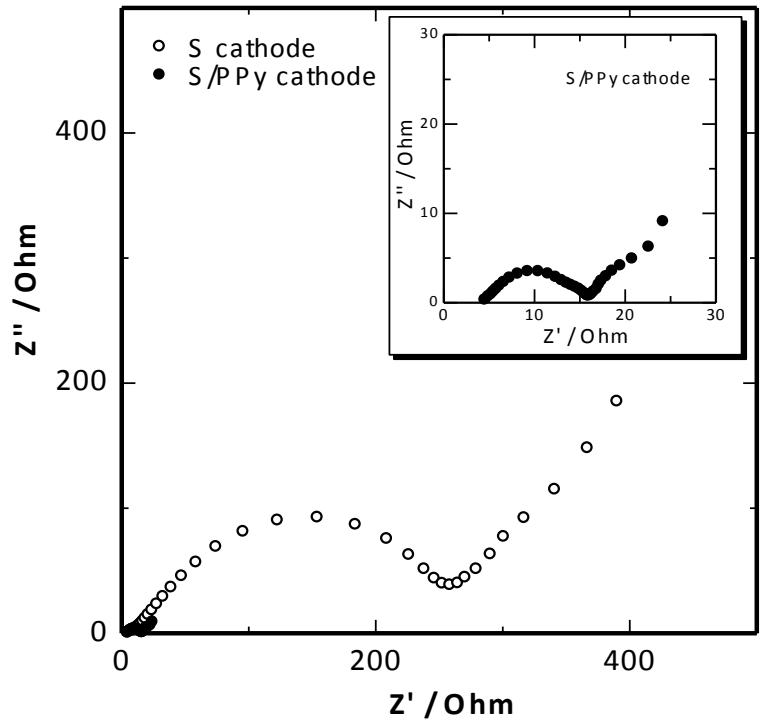

Fig 3.7 AC impedance plots of lithium cells with S and S/PPy composite cathodes in the frequency range of $0.01\text{-}10^6$ Hz.

The enhancement of cathode conductivity could be confirmed by a comparison of AC impedance behavior of the cells with S and S/PPy cathodes as given in **Fig. 3.7**. Both cathodes exhibited the Nyquist plots comprising of a depressed semicircle in the high to intermediate frequency range and an inclined line in the lower frequency range. For the composite electrodes containing highly conductive carbon, the depressed semicircle could be related to the interfacial charge transfer **[11,12]**. The inclined line in the lower frequency represented the Warburg impedance, associated with lithium-ion diffusion in the electrode particles. A much smaller high-to-medium frequency semicircle can be seen in the S/PPy

electrode AIS spectra compared with that of the sulfur cathode. This indicates a significant decrease in charge transfer resistance in the S/PPy composite compared with the pristine S electrode. This may be due to the high conductivity polypyrrole. This charge transfer enhancement leads to the electrochemical performance improvement of the composite cathode. The S/PPy composite was prepared in this work via a simple one-step technique and no heat-treatment was used. This can be considered as an economic and environmentally friendly approach because exclusion of heating prevents the sulfur loss and the formation of harmful sulfur compounds during the synthesis. The material exhibits enhanced electrochemical performance in a lithium cell with liquid electrolyte, which is comparable with that of the sulfur-containing cathodes prepared via complicated techniques using expensive conductive carbons **[14-16]**. Therefore, the current preparation technique could be considered as a promising approach to prepare high performance sulfur cathodes for lithium battery application.

3.1.4 Summary

The polypyrrole nanowires were prepared via chemical polymerization of pyrrole. These nanowires were used as a conductive matrix to prepare a branched binary S/PPy nanocomposite by a simple, one-step ball-milling without any heat treatment. The S/PPy composite consisted of the branched conductive PPy matrix coated with S. The use of conductive PPy matrix has improved the electrochemical performance of the composite cathode in lithium battery via the enhanced charge transfer in the system. Furthermore, the branched structure of the nanocomposite and high porosity of the PPy matrix could accommodate the mechanical stresses induced by the volume changes upon charge-discharge

and hinder the polysulfide dissolution. The S/PPy composite cathode exhibited enhanced electrochemical performance and allowed stable cycling of the lithium half-cells. One-step preparation technique developed in this work allows the preparation of high performance two-component S/PPy composite cathode with three-dimensional-branched structure.

3.2 Three-dimensional Carbon fiber as Current Collector for Li/S Batteries

3.2.1 Introduction

Due to the importance of the development of this type of batteries, especially for large scale applications, tremendous efforts have been devoted by many teams worldwide to solve the conductivity problems *via* preparation of new cathode materials based on the sulfur composites with various carbon and conductive polymer materials. At the same time, it was emphasized that the cathode current collector materials significantly impact on the battery performance **[17-29]**. Various metals such as Cu, Ni, stainless steel or wide range of carbon materials are used as current collectors in the forms of thin foil, mesh or foam to improve electrical conductivity and adhesion of active electrode materials **[30]**. Three-dimensional materials such as metal foams and carbon fiber cloth could be considered as promising systems due their high surface area. Therefore, owing to the three-dimensional (3D) structure, carbon fiber cloth has attracted great interest as a substrate and/or current collector, which has the ability to incorporate different materials into its 3D structure, providing the higher interfacial interaction compared with the 2D collectors, where a cathode film is attached and interacts with only its surface **[31-35]**. The use of carbon fiber current collector in Li/S battery particularly, permits for a high sulfur content deposited in its 3D geometry structure, which provides enhanced electronic conductivity between the high conductive carbon and

low conductive sulfur particles **[36]**.

In this chapter, carbon fiber cloth and nickel foam were studied as the current collectors for sulfur composite cathode in a lithium cell structure. The effect of these 3D substrates on the electrochemical performance of sulfur cathode has been investigated.

3.2.2 Experimental

A branched sulfur/polypyrrole (S/PPy) nanocomposite cathode was prepared by a simple ballmilling as described in our previous work **[25]**. 12.4 g CTAB was dissolved in 0.75 L deionized water, and then 0.015 L of Py was added into the CTAB solution, stirred for 3 h. Subsequently, 0.045 L aqueous solution of 5.1 g ammonium persulfate was added, as an oxidizing agent, to initiate the polymerization, and the solution was stirred for 24 h. All synthesis procedures were carried out in a temperature range between 0 and 5 ^{o}C. The final precipitate of PPy was separated via filtration, thoroughly washed with deionized water and ethanol, and then vacuum dried overnight at 70 ^{o}C. To makeS/PPy composite, PPy was mixed with S in the weight ratio PPy:S = 1:2, by ballmilling for 3 h at 600 rpm.

The sample surface morphology was examined by FESEM. The cell was composed of lithium metal anode and S/PPy carbon fiber cathode separated by a microporous polypropylene separator soaked in 1 mol L^{-1} LiTFSI solution of in TEGDME electrolyte. The composite cathode was prepared by mixing 80 wt% S/PPy composite, 10 wt% PVDF as a binder and 10 wt% acetylene black conducting agent in NMP. The carbon fiber cloth is a commercial product and used as received. The electrode was prepared by a conventional slurry-coating method, followed by drying in a vacuum oven for 12 h at 60 ^{o}C. The sulfur cathode, with Ni foam as current collector, was also prepared in the same way as the carbon

fiber cathode. The coin cells were assembled in a Braun glove box filled with high purity argon. The cells were tested galvanostatically between 1 and 3 V *vs*. Li^+/Li electrode at a current density of 100 mA g^{-1}. Applied currents and specific capacities were calculated on the basis of the weight of S in the composite cathode. The electrochemical impedance spectroscopy measurements were carried out by applying an ac voltage of 10 mV over the frequency range from 0.1 Hz to 1 MHz.

3.2.3 Results and discussion

Figure 3.8 shows the SEM images of both pure Ni foam and carbon fiber and these substrates coated with S/PPy composite cathode. One can see in **Fig. 3.8a** that the nickel foam has large pores of several tenths of micrometers. The morphology of the carbon fiber substrate reveals a scaffold-like morphology formed by carbon fibers with about 10 μm diameter with smooth surface as shown in **Fig. 3.8c**. From **Fig. 3.8b** and **3.8d**, it can be seen that both type current collectors could be homogeneously coated by S/PPy composite. It can also be seen, that carbon fiber have smaller dimensions compared with its Ni foam counterpart, thus may provide better conditions for charge transfer than Ni foam. This could play very positive effect on the cathode performance.

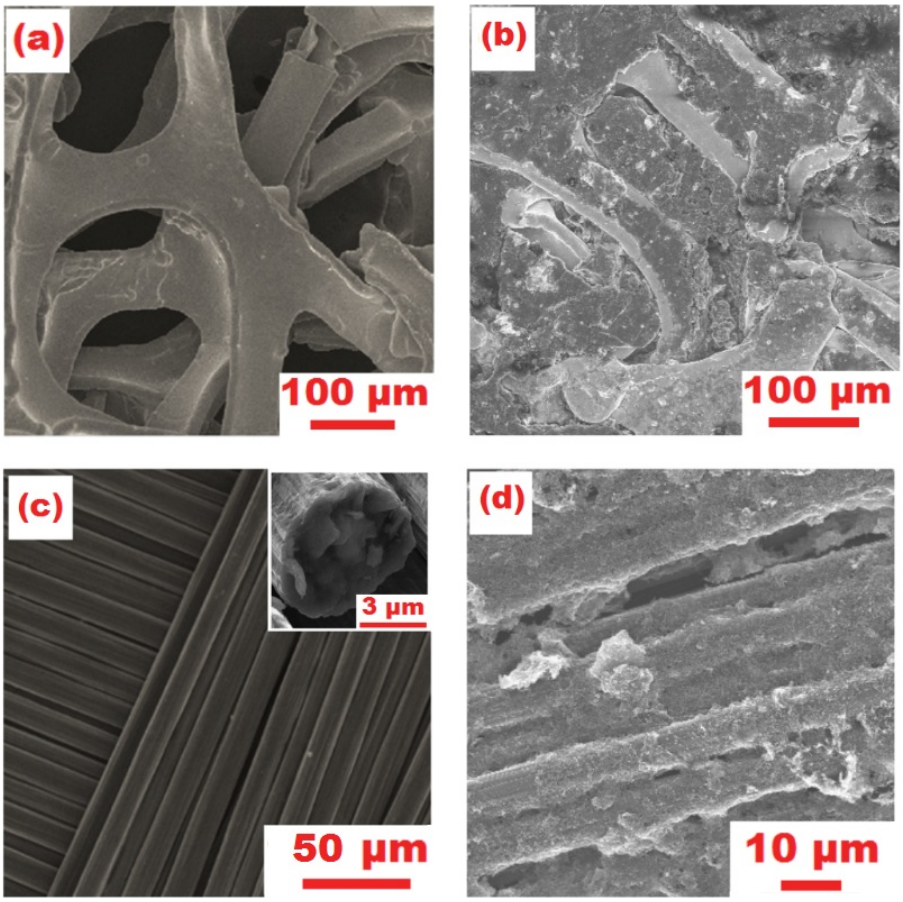

Fig 3.8 The SEM images of **(a)** parent Ni foam, **(b)** cathode material coated Ni foam; **(c)** carbon fiber (inset: the cross-section of carbon fiber) and **(d)** cathode material coated carbon fiber.

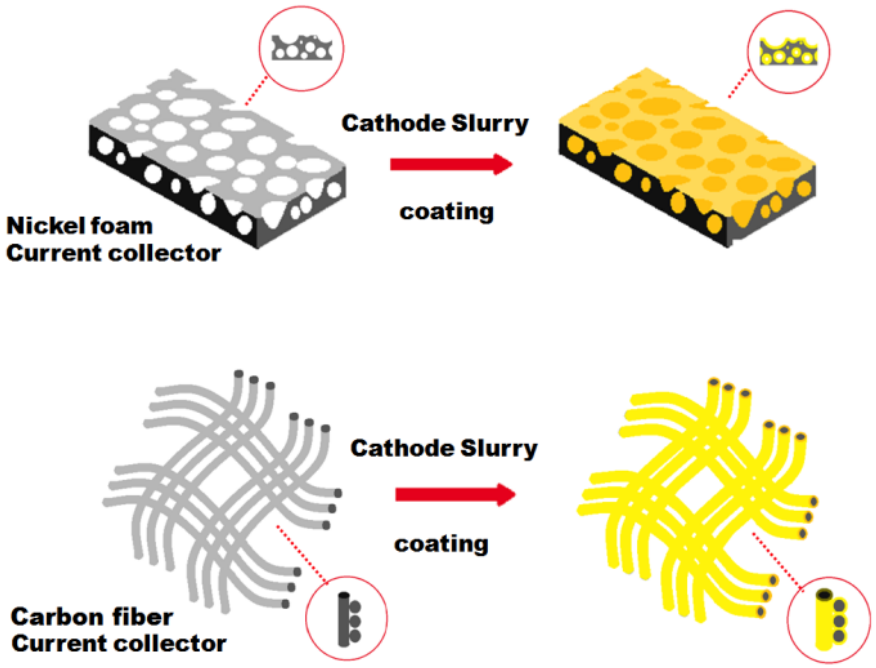

Fig 3.9 Schematics of the cathode material coating process on Ni foam and carbon fiber substrates.

Figure 3.9 schematically represents the process of the cathode material coating on the Ni foam and carbon fiber substrate. Due to its highly developed 3D structure and high conductivity, the carbon fiber current collector may accommodate more cathode material per weight and volume than its Ni foam counterpart; and, furthermore, it can enhance the electronic conductivity of the cathode coated on its surface, and provide mechanically flexible framework, which can accommodate the volume changes upon cycling, and retain soluble products of the electrochemical reactions as well, positively affecting and enhancing the electrochemical performance of the cell.

The comparison of the charge/discharge curves (the 2nd cycle) of the S/PPy composite cathode with the Ni foam and carbon fiber current collectors are shown in **Fig. 3.10**. Both the

electrodes show large discharge capacity above 1000 mAh g^{-1}. It can be seen that two main plateaus appear in the potential profiles, with different current collectors, which could be attributed to two main electrochemical reactions taking place at all the sulfur cathodes upon cycling in Li/S battery. The first electrochemical reaction is presented by a short discharge plateau about 2.4 V and related to the formation of higher-order lithium polysulfides (Li_2S_n, $n \geq 4$), which are soluble in the liquid electrolyte **[37-39]**. The following prolonged plateau around 2.0 V in the discharge profiles reflects the following electrochemical transition of the polysulfides to lithium sulfide Li_2S, and this reaction kinetics is slower than that of the polysulfide formation **[9,10,20,40]**.

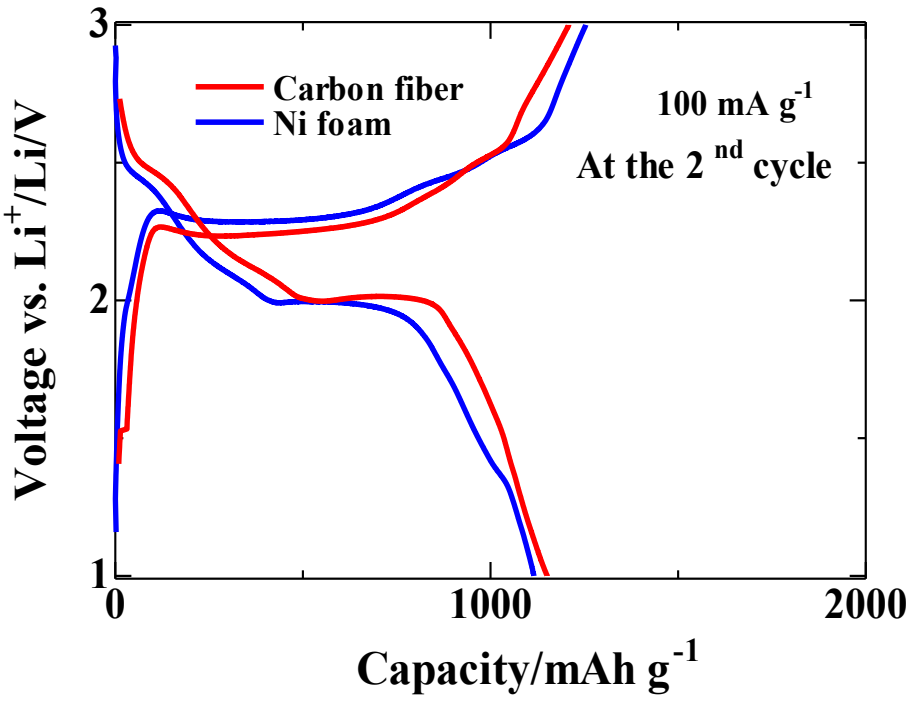

Fig 3.10 Galvanostatic charge/discharge profiles (the 2nd cycle) of lithium cell with Ni foam and carbon fiber current collector at a current density of 100 mA g^{-1}.

The use of the carbon fiber collector has significantly improved the cell cyclability, as it can be seen from **Fig. 3.11**. The carbon fiber based electrode shows a better cycling stability compared with the Ni foam counterpart, with a reversible capacity of 810 mAh g^{-1} after 40 cycles, which corresponds to an increase of this value for about 285 mAh g^{-1} during cycling at a current density of 100 mA g^{-1}. This enhanced cell reversibility can be attributed to the large interfacial/conducting area of the carbon fiber collector boosting the electrochemical activity of the cathode coated on its surface. Along with an effective electron conduction path, carbon fiber provides its network-like structure for the formation of stable morphology and structure of the S cathode preventing its agglomeration and separation.

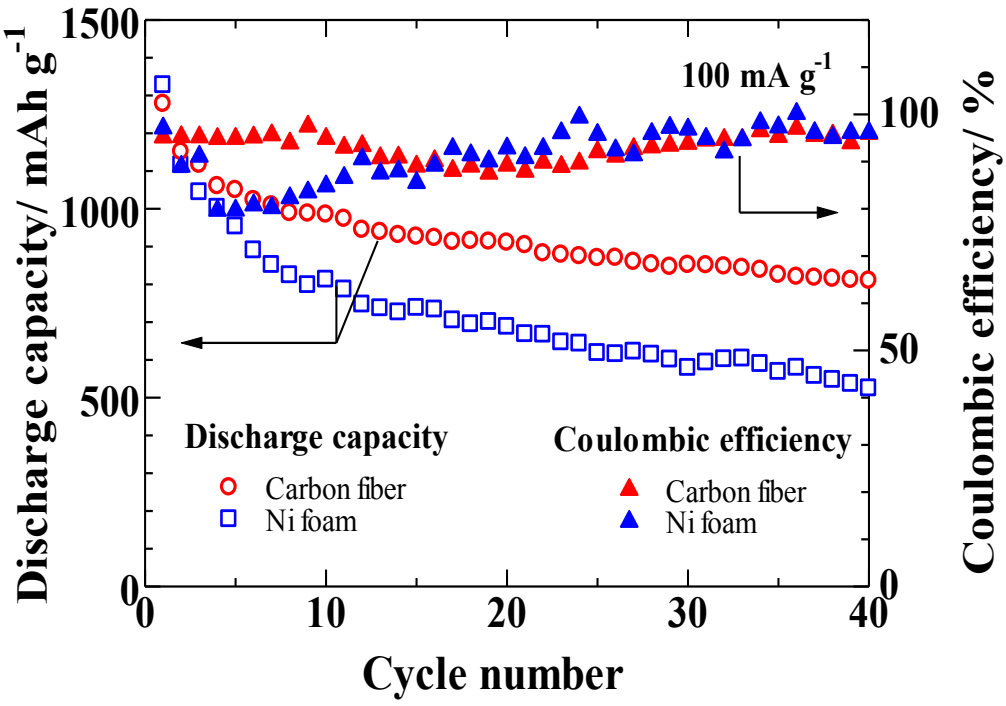

Fig 3.11 Cycle performance and Coulombic efficiency of lithium cells with carbon fiber and Ni foam current collectors at a current density of 100 mA g^{-1}.

EIS is a powerful tool to put some light on the interfacial effect in an electrochemical cell. And the observation of the trends in the impedance spectra upon the cells operation could deliver useful information related to the changes in the systems upon operation. **Figure 3.12a** presents the Nyquist plots of the cells with the carbon fiber current collectors. The impedance spectra for the carbon fiber system are complex and represented by two depressed semicircles in the high-to-medium frequency range. These semicircles, related to the interfacial charge transfer impedance, followed by a declined line of the Warburg impedance in low frequency part attributed to the bulk diffusion resistance of the composite cathode **[37]**. Carbon fiber can act as adsorbents improving the cathode material onto its surface, and, furthermore, could provide conditions for the electrochemical redox reaction products adsorption, which is impossible in the case of the metal surface of the Ni foam current collector. Furthermore, the carbon fiber based system impedance rapidly decreases upon initial charge/discharge cycles, which could be due the formation of a conductive SEI layer, favorable for the charge transfer in the system. After decreasing during a few initial cycles, the carbon fiber system charge transfer impedance stabilizes and does not change such remarkably on cycling (not shown) like in a cell with Ni foam current collector in our previous study, where the cell impedance increases on charge/discharge operation. These phenomena could be due to a partial separation of the cathode films from the Ni foam current collector surface, visually observed when the cell was disassembled after the cycling experiments. In contrast, the carbon fiber current collector provided good adhesion and stable coating of the cathode on its surface, and there were no visible

changes in the coating conditions when the cell with this current collector was disassembled after cycling.

The equivalent circuit (EC) fitting applied to the experimental EIS data provides the opportunities for the further optimization and enhancement of the electrochemical cell [**37-39**]. Therefore, using the EIS experimental data for the carbon fiber based system were analyzed using the tools of EC-Lab V10.32 (Bio-Logic Science Instruments). This analysis could be represented by the best fitting model (fitting goodness about 1), consisting of the following multicomponent equivalent circuit represented in **Fig. 3.12b** and by a scheme

$$R_0+C_1/(R_1+W_1)/(R_2+CPE_1)+(C_2+CPE_2)/(R_3+W_2)/(R_4+W_3)/R_5 \qquad (1)$$

where R_i, C_i, CPE_i and W_i are resistivity, capacitance, constant phase element and a Warburg components, respectively. It should be noted, that due to the multi-interface structure of the studied system, the resulted equivalent circuit model has a complicated character. The first member of Eq. 1, R_0, could be attributed to the electrolyte impedance [**37**]. Each of the following two complex addendums in Eq. 1 consisting of the parallel combinations of electrical scheme elements could be a representation of the interfaces/components impedances of this multi-interface system. Furthermore, these members contain both charge transfer impedance part and a Warburg (bulk diffusion impedance) component. This confirms that the studied system has multiple charge transfer borders combined with multiple regions of charge (both lithium-ion and electrons) paths through the bulk conductors. The EC model used in this work has demonstrated that the R_0 component of the circuit does not remarkably change upon cycling, so are all W_i components, which could be the indications of the relatively stable nature/conductivity of the electrolyte

and the materials composing the system. However, the C_i and CPE_i components of the circuit vary, resulting in a gradual increase of charge transfer impedance of the system upon cycling. These results follow the trends in the cell cyclability presented in **Fig. 3.11**, showing gradual decrease of the cell capacity. This allows for a suggestion, that the cell capacity decay for the carbon fiber current collector happens due to the gradual degradation of the charge transfer conditions in the system, and the further enhancement of the cathode could be achieved by the stabilization of the interfacial structure, probably, by the application of inert coatings or additives of high conductive components such as graphene, carbon nanotubes *etc*.

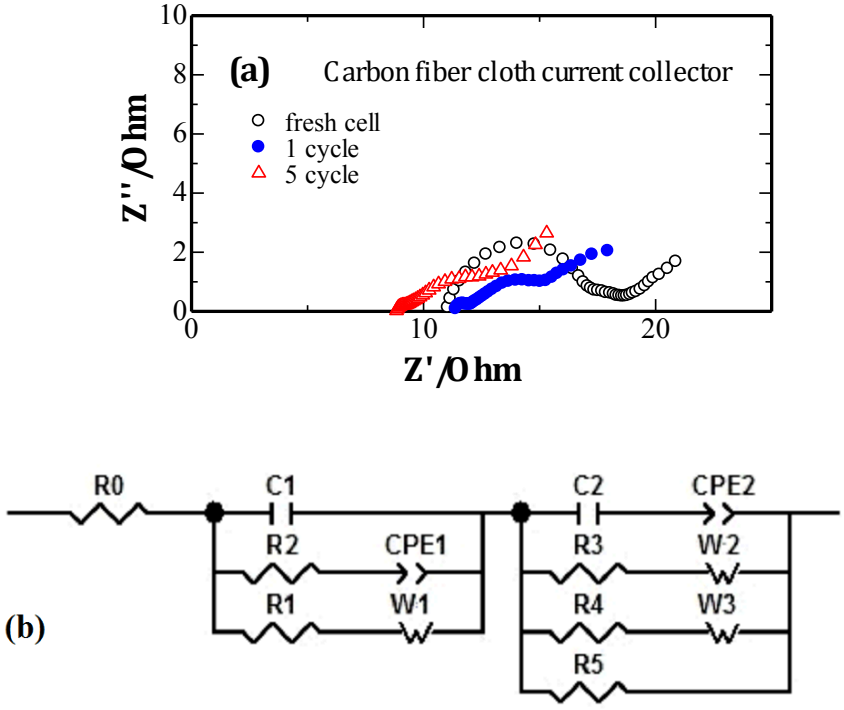

Fig 3.12 Nyquist plots of EIS of lithium cells with **(a)** carbon fiber and **(b)** equivalent circuit obtained from the experimental data analysis.

3.2.4 Summary

Two different types of 3D structures, Ni foam and carbon fiber cloth, were studied as current collectors for the S/PPy composite cathode in a lithium battery. By comparison with its Ni foam counterpart, the carbon fiber current collector remarkably improves the cycle performance of the S/PPy composite cathode. The advantages of carbon fiber over Ni foam were suggested to be due to its inherent chemical, structural and morphological uniqueness, which, along with its known high conductivity and chemical inertness, provides an enhanced affinity towards the sulfur composite cathode, suppress the agglomeration of the composite cathode particles, and, finally, enhances stable charge transfer conditions during the battery operation. Considering inexpensiveness of carbon fiber cloth (average market price USD15/m^2), the results of these studies allow us to conclude that carbon fiber is a very promising material for current collectors in high energy Li/S batteries.

3.3 One Pot Approach to Synthesize PPy@S Core-shell Nanocomposite Cathode for Li/S Batteries

3.3.1 Introduction

Among the many approaches explored, the use of conductive polymers surface coatings shows good potential in tackling the drawbacks of sulfur cathodes **[23,24,41]**. Conductive polymers can act both as an electronic conductivity enhancer and as a sulfur vault. Attempts using this strategy have yield core-shell type particles or agglomerates, usually of hundreds of microns in size, that show improved performance as cathodes for sulfur batteries [**41-43**]. Nevertheless, the multi-step synthetic procedures are complicated, time and energy consuming. Moreover, sulfur is evaporated and lost during the required heat treatment steps.

Hence, the development of simple techniques to prepare sulfur composites without heat treatment is of technological and economical interest. To the best of our knowledge, there are no reports on the synthesis of nanoscopic conductive polymer coated nano-sulfur particles without heat treatment and/or their use in Li/S battery.

Herein we describe a simple one pot method to synthesize a core-shell structured sulfur/polypyrrole (PPy@S) composite by *in situ* chemical oxidative polymerization of pyrrole on the surface of spherical nano-sulfur particles. The physical and electrochemical properties of the composite as a cathode material for lithium secondary batteries are also reported.

3.3.2 Experimental

Polypyrrole was synthesized from Py by chemical oxidative procedure, using $FeCl_3$ as oxidant. Polypyrrole coated sulfur (PPy@S composite) was obtained by *in situ* polymerization of pyrrole on the surface of nano-sulfur particles. 0.2 g pyrrole was added into 4 g aqueous suspension of nano-sulfur and stirred for 0.5 h. 15 mL of 0.5 M $FeCl_3$ aqueous solution was added dropwise with constant sonication at ambient temperature. After sonication for 2 h, the precipitate was filtered, thoroughly washed with deionized water and methanol, and then vacuum dried overnight at 70 °C.

FTIR spectra of PPy and PPy@S were obtained between 750 and 2000 cm^{-1} using a Bruker Vertex 80. The crystalline nature of the samples were analysed by XRD using a Bruker D8 Discover equipped with Cu Kα radiation. The composite surface morphology was examined by FESEM. The interior structure of PPy@S composite was observed using HRTEM equipped with Energy Dispersive Spectroscopy (EDS). The diameter distribution of

PPy@S composite, the calculation of the geometric mean diameter $d_{g,p}$ and the geometric standard deviation σ_g was calculated by random sampling of the nanoparticles from the SEM images. The sulfur content in the PPy@S composite was determined using chemical analysis (CHNS, Vario Micro Cube, Elementar).

The cell was composed of lithium metal anode and PPy@S cathode separated by a microporous polypropylene separator soaked in 1 mol L^{-1} solution of LiTFSI in TEGDME. The composite cathode was prepared by mixing 80 wt% PPy@S composite, 10 wt% PVdF as a binder and 10 wt% acetylene black conducting agent in NMP. The resultant slurry was cast onto an Al foil and dried in a vacuum oven for 12 h at 60 $^{\circ}$C, after which disk of 1 cm diameter was cut out to be used as cathode. Cathode with the composition PPy:AB:PVdF = 6:3:1 was also prepared in the same way as the PPy@S composite cathode and tested for comparison. The coin cells were assembled in a MBraun glovebox filled with high purity argon. CV was performed between 1 and 3 V *vs.* Li/Li^+ at a scanning rate of 0.1 mV s^{-1}.

3.3.3 Results and discussion

The FTIR spectrum of PPy (**Fig. 3.13**) displays the characteristic bands of the PPy: the pyrrole ring fundamental vibrations at 1545 cm^{-1} and 1458 cm^{-1}, the =C-H in-plane vibrations at 1291 cm^{-1} and 1043 cm^{-1}, and the C-N stretching vibration at 1175 cm^{-1}. This signifies that the PPy structure was successfully obtained *via* the chemical polymerization method. The aforementioned characteristic peaks of PPy are also observed in the PPy@S composites, albeit with reduced intensity due to the lower content of PPy.

The XRD patterns of as prepared PPy, elemental S and PPy@S composite samples are shown in **Fig. 3.14**. The broad feature at 26^{o} is characteristic of PPy and indicates a low

degree of crystalinity of this phase. In contrast, the XRD patterns of S exhibit the characteristics features of orthorhombic sulfur in the *Fddd* space group. These sharp peaks are also present in the PPy@S composite showed but with reduced intensity. This is most likely consequence of the well-dispersed character of nanoscopic sulfur in the core-shell structure, as evidenced by electron microscopy analysis.

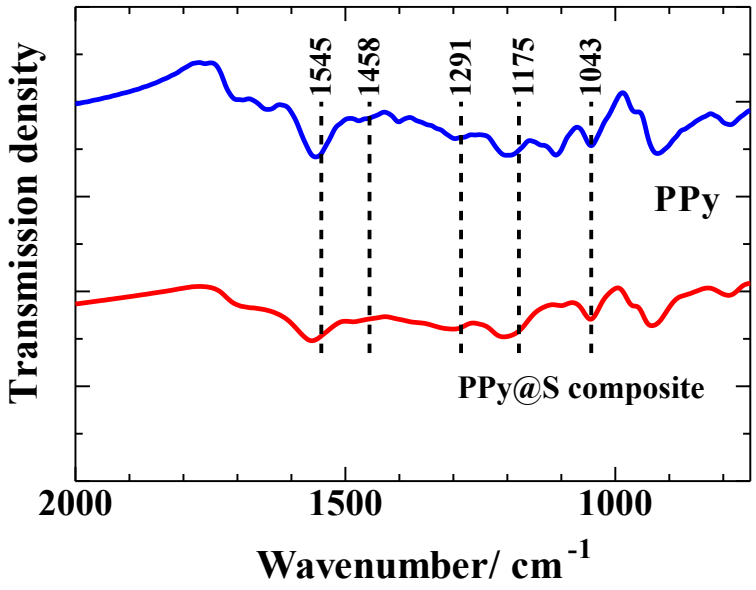

Fig 3.13 FTIR spectrums of PPy and PPy@S composite.

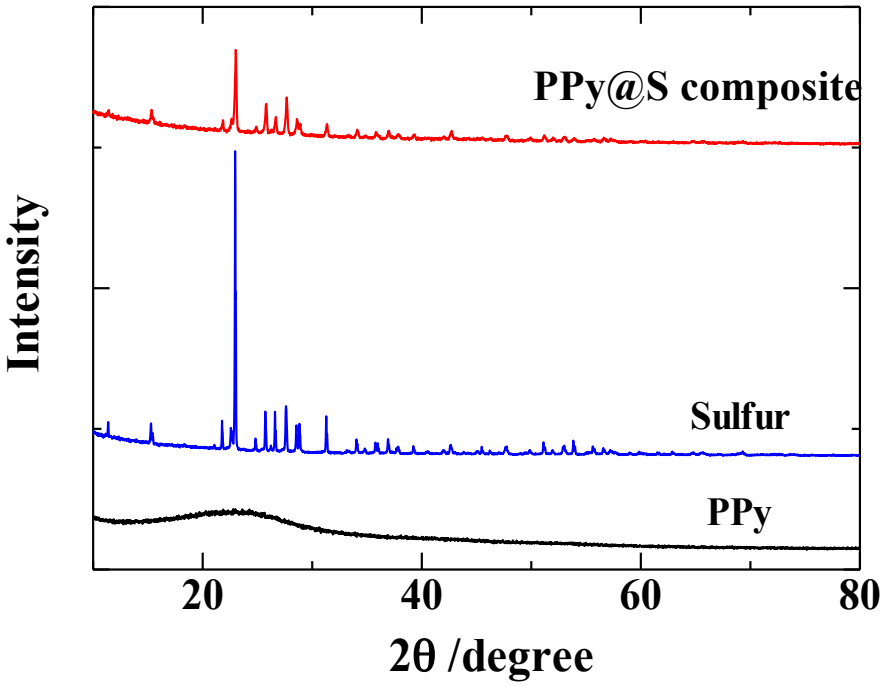

Fig 3.14 XRD patterns of Sulfur, PPy and PPy@S composite.

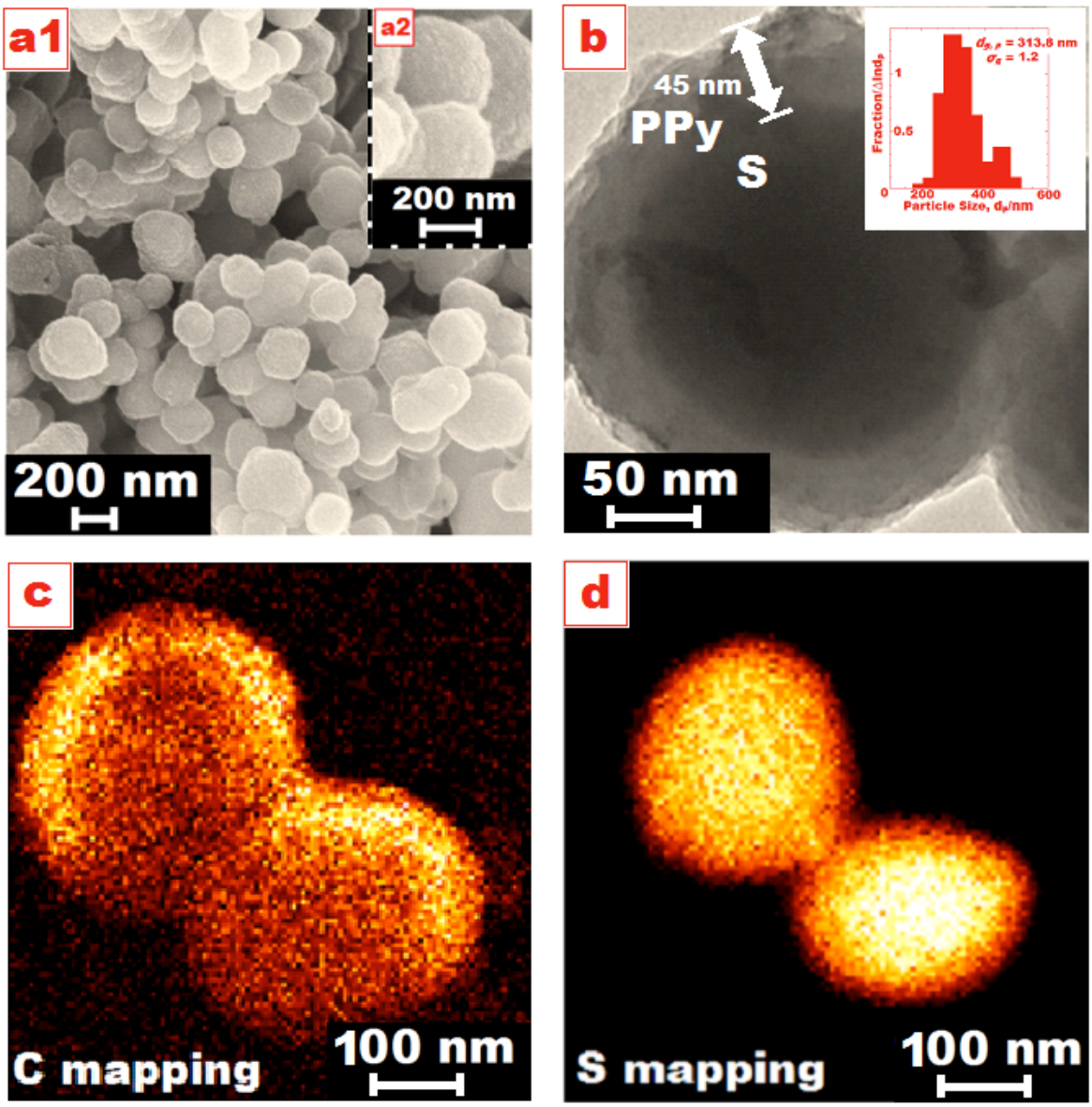

Fig 3.15 (a) SEM image of PPy@S composite at different magnifications; **(b)** HRTEM images of PPy@S composite and particle size distribution of PPy@S composite; **(c and d)** EDS mapping showing distribution of Carbon (C) and Sulfur (S) in composite of PPy@S.

The SEM image of the PPy@S composite is shown in **Fig. 3.15a**. Most particles are discrete, nearly spherical, and of uniform size, although a small amount of larger aggregates is also observed. And at higher magnification, the SEM images reveal that the PPy coating is rough as shown in the inset of **Fig. 3.15a(2)**. The HRTEM (**Fig. 3.15b**) clearly depicts sulfur particles coated with a PPy layer (also as indicated by the arrows): well-defined particles of PPy shells and dense sulfur cores are readily observed. The inset of **Figure 3.15b** presents the particle size distribution of PPy@S composite powders obtained from the SEM data. The particles have geometric mean diameter of $d_{g,p}$ = 313.8 nm and a geometric standard deviation of σ_g = 1.2. The well developed core-shell structure was also confirmed by the EDS mapping results shown in **Fig. 3.15c and 3.15d**. The core-shell structure of the PPy@S composite may effectively prevent sulfur dissolution into the electrolyte. In addition, the PPy matrix is thought to enhance the composite electrical conductivity, by reducing the particle-to-particle contact resistance, and to increase the contact area between the electrode and the electrolyte facilitating lithium diffusion.

The curves for the initial three CV cycles of Li/S cell with PPy@S composite cathode are shown in **Fig. 3.16**. Two major redox processes are observed and can be attributed to the transition of S to polysulfides (Li_2S_n, $n \geq 4$), and their further transformation to lithium sulfide Li_2S **[44]**. During the 1st cycle, the activation process associated with the penetration and transport of the electrolyte and lithium-ions through the PPy layer on the PPy@S composite lead to an anodic peak at slightly lower potential (2.3 V *vs.* Li/Li^+). The intensity and position of the main peaks remain nearly unchanged on subsequent cycles, suggesting good reversibility of the redox processes. The inset of **Figure 3.16** confirms that the PPy is not

electrochemically active in the selected voltage region.

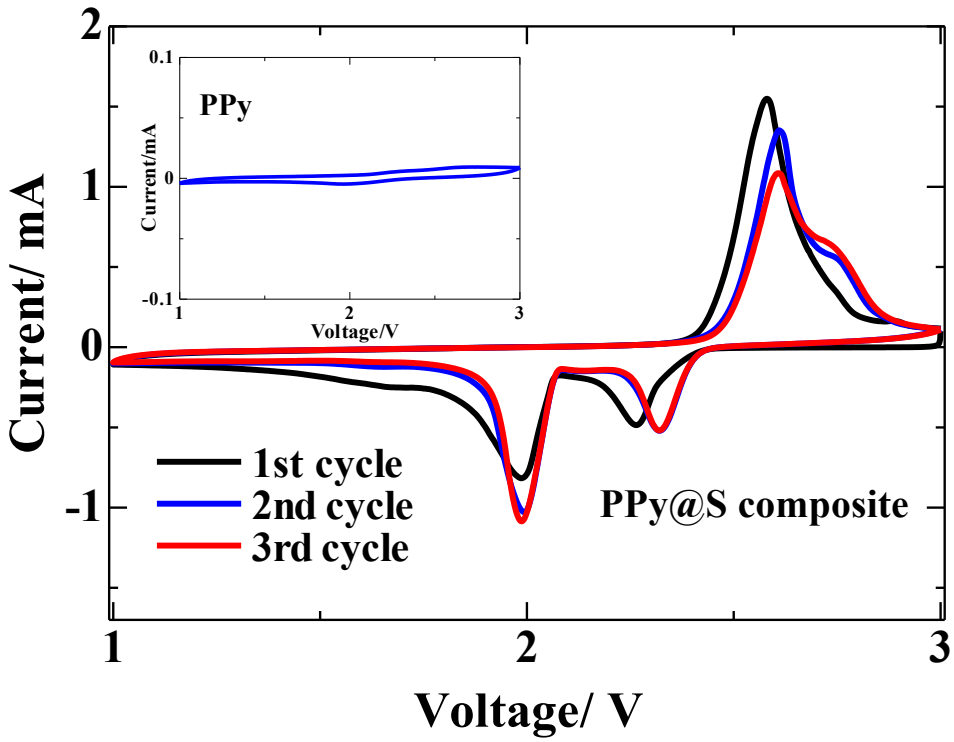

Fig 3.16 CV profiles of lithium cells with PPy and PPy@S composite cathodes (The potential sweep rate is 0.1 mV s^{-1}).

The electrochemical performance of the PPy@S composite in galvanostatic charge/discharge tests is shown in **Fig. 3.17**. The voltage profile for the 2nd cycle (see **Figure 3.17, inset**) shows two main discharge plateaus at 2.4 V and 2.0 V *vs.* Li/Li^+, in good agreement with the CV data. Up to 1309 mAh g^{-1} discharge capacity is attained by the PPy@S nanocomposite at 0.2 C on the 2nd cycle. Although some capacity loss was observed (913 mAh g^{-1} reversible capacity after 50 cycles), we observed improved cycling

performance in comparison to the PPy/S composite with branched structure previously reported **[25]**. This is likely due to the ability of the core-shell structure of the PPy@S composite to minimize losses of active material during cycling and enhance electronic conductivity of the cathode material. **Figure 3.17** shows a Coulombic efficiency in the range of 93.5 to 101.1%, suggesting that the PPy coating layer effectively blocks the severe shuttle reaction of the soluble lithium polysulfides **[45]**.

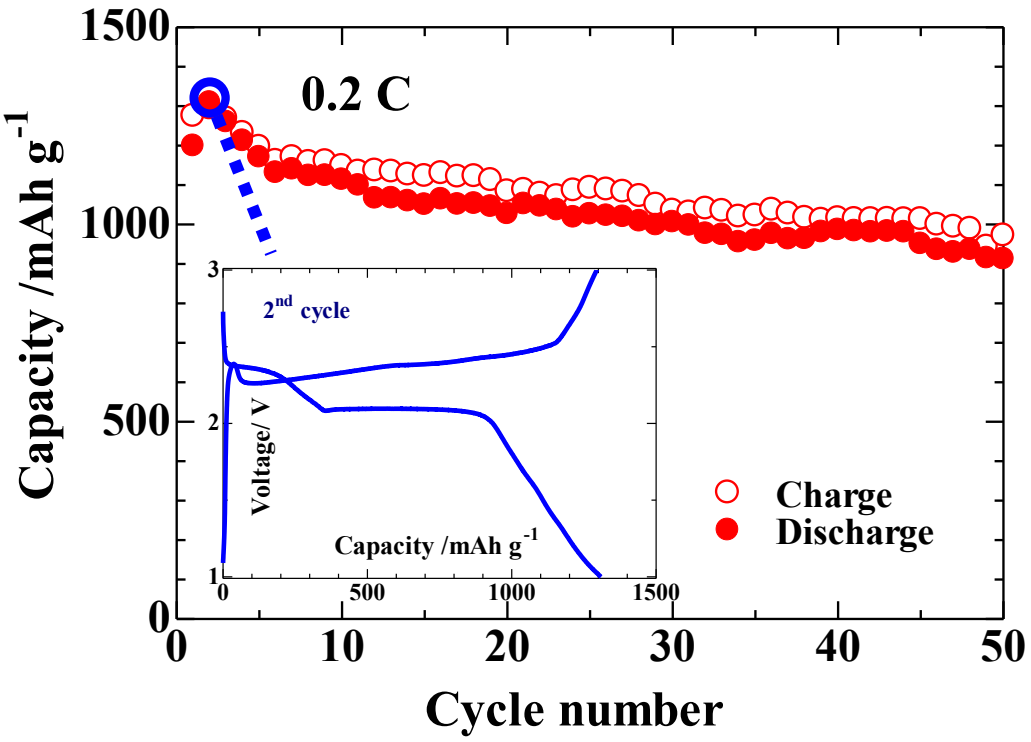

Fig 3.17 Cycle performance of lithium cells with PPy@S composite cathodes at 0.2 C and charge/discharge profiles at the 2nd cycle.

The rate capability results, as depicted in **Figure 3.18a,** reveal excellent performance for the PPy@S composite. After the two initial activation cycles at 0.2 C, the composite achieves a discharge capacity of 1023 mAh g^{-1} at 0.5 C. There is a gradual capacity reduction with the increasing current rate, although 437 mAh g^{-1} reversible capacity was sustained even at 2.5 C. More importantly, the composite regains most of its reversible capacity (773 mAh g^{-1}) when the discharge rate is modulated back to 0.5 C, showing the high abuse tolerance of the PPy@S. This superb rate performance can be attributed to the electronic conductivity enhancement by the introduction of conductive PPy layer coating on the nano-sulfur particles. The charge/discharge profiles for the PPy@S composite at various discharge rates, presented in **Figure 3.18b**, reveal that the polarization augments upon increasing current rate. Noteworthy, the capacity corresponding to the higher plateaus on the discharge curves does not decrease appreciably with the increasing current rate, whereas that corresponding to the formation of lower polysulfides and Li_2S is notably reduced **[46]**.

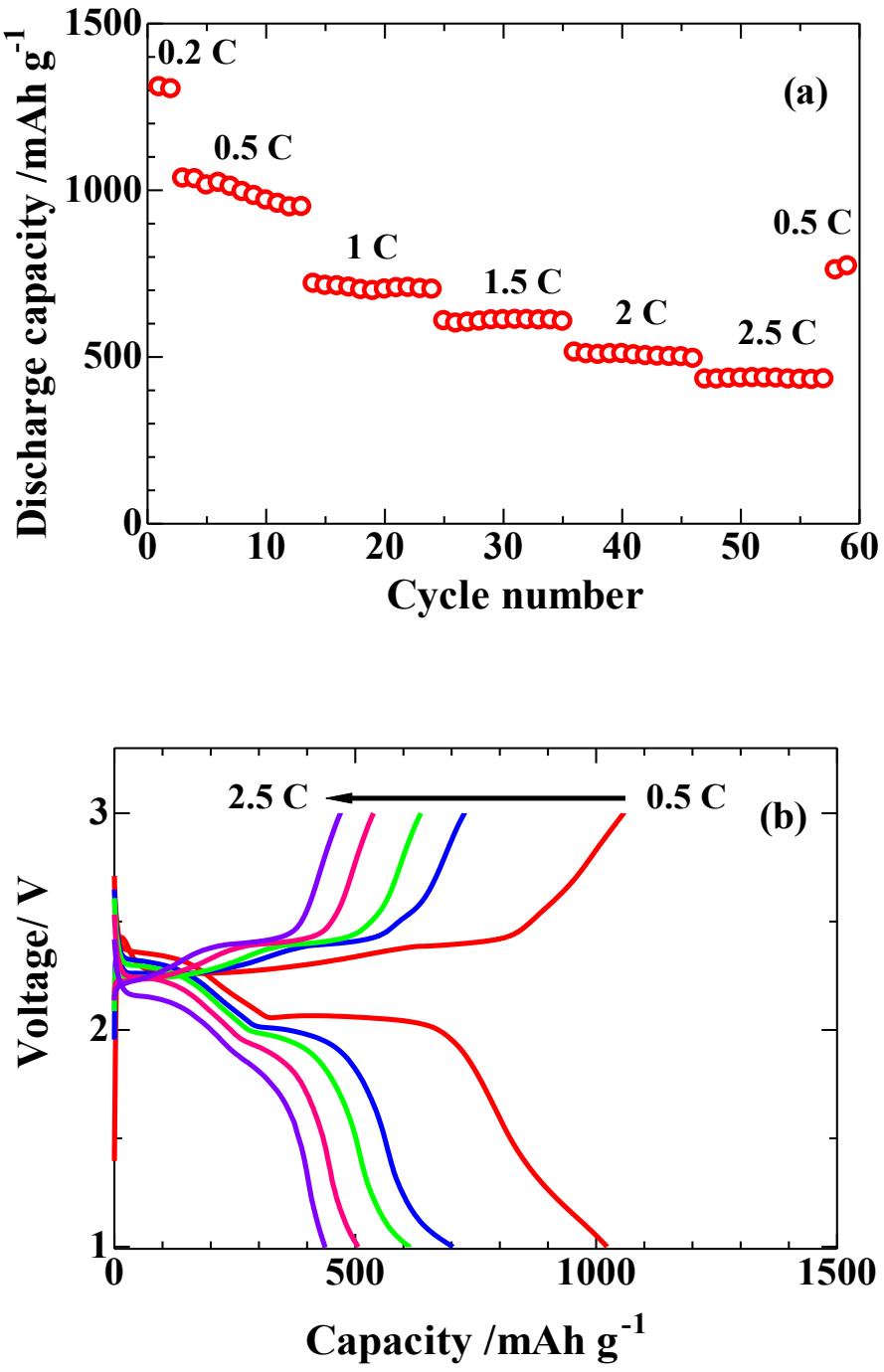

Fig 3.18 (a) Rate capability of lithium cells with PPy@S composite cathodes; **(b)** Charge/discharge profiles of lithium cells with PPy@S composite cathodes at various rates.

3.3.4 Summary

A polypyrrole coated sulfur composite was synthesized by the *in situ* polymerization of pyrrole on the surface of nano-sulfur particles. The composite showed good capacity and cycling stability in Li/S rechargeable batteries. The initial discharge capacity was 1200 mAh g^{-1} at 0.2 C, with 913 mAh g^{-1} remaining after 50 cycles, and 437 mAh g^{-1} at 2.5 C. The electrochemical performance of the composite show that the conductive PPy nanolayer coating provides both an effective electron conduction path and a strong physical and chemical confinement setting for elemental sulfur and resident polysulfides, minimizing the loss of active material during cycling.

Chapter 4 The Preparation of Sulfur/Polypyrrole/Conductive Carbon Ternary Composite for Li/S batteries

4.1 Novel Sulfur/Polypyrrole/Multi-walled Carbon Nanotubes Nanocomposite Cathode with Core-shell Tubular Structure for Li/S Batteries

4.1.1 Introduction

As is well known, polypyrrole (PPy) is one of the most important conductive polymers due to its relatively easy synthesis, electrical conductivity, and environmental stability **[1,2]**. Furthermore, PPy has a high absorption ability, which can help to hold back the dissolving of polysulfides in the electrolyte **[3-5]**. Introduction of multi-walled carbon nanotube (MWNT) to the conductive polymer is highly favorable, due to the effective improvement of the electrical and thermal properties, compared to pure PPy **[6]**. Among a variety of methods, *in situ* polymerization of pyrrole on the MWNT- is an effective method for obtaining a homogeneous dispersion of MWNT in the polymer matrix, and can form a strong chemical interaction between the -COOH groups of chemically modified MWNT and =NH groups of the PPy **[7]**. In this chapter, we study the preparation of a novel sulfur/polypyrrole/MWNT (S/PPy/MWNT) composite with a core-shell nano-tubular structure, and its physical and electrochemical properties as a cathode for lithium secondary batteries.

4.1.2 Experimental

The preparation route of the composite is represented schematically in **Fig. 4.1 and 4.2**. The MWNT was treated in a mixture of concentrated H_2SO_4/HNO_3 (3:1) at 70^oC for 1h in an ultrasonic homogenizer, followed by washing with deionized water until pH=7. Polypyrrole was synthesized from Py by a chemical oxidative procedure, using $FeCl_3$ as oxidant **[8]**.

Polypyrrole-coated MWNT (PPy/MWNT composite) was obtained by *in situ* polymerization of pyrrole on MWNT as described in Sahoo *et al*'s work **[7]**, with slight modifications in the preparation procedure. 0.1 g MWNT was first dispersed in 40 mL of a methanol: acetonitrile (1:1, v/v) mixture by sonication for 2 h using an ultrasonic homogenizer. 0.2 g pyrrole was added into this solution and stirred for 0.5 h. 15 mL of 0.5 M $FeCl_3$ aqueous solution was added dropwise with constant sonication at ambient temperature. After continuous sonication for 2 h, the precipitate was separated via filtration, thoroughly washed with deionized water and methanol, and then vacuum dried overnight at 70°C.

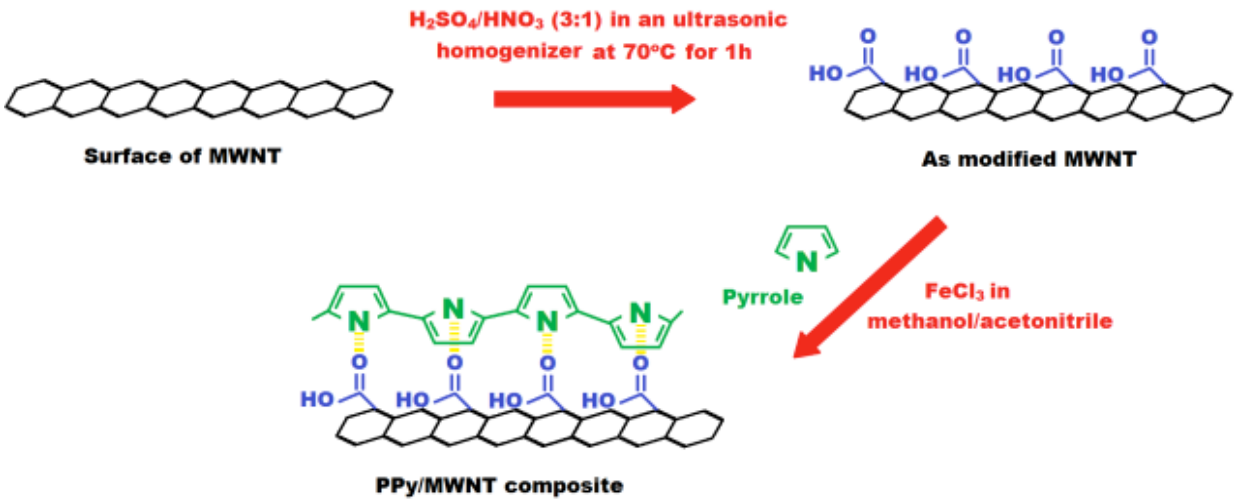

Fig 4.1 Schematic of a possible interaction of hydrogen bonding existed between for PPy chain and as-modified MWNT.

To make the S/PPy/MWNT composite, the as-prepared PPy/MWNT composite was added into 6 g aqueous suspension of nano-sulfur. The mixture was sonicated for 0.5 h, and

then dried in a vacuum oven at 65°C for 5 h. Finally, the mixture was heated to 150°C and kept for 3 h in Ar gas atmosphere to obtain the S/PPy/MWNT composite.

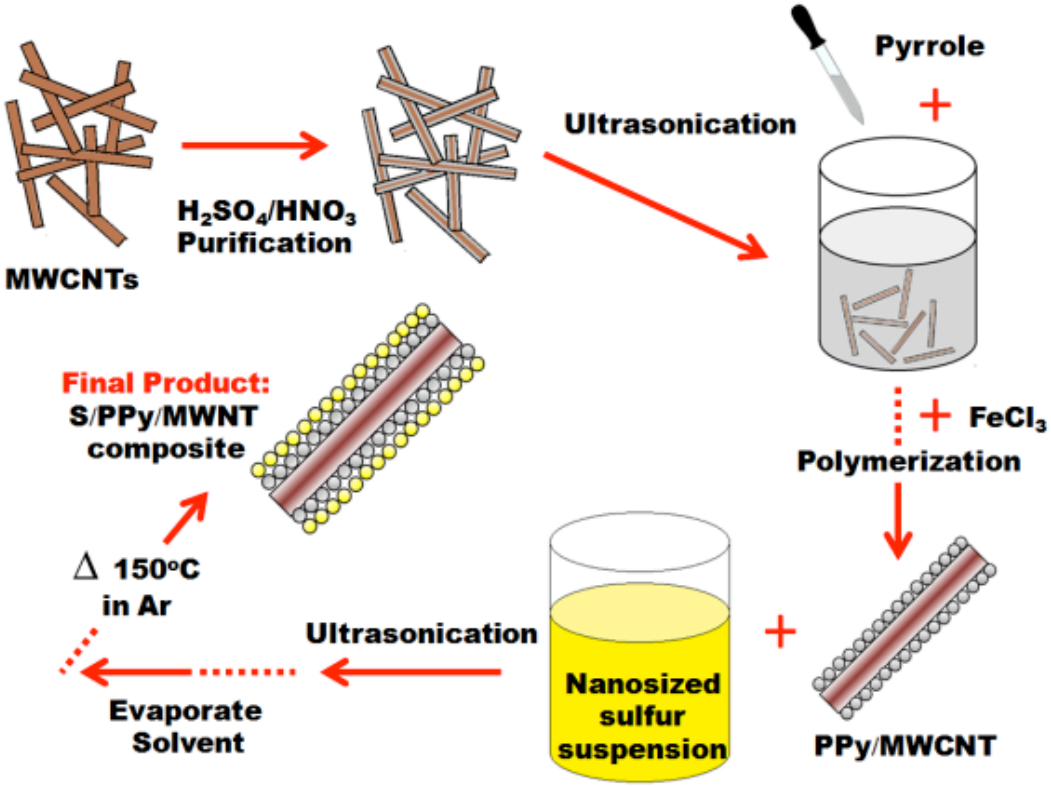

Fig 4.2 Schematic of the S/PPy/MWNT composite preparation.

PPy, PPy/MWNT and S/PPy/MWNT composites were characterized by FTIR. The crystalline phases of the sample were determined by XRD using Cu Kα radiation. The interior structure of the MWNT, PPy/MWNT and S/PPy/MWNT composites was observed using TEM at 60 kV and HRTEM equipped with EDS. The Sulfur content in S/PPy/MWNT composite was determined as 52.6 wt% using an elemental analyzer.

The cell was composed of lithium metal anode and S/PPy/MWNT cathode separated by a microporous polypropylene separator soaked in 1 M solution of LiTFSI in TEGDME electrolyte. The composite cathode was prepared by mixing 80 wt% S/PPy/MWNT composite, 10 wt% PVdF as a binder and 10 wt% acetylene black conducting agent in NMP. The resultant slurry was painted onto a circular piece of nickel foam with 1 cm in diameter. After drying in a vacuum oven for 12 h at 60^{o}C, the cathode was pressed at 8 MPa in order to achieve good contact between the active material and nickel foam. The sulfur loading in each electrode was about 4 mg cm^{-2}. The coin cells were assembled in an Ar filled glove box and tested galvanostatically between 1 and 3 V vs. Li^{+}/Li electrode at different current densities.

4.1.3 Results and discussion

The FTIR spectra of PPy, PPy/MWNT and S/PPy/MWNT composites are shown in **Fig. 4.3a**. The characteristic bands of the PPy are consistent with the literature values [**9,10**]. The pyrrole ring fundamental vibration, the =C-H in-plane vibration, and the C-N stretching vibration occur at 1545 cm^{-1}, 1043 cm^{-1}, and 1175 cm^{-1}, respectively. Therefore, we conclude that the PPy structure was successfully obtained via the chemical polymerization method. All the above-mentioned characteristic peaks of PPy are also observed in PPy/MWNT and S/PPy/MWNT composites, with a reduction of intensity due to the lower content of PPy in comparison to the pure PPy.

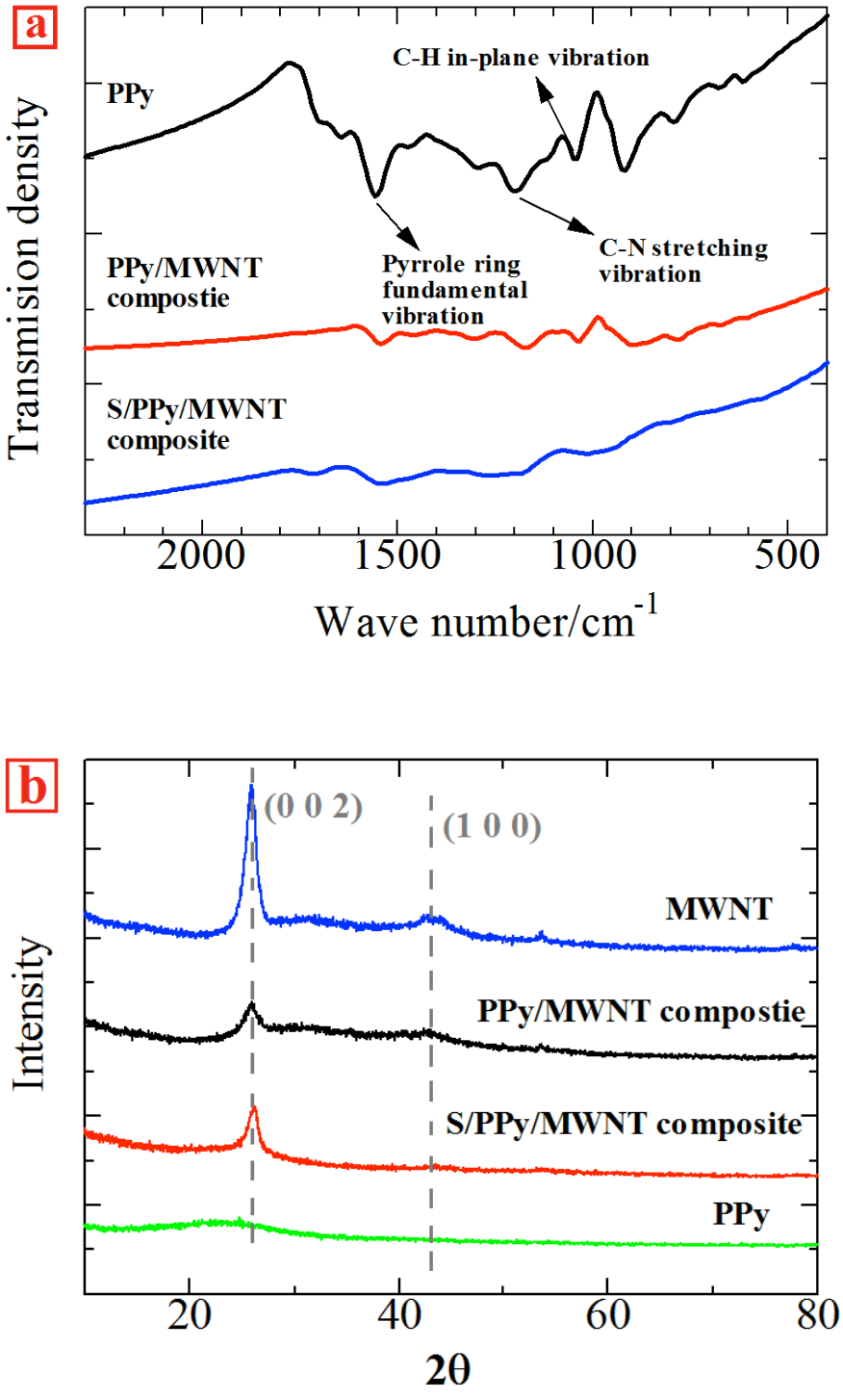

Fig 4.3 (a) FTIR spectrum of PPy, PPy/MWNT and S/PPy/MWNT composite; **(b)** XRD pattern of as-modified MWNTs, PPy, PPy/MWNT and S/PPy/MWNT composite samples.

The XRD patterns of as-modified MWNT, PPy, PPy/MWNT and S/PPy/MWNT composite samples are shown in **Fig. 4.3b**. PPy appears in amorphous phase with a broad feature of at around 26^{o} **[11]**. The modified MWNT displays a strong diffraction at 25.8^{o} and a weak one at 42.7^{o}, corresponding to the (0 0 2) and (1 0 0) planes **[12,13]**. The characteristic features of both PPy and MWNT are presented in the XRD pattern of PPy/MWNT composite, and the S/PPy/MWNT composite also displays the lines for peaks of PPy and MWNT, although with reduced peak intensity, but lines for sulfur could not be observed. This indicates the absence of crystalline sulfur phases, more likely due to nanosized sulfur well-dispersed in the core-shell structure as below discussed.

Figure 4.4 shows the morphological characterization and the tube diameter distribution obtained from the TEM data. **Figure 4.4a** and **4.4b** clearly show that the surface of carbon nanotubes was uniformly coated with a tubular layer of PPy film. During the polymerization, the pyrrole monomer is oxidized by $FeCl_3$, generating a layer of PPy on the surface of the carbon nanotubes. The average diameter of nanotubes increases from 26.7 nm to 61.7 nm upon polymerization. In **Fig. 4.4c**, one can see that S/PPy/MWNT composite has a typical core-shell structure, and the diameter of the S/PPy/MWNT composite (*dp* = 81.0 nm) becomes larger than that of the PPy/MWNT composite (*dp* = 61.7nm).

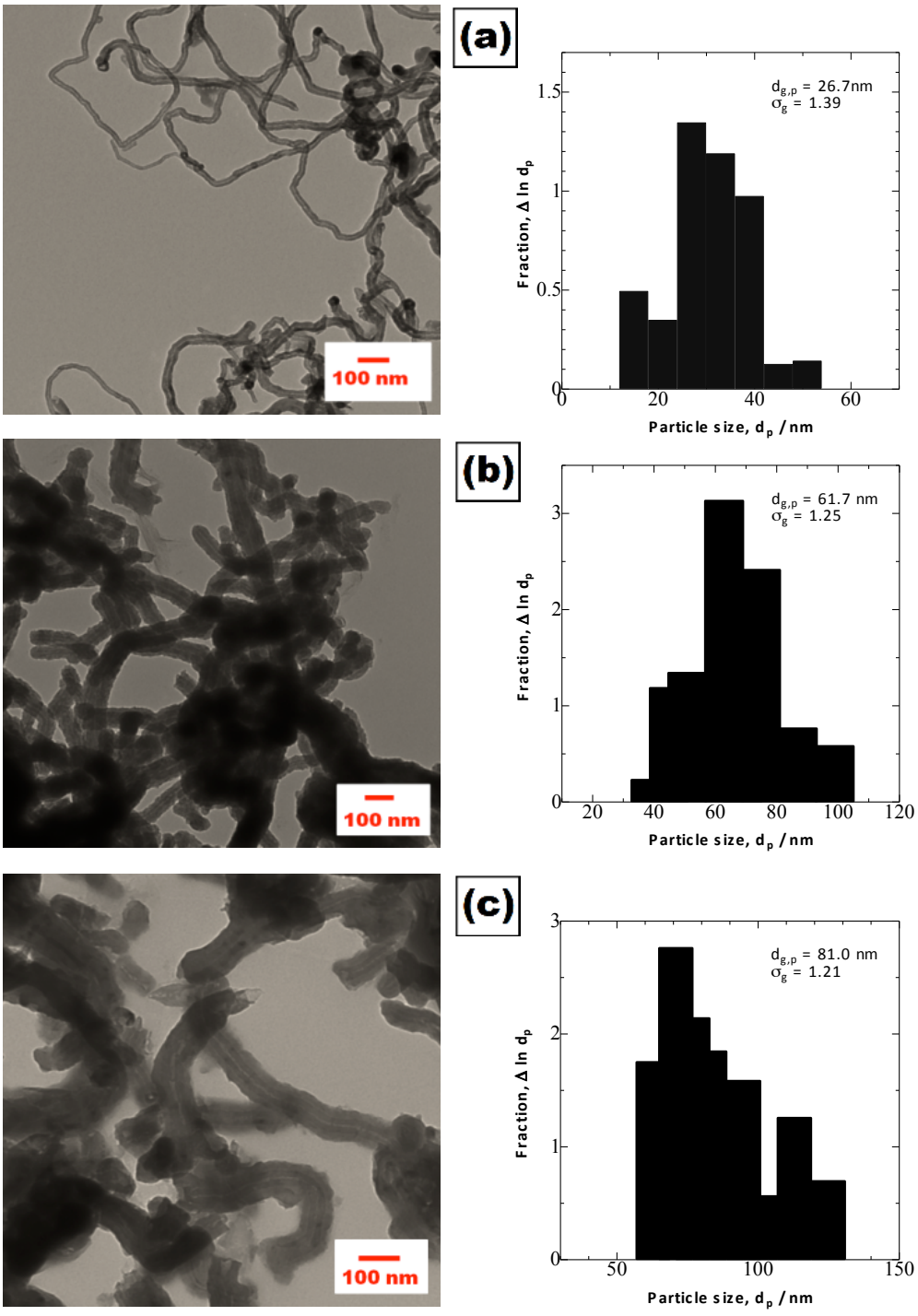

Fig 4.4 TEM images and the diameter distributions of **(a)** as-modified MWNT, **(b)** PPy/MWNT and **(c)** S/PPy/MWNT composite samples.

We postulate that the nanosized sulfur is melted and absorbed on the surface of PPy/MWNT nanotubes during heat treatment, leading a larger diameter of the composite nanotubes. This is in good agreement with the TEM-EDS mapping results depicted in **Fig. 4.5**, which show that sulfur homogeneously coats the PPy/MWNT nanotubes and PPy is sandwiched between MWNT and sulfur. In this core-shell structure, PPy acts as an effective binder connecting sulfur and MWNT. PPy also serves as a sponge to absorb polysulfides into its porous structure, improving the cyclability of the cells. Furthermore, as a core in this composite, the MWNT can provide a high electronic conductivity and mechanically flexible framework, enhancing the rate capability of the cathode material.

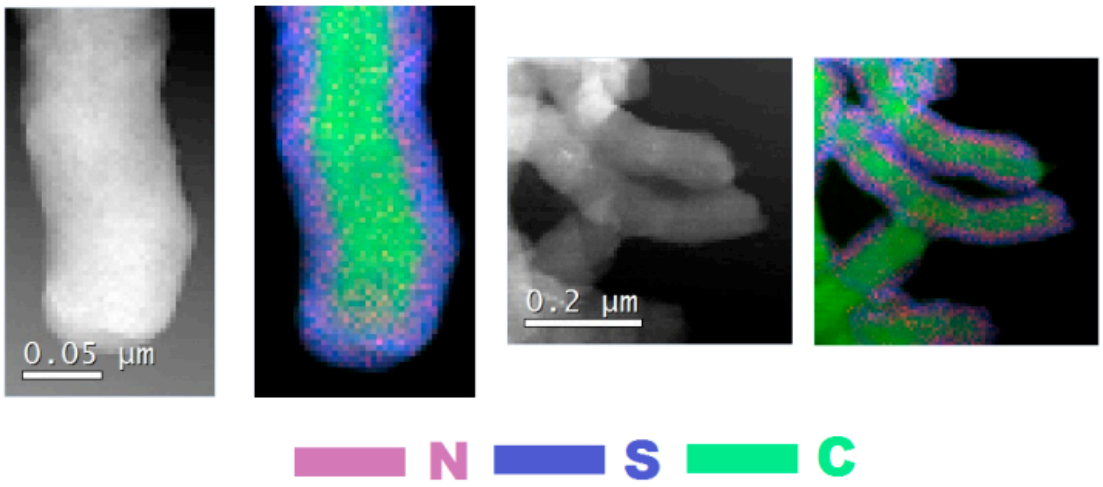

Fig 4.5 HRTEM images of the S/PPy/MWNT composite sample with carbon, sulfur and nitrogen elemental mapping.

The galvanostatic charge-discharge profile of the S/PPy/MWNT composite is shown in **Fig. 4.6a**. The discharge curves show two plateaus, which can be attributed to two main electrochemical processes that take place in the composite cathode. The first short plateau at about 2.4 V is related to the formation of high order lithium polysulfides (Li_2S_n, $n \geq 4$), which are soluble in the liquid electrolyte **[13-15]**. The following prolonged plateau around 2.0 V reflects the electrochemical transition of the polysulfides to lithium sulfide Li_2S. The kinetics of this reaction is slower than that of the polysulfide formation **[14-17]**.

Even though no remarkable difference in the 2 V discharge plateaus is observed between the first and third cycles, the higher voltage plateau diminishes and almost disappears after a few cycles. This is probably due to the activation energy needed in the cycling upon achieving a steady state of polysulfide formation. It can be seen here that a discharge capacity of 1245.2 mAh g^{-1} was obtained at the third cycle, the 2.4 V plateau is short, and the system's discharge capacity mainly depends on the 2 V plateau.

The S/PPy/MWNT composite cathode shows an outstanding cyclability as shown in **Fig. 4.6b**. The discharge capacity of the S/PPy/MWNT composite was stabilized after 2 cycles at 1278.1 mAh g^{-1} and a discharge capacity of 960.7 mAh g^{-1} was retained after 40 cycles. The reversibility indicates that MWNT core can provide an effective electron conduction path and their network-like structure forms a stable structure for the S electrode. On the other hand, PPy has a strong adhesion to the surface of MWNT and absorb polysulfides into its porous structure thwarting of the shuttle effect **[3-5, 8]**.

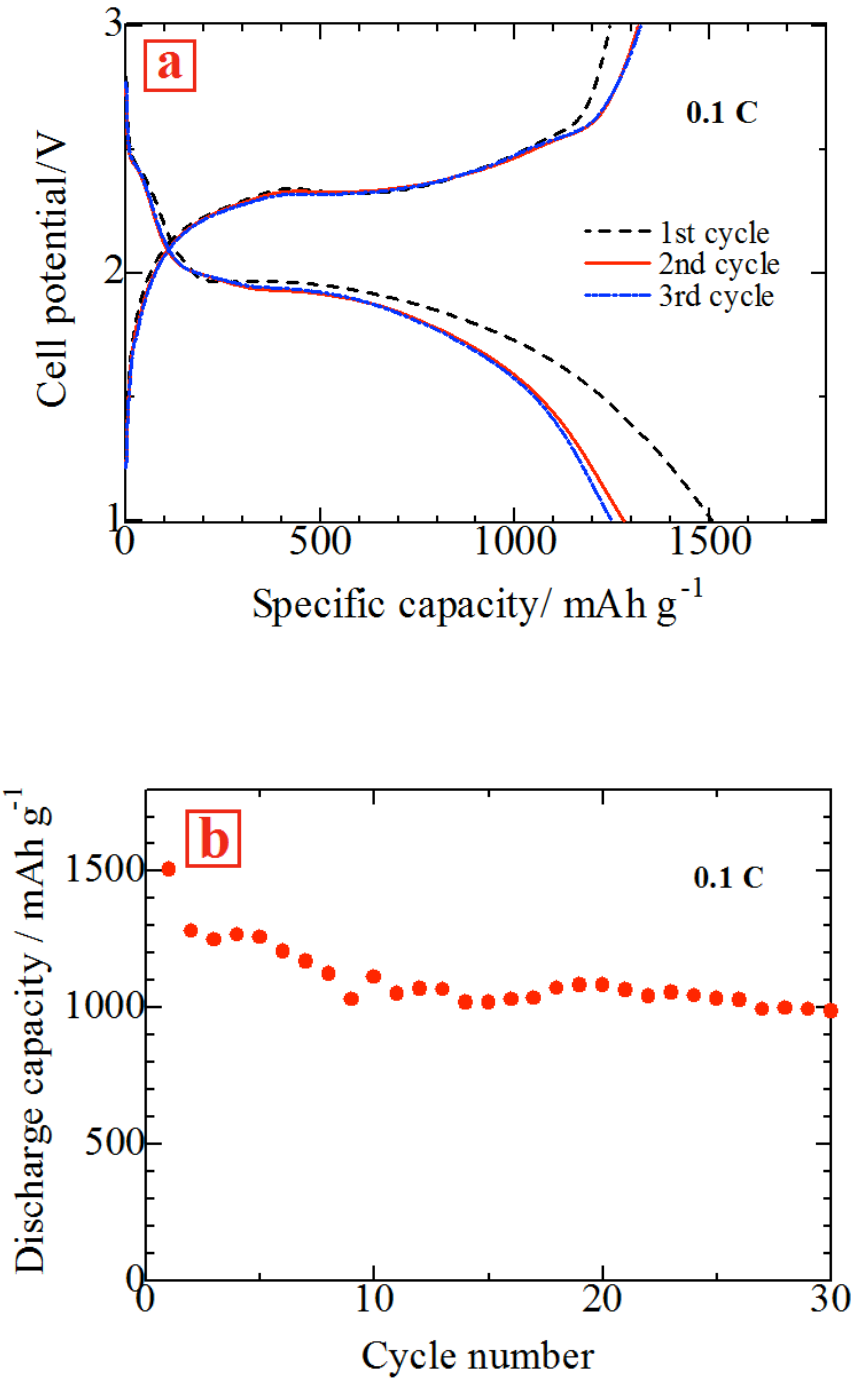

Fig 4.6 (**a**) Charge/discharge profiles of Li/S cell with S/PPy/MWNT composite cathode at 0.1C; (**b**) Cycle performances of lithium cell with S/PPy/MWNT composite cathode at 0.1C.

To further investigate the rate performance of the S/PPy/MWNT composite, a rate capability study was carried out at various rates as shown in **Fig. 4.7**. With the increase in the current rate from 0.25 C to 0.5 C, the discharge capacity dropped from about 971.7 mAh g^{-1} to 492.4 mAh g^{-1}. Notwithstanding, the discharge capacity is mostly recovered when the rate is decreased from 0.5 C to 0.2 C, owing to the good electrical conductivity of MWNT core as conductive matrices in the sulfur electrode.

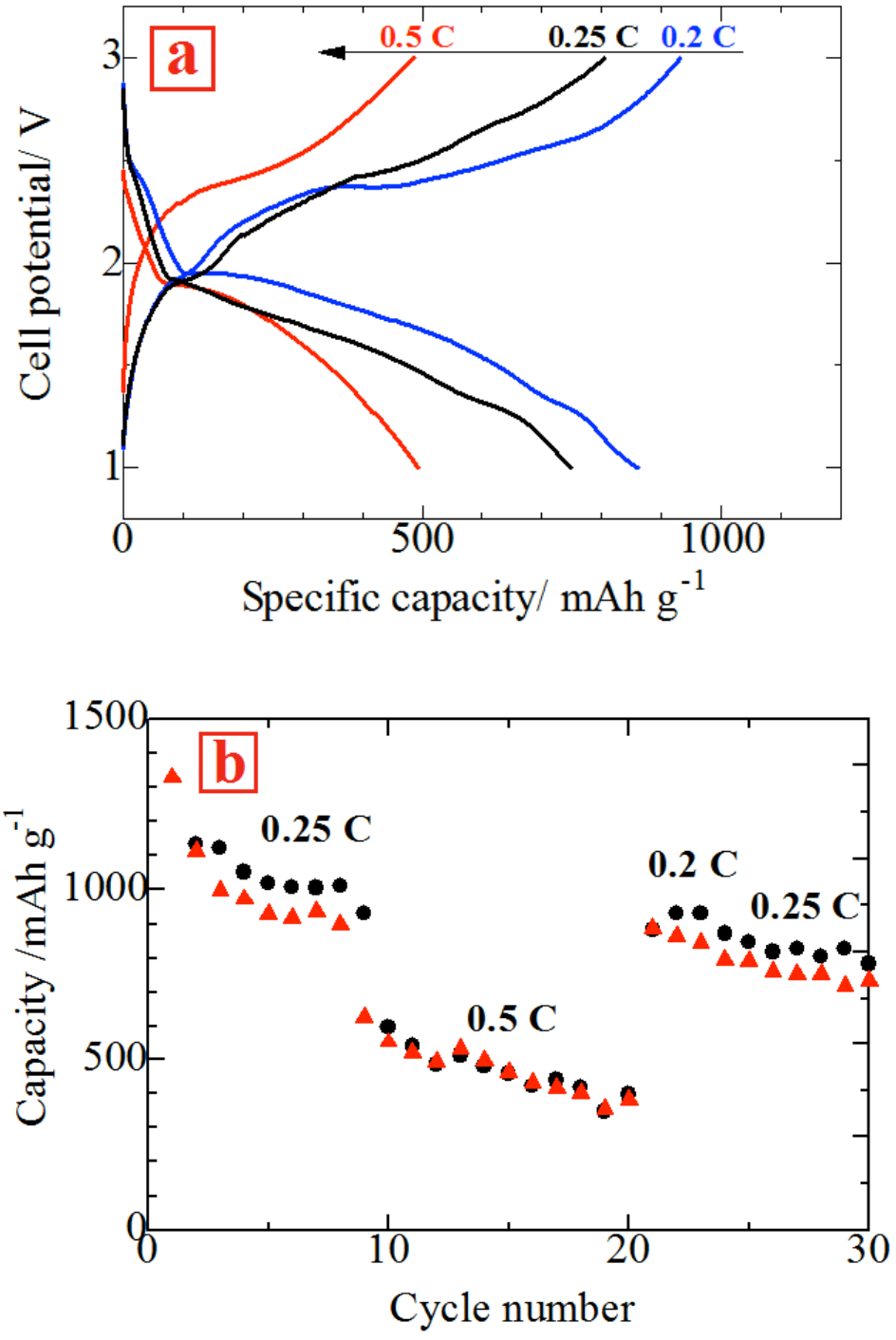

Fig 4.7 **(a)** Charge/discharge profiles of the S/PPy/MWNT composite at various rates. **(b)** Rate capability of the S/PPy/MWNT composite.

4.1.4 Summary

A method for fabricating a ternary S/PPy/MWNT composite cathode has been developed. The method, based on previous work to synthesize PPy/MWNT composite by *in situ* chemical polymerization of pyrrole on the carbon nanotubes, employs nanosized sulfur particle suspension to produce a novel cathode material with a core-shell, nano-tubular structure. The electrochemical results show that MWNT can provide an effective electron conduction path and their network-like structure forms a stable matrix for the S electrode. On the other hand, PPy has a strong adhesion to the surface of MWNT and absorb polysulfides into its porous structure. This novel core-shell tubular structure accommodates the mechanical stresses induced by the volume changes upon charge-discharge of Li/S battery and hinders the polysulfides dissolution. Consequently, the S/PPy/MWNT composite cathode exhibits good cycle and rate performances for rechargeable lithium/sulfur batteries.

4.2 A Novel Nano-sulfur/Polypyrrole/Graphene Nanocomposite Cathode with a Dual-layered Structure for Li/S Batteries

4.2.1 Introduction

Since the discovery of graphene in 2004, much attention has been drawn to its large surface area, superior electronic conductivity, and high mechanical flexibility **[18-20]**. Polypyrrole/graphene nanosheet (PPy/GNS) composite has been synthesized and used as electrochemical sensors and supercapacitors **[21-28]**. To the best of our knowledge, this composite has not been used in a battery electrode. In this report, we demonstrate the introduction of PPy/GNS to sulfur cathode in a Li/S battery.

In this part, we describe the preparation of a novel sulfur/polypyrrole/graphene (S/PPy/GNS) nanocomposite and assess its physical and electrochemical properties as a cathode for lithium secondary batteries.

4.2.2 Experimental

Polypyrrole was synthesized from pyrrole monomer by chemical oxidative procedure, using $FeCl_3$ as an oxidant. Polypyrrole-coated graphene (PPy/GNS) was synthesized by *in situ* polymerization of pyrrole in the presence of graphene **[23-26]**.

0.1 g graphene nanosheet was first dispersed in a 40 mL mixture of methanol and acetonitrile (1:1 vol) by sonication at room temperature for 2 h. After addition of 0.2 g of pyrrole this solution was stirred for 0.5 h. Afterwards, 15 mL of 0.5 mol L^{-1} $FeCl_3$ aqueous solution was added dropwise to the above solution with constant sonication at ambient temperature. The mixture was sonicated again for 2 h. The final precipitate of PPy/GNS was separated via filtration, thoroughly washed with deionized water and methanol, and then vacuum dried overnight at 70 °C.

To make S/PPy/GNS composite, as-prepared PPy/GNS was added into a 6 g nano-sulfur suspension. The mixture was dispersed homogeneously for 0.5 h using an ultrasonic homogenizer, and then dried in a vacuum oven at 65 °C for 6 h to remove the solvents. Finally, the mixture was heated to 150 °C and kept for 3 h in Ar gas atmosphere to obtain the S/PPy/GNS composite, in which the sulfur content, determined using chemical analysis, was 52 %.

PPy, PPy/GNS and S/PPy/GNS composites were characterized by FTIR. The surface morphology of PPy/GNS and S/PPy/GNS composite were examined by FESEM. The interior

structures of GNS, PPy/GNS and S/PPy/GNS composite were observed using TEM at 60 kV and HRTEM equipped with EDS.

The cell was composed of lithium metal anode and S/PPy/GNS cathode separated by a microporous polypropylene separator soaked in 1 mol L^{-1} solution of LiTFSI in TEGDME electrolyte. The composite cathode was prepared by mixing 80 wt% S/PPy/GNS, 10 wt% PVdF as a binder and 10 wt% acetylene black conducting agent in NMP. The resultant slurry was coated onto Al foils and dried at 60 ^{o}C under vacuum overnight. The coin cells were assembled in a glovebox filled with argon. The cells were tested galvanostatically between 1 and 3 V vs. Li^{+}/Li electrode at different current densities. CV was performed with a potentiostat between 1 and 3 V vs. Li^{+}/Li at a scanning rate of 0.5 mV s^{-1}.

4.2.3 Results and Discussion

Figure 4.8 shows the FTIR spectra of PPy, PPy/GNS and S/PPy/GNS. The pyrrole ring fundamental vibration, C-N stretching vibration, and =C-H in-plane vibration occur at 1545 cm^{-1}, 1175 cm^{-1}, and 1043 cm^{-1}, respectively. These data are consistent with the literature **[29,30]** and indicates that the PPy structure was successfully obtained *via* the polymerization method. The characteristic bands of PPy are also observed in the PPy/GNS and S/PPy/GNS composites, although a reduction of intensity of is observed with the decrease of PPy content.

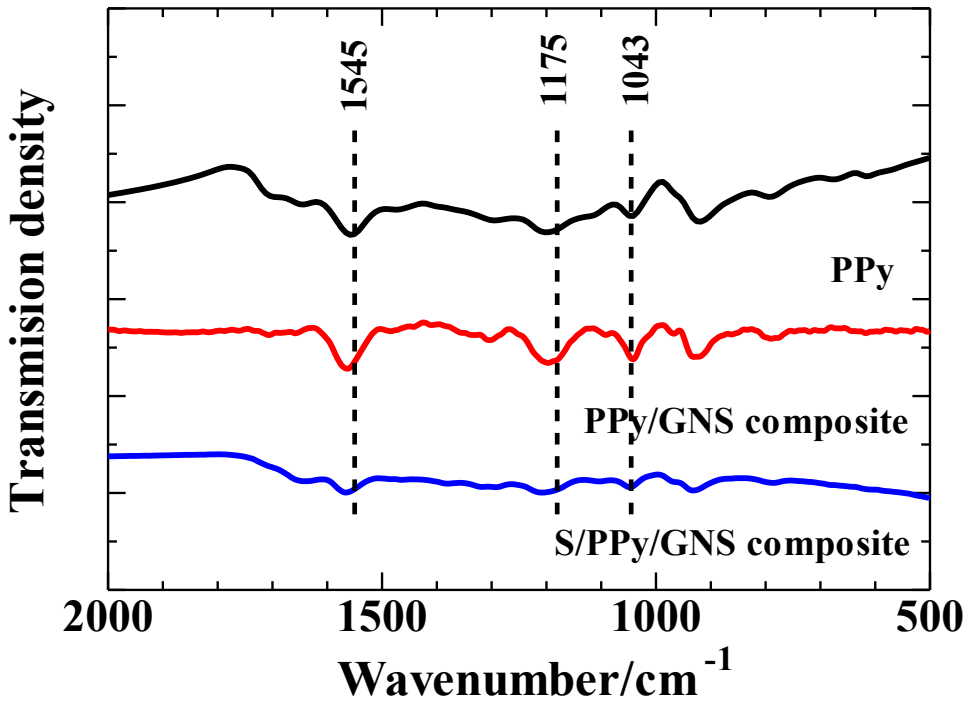

Fig 4.8 FTIR spectrums of PPy, PPy/GNS and S/PPy/GNS composite samples.

The surface morphology of the as-synthesized PPy/GNS and S/PPy/GNS composites are depicted in SEM micrographs (**Fig. 4.9a and 4.9b**). PPy is formed and fixed to the surface of GNS after polymerization as shown in **Fig. 4.9a**. Pyrrole monomers are adsorbed onto the larger surface of GNS *via* π-π interactions, hydrogen bonds and Van der Waals **[22]** serving as anchor points to the forming polymer. As for the S/PPy/GNS composite (**Fig. 4.9b**), it forms irregular stacks of interlaced nanosheet-like leading to a rough surface, densely covered with sulfur particles. This probably stems from the high absorption ability of PPy to sulfur **[5,31]**. The EDS mapping (**Fig. 4.9c**) shows the distribution of sulfur in the S/PPy/GNS composite, confirming the highly homogeneous dispersion of nanoscopic sulfur on the surface of the parent PPy/GNS composite. **Fig. 4.9(d-f)** shows HRTEM images of as

prepared PPy/GNS composite. At a high magnification (**Fig. 4.9e**), no obvious lattice fringes can be observed confirming the amorphous character of the PPy portion, in agreement with the literature data **[29,30]**. The EDS carbon and nitrogen mapping of PPy/GNS (**Fig. 4.9f**) show GNS homogeneously coated by PPy layer.

\

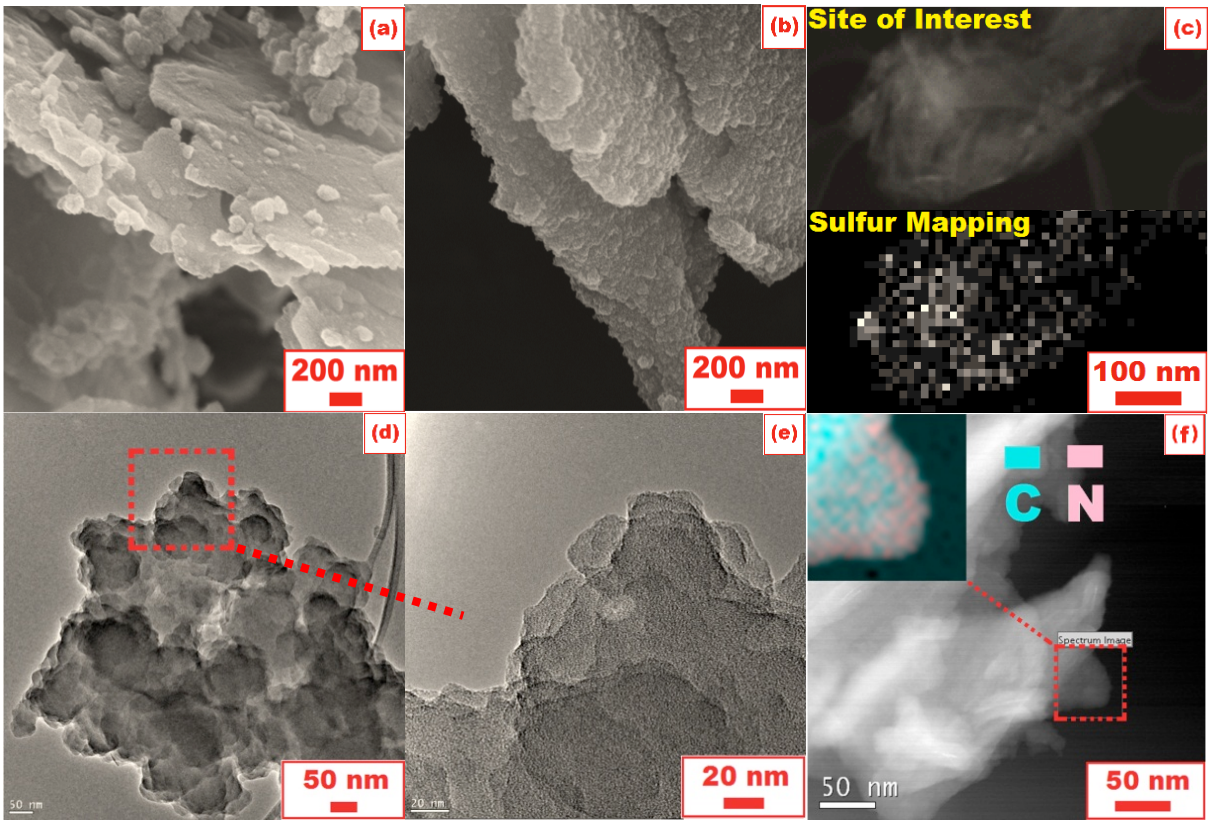

Fig 4.9 (a and b) SEM image of PPy/GNS and S/PPy/GNS composite samples; **(c)** EDS mapping showing distribution of Sulfur (S) in composite of S/PPy/GNS; **(d, e and f)** HRTEM images of PPy/GNS samples at different magnifications and EDS mapping showing distribution of carbon (C) and nitrogen (N).

Based on these observations, a possible mechanism for the composite formation is proposed as shown in **Fig. 4.10**. According to this mechanism, pyrrole is polymerized on the

surface of the graphene nanosheets and the formed polypyrrole, which is known to have strong affinity towards sulfur, serves as an anchor point for the sulfur nanoparticles during the subsequent step. The result is a dual-layered composite with architecture hierarchical to the graphene nanosheet structure.

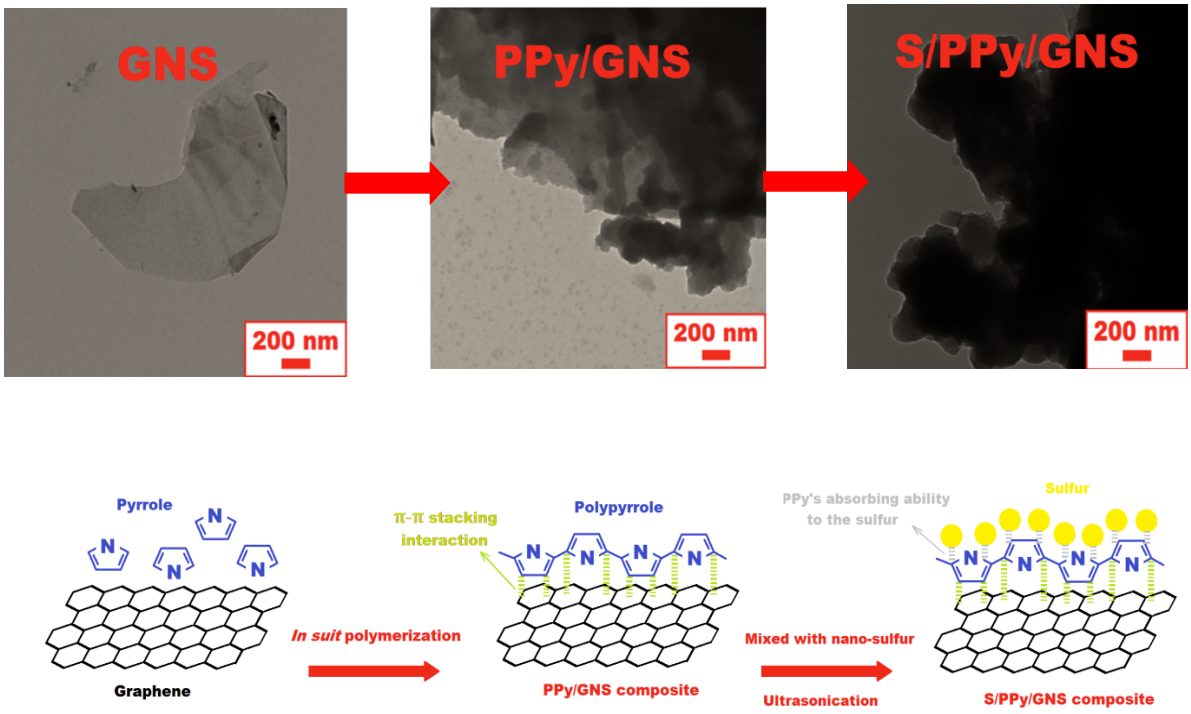

Fig 4.10 Schematic of the S/PPy/GNS composite formation.

Figure 4.11 shows the cyclic voltammetry (CV) of the cell containing S/PPy/GNS composite cathode at initial two cycles. During the first cycle, three cathodic peaks and two anodic peaks are observed. The cathodic peak at 2.4 V can be assigned to the reduction of sulfur to polysulfides (Li_2S_n, $2<n\leq8$) while the strong cathodic peak at 2.0 V is associated

with the reduction of soluble polysulfides into Li_2S_2/Li_2S. The appearance of a small peak at around 1.7 V can be attributed overcome the strong absorbing energy between the sulfur and the conductive matrix. During the second cycle, the peak corresponding to the oxidation of polysulfides to S_8 becomes stronger and shifts to higher potential, indicating improvement of the reaction kinetics.

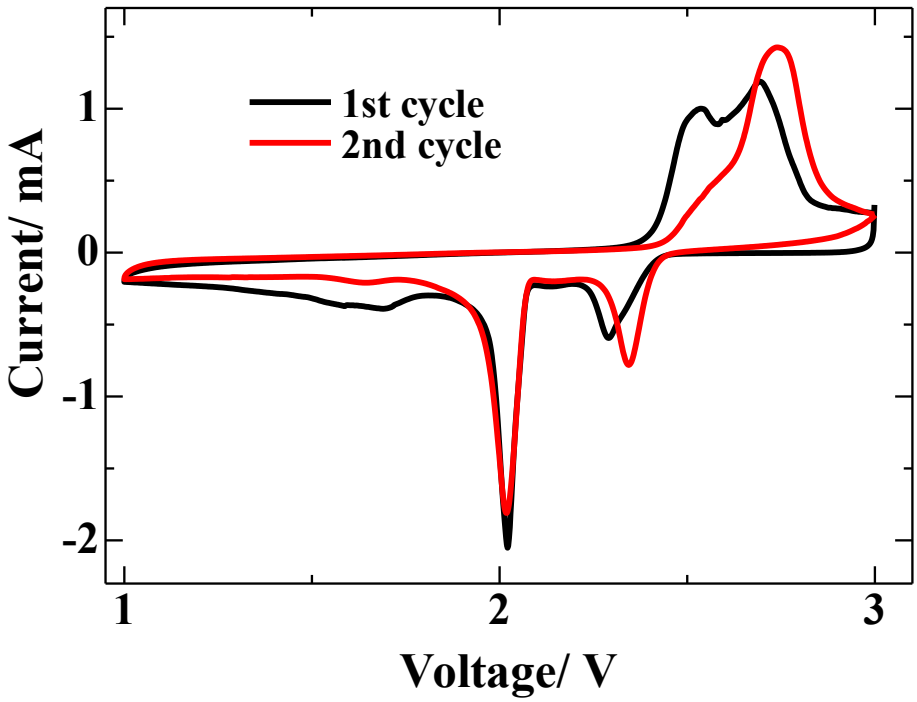

Fig 4.11 Initial CV profiles of S/PPy/GNS composite, used as a cathode active material in the lithium half-cell. The measurement is conducted at a scan rate of 0.5 mV s^{-1} in the voltage range of 1.0 to 3.0 V vs. Li/Li^+.

The electrochemical performance of the S/PPy/GNS composite as cathode materials in Li/S batteries was investigated by galvanostatic discharge-charge tests and the results are shown in **Fig. 4.12**. The discharge curves show two plateaus that can be assigned to the two

step reaction of sulfur with lithium. This result is in good agreement with the CV data as well as with literature values.

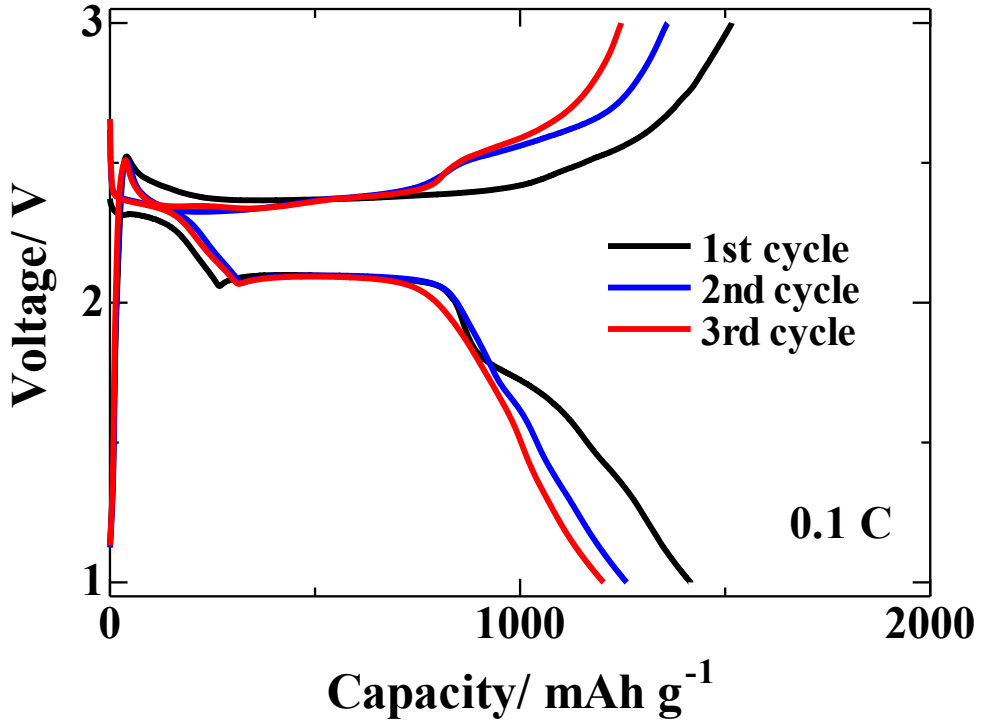

Fig 4.12 Discharge/charge profiles of lithium cell with S/PPy/GNS composite cathode at 0.1 C.

Figure 4.13 presents the cycling performance of a Li/S cell containing S/PPy/GNS composite cathode. The nanocomposite delivers a high initial discharge capacity of about 1415.7 mAh g^{-1} and maintains a reversible capacity of 641.5 mAh g^{-1} after 40 cycles at 0.1 C rate. This represents a better cycling performance than that observed for S/PPy composites

without graphene, at a cycling rate twice as fast **[5,31]**. Furthermore, the Coulombic efficiency higher or equal than 90% during the 40 cycles indicates that PPy in the composite plays the significant role of absorbing the polysulfides and suppressing the shuttle effect.

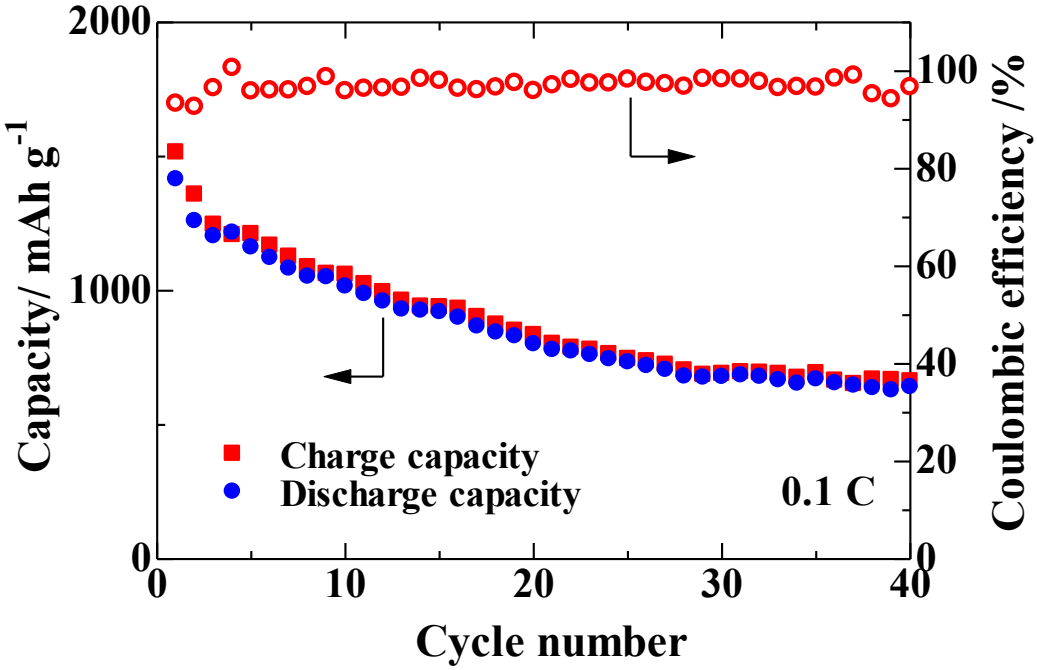

Fig 4.13 Discharge/charge capacity and Coulombic efficiency vs. cycle number for the S/PPy/GNS lithium cell at 0.1 C.

To further investigate the electrochemical performance of the S/PPy/GNS nanocomposite, a rate capability study is carried out as shown in **Fig. 4.14**. Initial capacities of 988.7 mAh g^{-1} and 830.1 mAh g^{-1} were obtained at rates of 0.5 C and 1 C, respectively. After 50 cycles the capacity remains at 424.5 mAh g^{-1} and 324.7 mAh g^{-1}, showing good cycling stability of the S/PPy/GNS composite cathode.

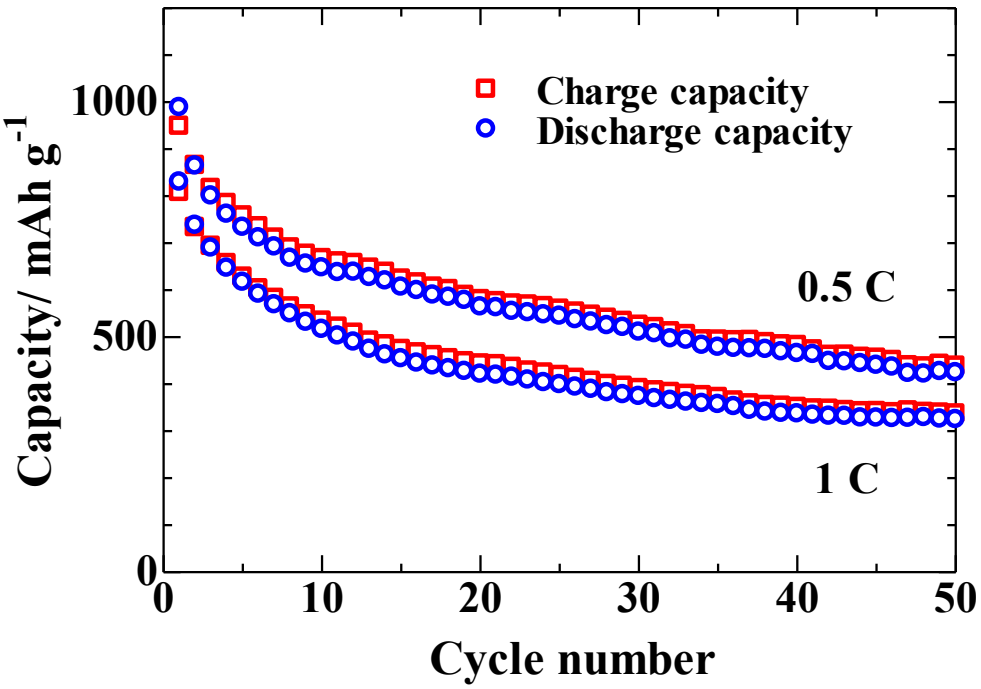

Fig 4.14 Reversible capacity vs. rate capability for the S/PPy/GNS lithium cell.

Based on our observations, we postulate that the combined effects of the individual components and dual-layered structure of the composite play a key role on its electrochemical performance. The high dispersion of nanoscale sulfur layer on the surface of PPy/GNS composite is beneficial to the excellent high rate discharge capability of the sulfur cathode owing to the good electrical conductivity of GNS and good lithium ion transport path. Concomitantly, PPy porous structure accommodates more volume change during cycling and also plays an important role in retarding diffusion of polysulfides out of the electrode.

4.2.4 Summary

A method for fabricating a ternary sulfur/polypyrrole/graphene nanosheet composite has been developed. The method, based on previous work to synthesize PPy/GNS composite by the *in situ* chemical polymerization of pyrrole on the graphene nanosheet, employs nanosized sulfur particle suspension to produce a novel cathode material with dual-layered structure. The electrochemical results show that graphene can provide an effective electron conduction path and the S/PPy/GNS nanocomposite forms a stable dual-layered structure for the S electrode. PPy also has strong adhesion to the surface of graphene and absorb polysulfides into its porous structure. Consequently, the S/PPy/GNS composite cathode exhibits good cycling and rate performance for rechargeable lithium/sulfur batteries.

Chapter 5

Ternary Sulfur/Polyacrylonitrile/$Mg_{0.6}Ni_{0.4}O$ Composite Cathode for High Performance Li/S Batteries

5.1 Introduction

Various methods to address the above issues have been explored, including addition of various types of conductive carbon materials and conductive polymers, to enhance the electronic conductivity of the composite and hinder the dissolution of polysulfides into the electrolyte.

Among the different types of composites, the sulfur/polyacrylonitrile (S/PAN) composite has demonstrated high sulfur utilization and large capacity at initial cycles **[1]**. However, the poor electronic conductivity of the S/PAN binary composite hinders the cyclability and the performance at high C-rate. It is noted that Li/S batteries exhibit enhanced electrochemical performance with different kinds of additives to the sulfur cathode with morphology changing and/or absorbing properties **[2-4]**. These additives have advantages of small dosage and fast effect without increasing the cost of battery compared with the other technologies **[5]**. Therefore, employment of additives in Li/S batteries to enhance the performance by modifying the morphology of S composite is an effective approach in preparing high performance sulfur cathodes.

In this part, we report on the preparation of nanosized $Mg_{0.6}Ni_{0.4}O$ via self-propagating high temperature synthesis (SHS), its effect on the electrochemical performance of the S/PAN/$Mg_{0.6}Ni_{0.4}O$ ternary composite cathode, and characterization of the composite physical and electrochemical properties as a cathode in lithium secondary batteries.

5.2 Experimental

The synthesis of $Mg_{0.6}Ni_{0.4}O$ was carried out by the SHS method as follows. 0.6 mol $Mg(NO_3)_2$, 0.4 mol $Ni(NO_3)_2$ were dissolved in 100 mL deionized water and different amounts of glycine were added into the solution . The solution was thoroughly stirred and boiled to evaporate the excess water. Further, the resulting viscous liquid was placed and heated in an oven at 200°C, where ignited and underwent a self-sustaining combustion process as shown in **Fig. 5.1**. The final product was an ash composed of nickel and magnesium oxides. The powder was calcined at different temperatures for 6 h in air and then ground in an agate mortar.

The ternary composite preparation is schematically presented in **Fig. 5.2**. Sulfur, PAN and as-prepared $Mg_{0.6}Ni_{0.4}O$ were mixed in the weight ratio of 4:1:0.25 and ball milled at 800 rpm for 2 h with ethanol as dispersant. The mixture (precursor) was further dried in a vacuum oven at 60 °C for 3 h to remove the solvent and then heat treated at 350 °C for 3 h in a tubular furnace in Ar gas to melt sulfur and react it with PAN. For comparison with the ternary composite, the S/PAN binary composite cathode was prepared in the same way.

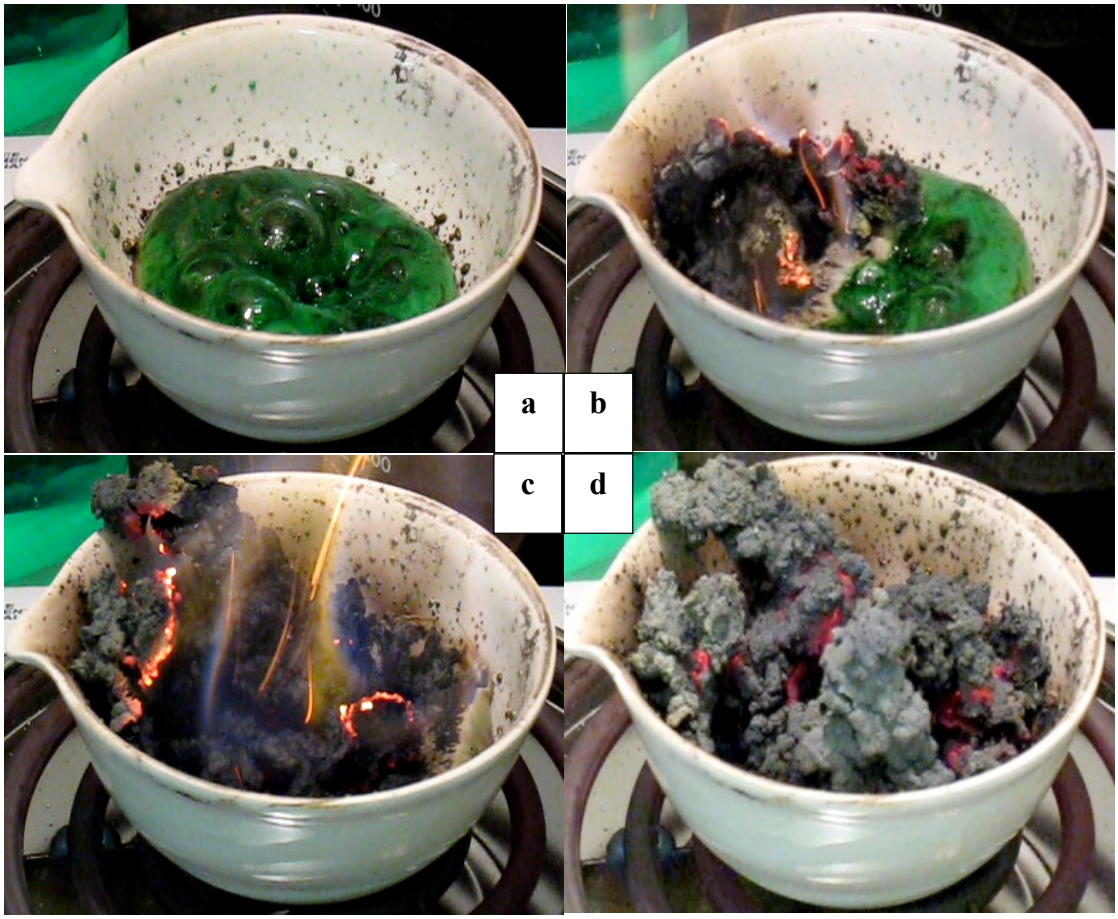

Fig 5.1 The synthesis of $Mg_{0.6}Ni_{0.4}O$ as prepared powder carried out by SHS method.

The crystalline phases of the samples were determined by XRD analysis equipped with Cu-Kα radiation and HRTEM with selected area electron diffraction (SAED). The sample surface morphology was examined by FESEM. The specific surface area was determined by BET. The S content of the samples was determined by chemical analysis (CHNS, Vario Micro Cube, Elementar). The interior structure of samples was observed using TEM at 60 kV and HRTEM equipped with EDS.

CR2032 coin-type cells were assembled inside a MBRAUN glove box filled with high purity argon by sandwiching a polypropylene separator between the composite cathode and lithium anode, and using 1 mol dm^{-3} $LiPF_6$ in EC:DMC:DEC=1:1:1 as electrolyte. The cathode was comprised of 80 wt% binary or ternary composite, 10 wt% acetylene black as conductive material and the rest was PVdF as a binder. These materials were dispersed in NMP. The resultant slurry was spread onto a circular nickel foam with 1 cm in diameter and then dried in vacuum for 12 h at 60 ^{o}C. Finally, the electrode was pressed at 8 MPa by a hydraulic press in order to achieve good contact between the active material and nickel foam current collector. The electrodes were prepared to make their weight and thickness the same by precise weighing, pressing and controlling its geometry. The cells were tested galvanostatically between 1 and 3 V vs. Li^+/Li at different current densities, and specific capacities were calculated on the basis of the weight of S in the composite cathode.

CV was performed between 1 and 3 V vs. Li^+/Li at a scanning rate of 0.1 mV s^{-1}. The EIS measurements were carried out by applying an ac voltage of 10 mV over the frequency range from 0.1 Hz to 1 MHz.

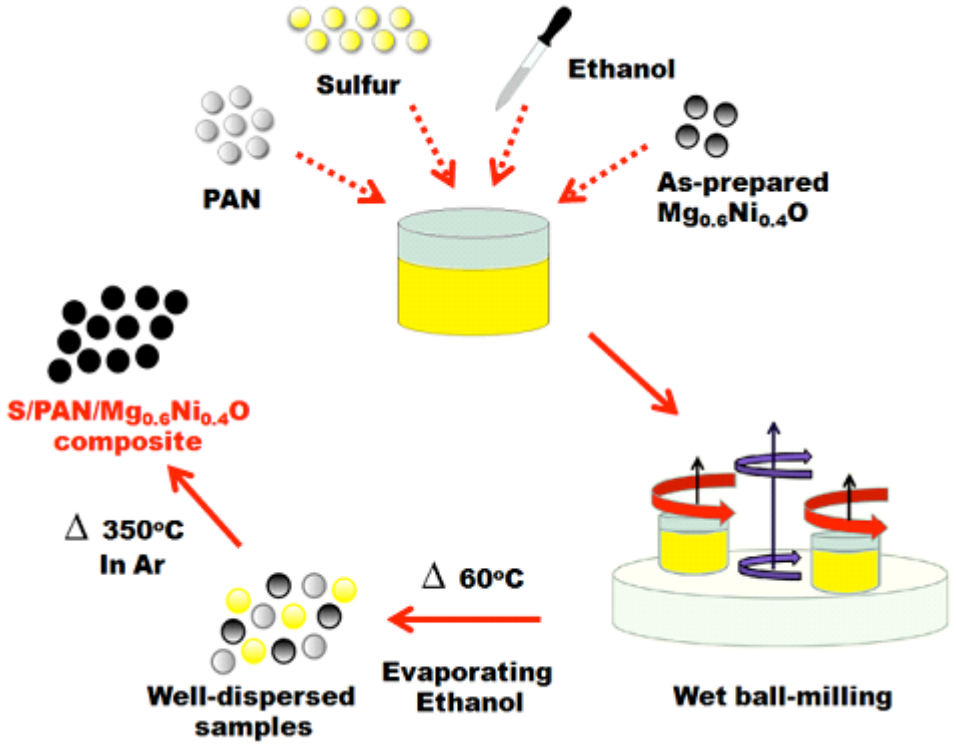

Fig 5.2 Schematic of the S/PAN/$Mg_{0.6}Ni_{0.4}O$ ternary composite preparation.

5.3 Results and Discussion

XRD analysis was used to investigate potential structural changes due to the starting material interactions including possible reactions of $Mg_{0.6}Ni_{0.4}O$ with other cathode components. **Figure 5.3** shows the XRD patterns of the starting components S, as-prepared $Mg_{0.6}Ni_{0.4}O$ and the S/PAN/$Mg_{0.6}Ni_{0.4}O$ ternary composite. One can see that the XRD patterns of the S/PAN/$Mg_{0.6}Ni_{0.4}O$ ternary composite has sharp peaks of a face-centered cubic structure $Mg_{0.6}Ni_{0.4}O$ with reduced peak intensity compared with that of the initial $Mg_{0.6}Ni_{0.4}O$.

On the other hand, the characteristic *Fddd* orthorhombic crystal structure peaks of

elemental sulfur disappear from the XRD patterns of the ternary composite, which could be due to the trapping of S in the internal structure of the composite. The XRD data do not show appearance of any new phases in the final product, which could be an indication of absence of chemical reaction between sulfur, PAN and $Mg_{0.6}Ni_{0.4}O$ during ball-milling and following heat treatment.

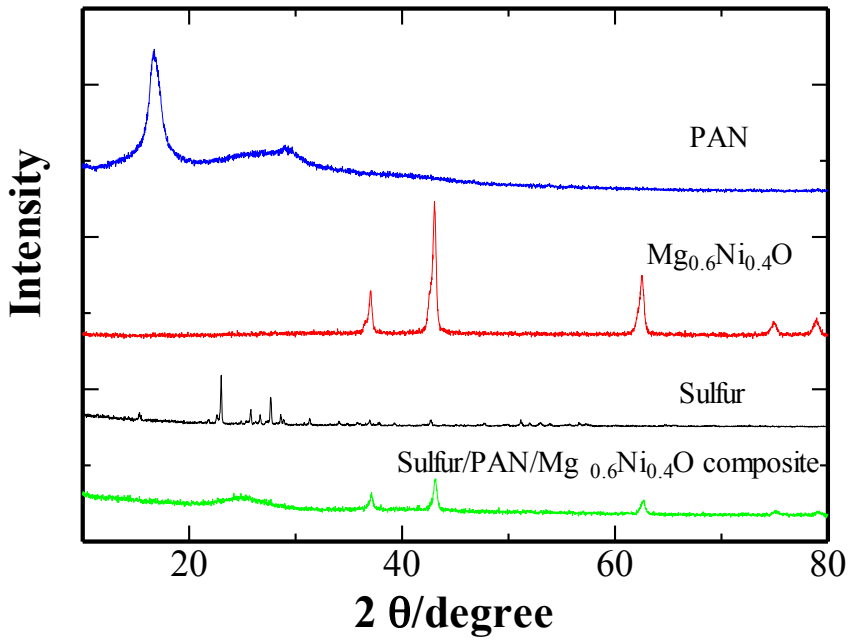

Fig 5.3 XRD patterns of starting components S, PAN, as-prepared $Mg_{0.6}Ni_{0.4}O$ and the S/PAN/$Mg_{0.6}Ni_{0.4}O$ ternary composite.

Figure 5.4a presents the HRTEM images of the $Mg_{0.6}Ni_{0.4}O$ particles. The sample exhibits nanostructure, which consisted of primary particles ranged from 20-50 nm. At a higher magnification (**Fig. 5.4b**), obvious lattice fringes could be observed, and $Mg_{0.6}Ni_{0.4}O$

has a highly crystalline structure, which is consistent with the XRD results. It is confirmed by the EDS mapping that the elements of Ni, Mg and O homogeneously dispersed into the $Mg_{0.6}Ni_{0.4}O$ bulk (**Fig. 5.4c-f**).

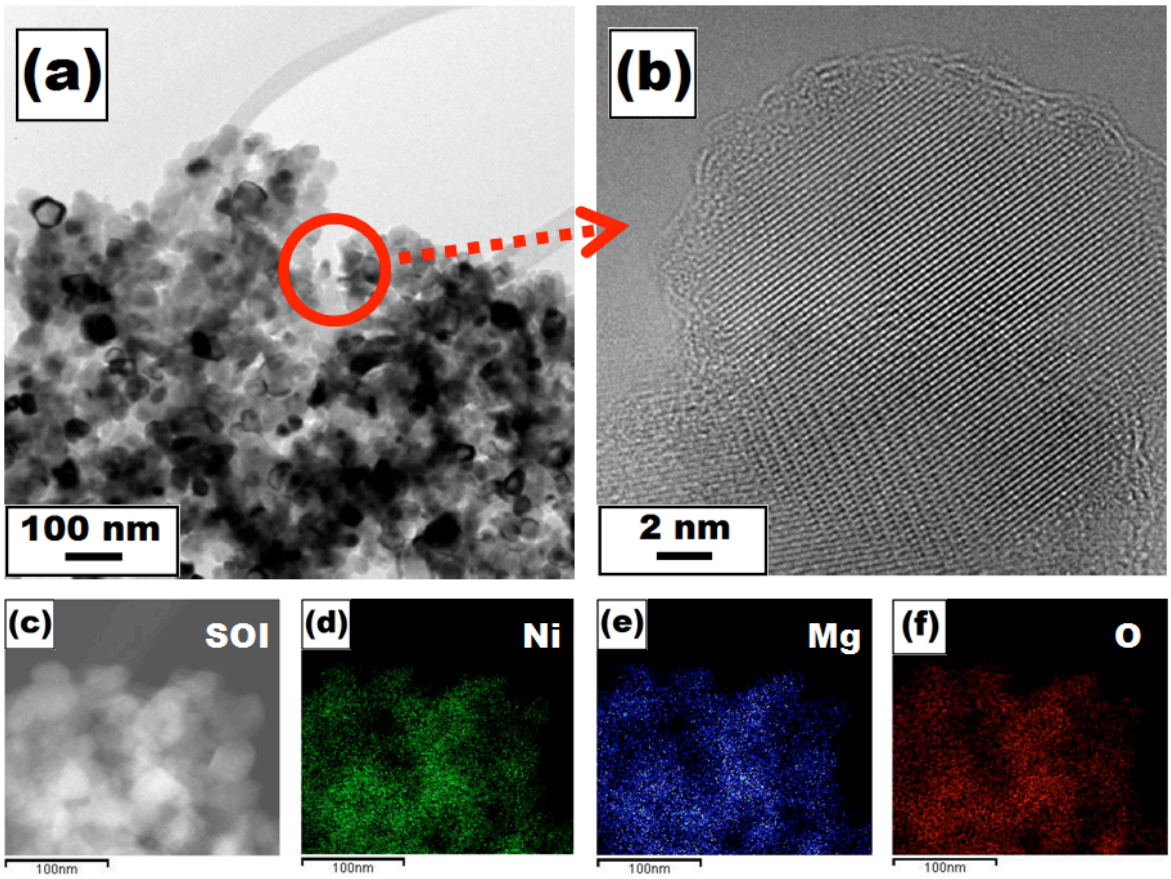

Fig 5.4 HRTEM images of $Mg_{0.6}Ni_{0.4}O$ samples at different magnifications (**a and b**); EDS mapping showing distribution of Mg, Ni and O element (**c-f**).

The effect of the $Mg_{0.6}Ni_{0.4}O$ nanoparticle addition on the composite morphology could be observed from the SEM images presented in **Fig. 5.5(a and b)**. It is noted that the surface

morphology of the S/PAN binary composite changes significantly by addition of about 4 wt% of $Mg_{0.6}Ni_{0.4}O$ nanoparticles. Figure **5.5a** shows typical S/PAN nanostructures containing agglomerated particles with diameters ranging from 0.1 μm to 1μm. In the bulk of S/PAN composite, the particles are very compact and have smooth surface, while the S/PAN/$Mg_{0.6}Ni_{0.4}O$ ternary composite has a rough surface with twice specific surface area of 17.1 m^2 g^{-1} compared with 8.0 m^2 g^{-1} of S/PAN composite, which was beneficial to the contact and interaction between the electrode and the electrolyte. On the other hand, the ternary composite contains many nanosized particles, creating a 3D porous nanostructure, which could be highly favourable to ion diffusivity and improve electrochemical performance in Li/S battery. By comparison between the TEM results of the binary composite and ternary composite (**Fig. 5.5c and 5.5d**), the dark dots are observed to well disperse in the ternary composite bulk.

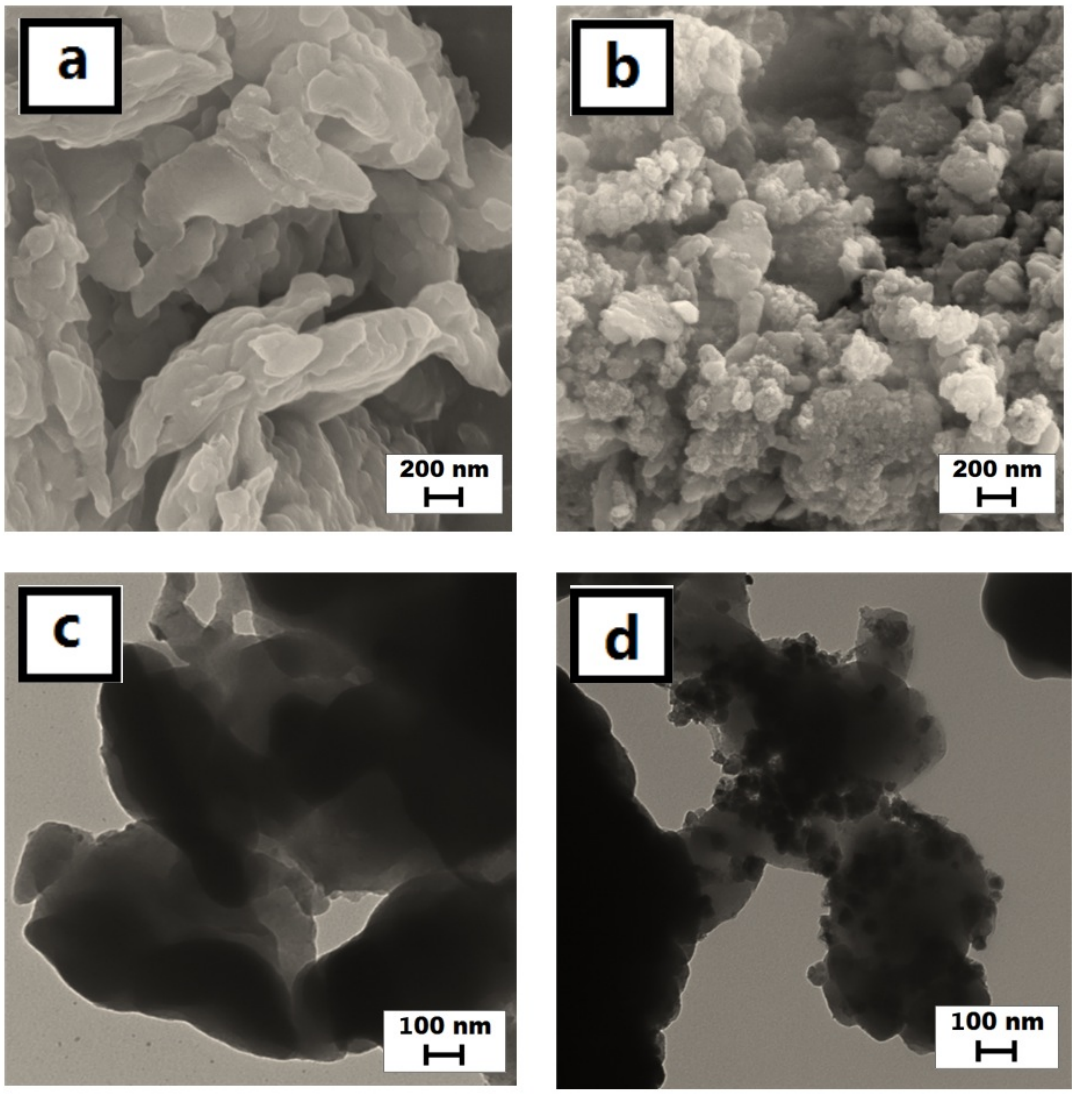

Fig 5.5 SEM images and TEM images of **(a, c)** S/PAN binary and **(b, d)** S/PAN/$Mg_{0.6}Ni_{0.4}O$ ternary composites.

The "dark dots" could be $Mg_{0.6}Ni_{0.4}O$ embedded in the composite bulk, which is confirmed by HRTEM equipped with SAED (**Fig. 5.6**). The SAED pattern in this phase, shown in **Fig. 5.6**, consists of a few rings which could be assigned to the face-centered cubic

structure of $Mg_{0.6}Ni_{0.4}O$. All d-spacing derived from SAED spectra are shown in **Table 5.1**. This agrees well with the sharp peaks in the XRD patterns.

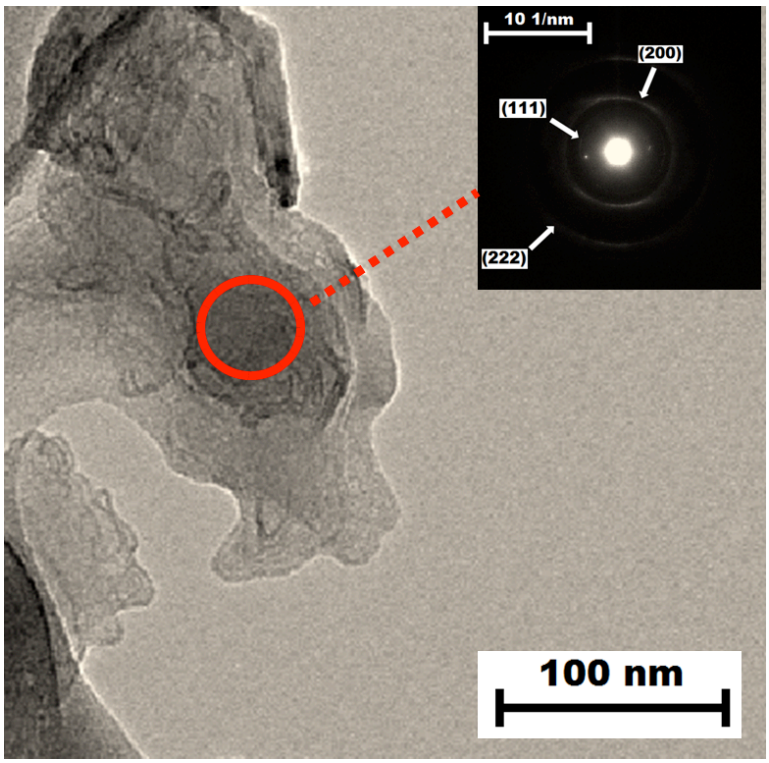

Fig 5.6 HRTEM image and SAED patterns of the S/PAN/$Mg_{0.6}Ni_{0.4}O$ ternary composite.

Table 5.1 *d*-spacing derived from SAED analysis of as-prepared $Mg_{0.4}Ni_{0.6}O$.

As-**prepared**	$Mg_{0.4}Ni_{0.6}O$*	
nm	*nm*	*d(h k l)*
0.236	0.242	(111)
0.202	0.209	(200)
0.119	0.121	(222)

*JCPDS 34-0410

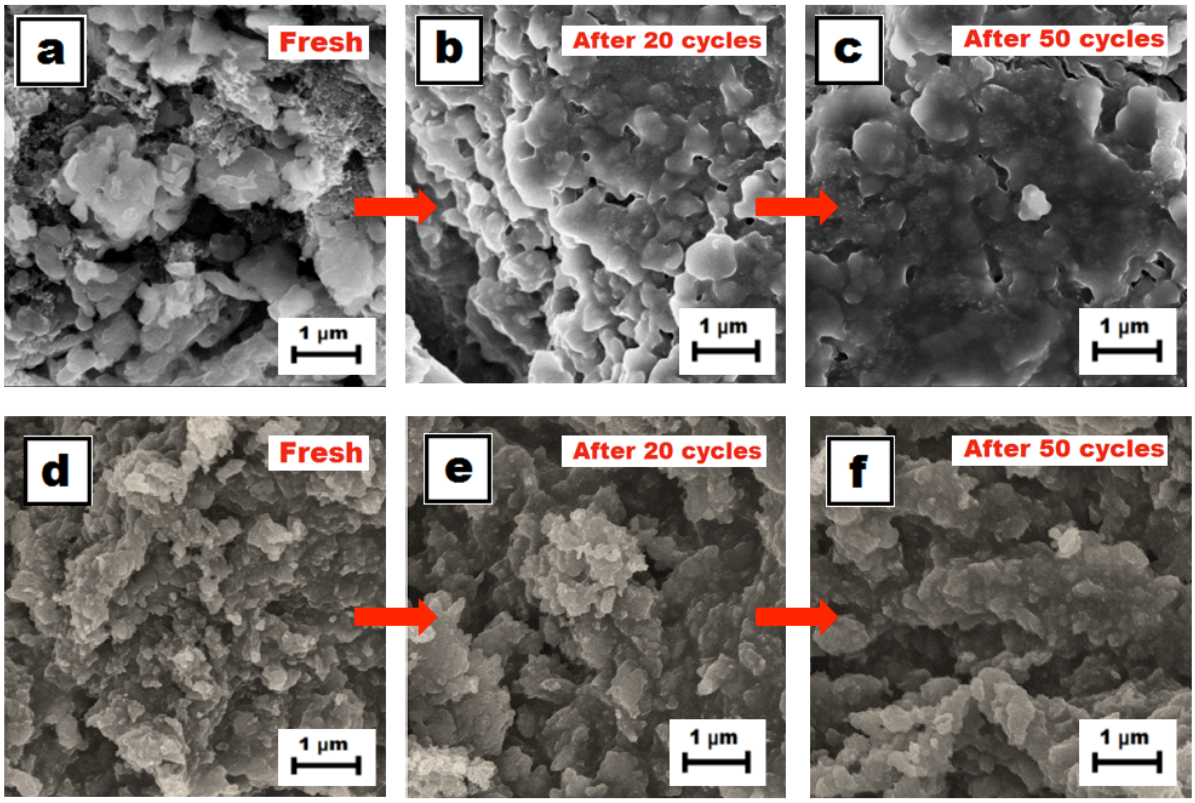

Fig 5.7 SEM of (**a, b, c**) binary and (**d, e, f**) ternary composites before and after charge-discharge cycles.

Fig. 5.7 shows the SEM images of fresh and cycled binary and ternary composite cathodes. It can be seen from **Fig. 5.7a-c** that the S/PAN binary cathode morphology drastically changed upon cycling, and active material particles in the binary composite continuously merged into a large solid bulk, which could be due to the separation of active material from conducting agent and binder and further agglomeration into poorly conductive S/PAN particles, negatively effecting the cathode conductivity and sulfur utilization. This process became stronger upon further cycling resulting in severe agglomeration of the active cathode material, which could be one of the major reasons of poor cyclability of the S/PAN binary composite. In contrast, the morphology of the S/PAN/$Mg_{0.6}Ni_{0.4}O$ ternary composite does not change remarkably even after 50 cycles (See **Fig. 5.7d-f**), and kept its nanostructured feature.

The SEM results presented in **Fig. 5.7** suggest that $Mg_{0.6}Ni_{0.4}O$ as doping material could suppress the separation and agglomeration of active material in the composite, improving the electrochemical performance of the cathode and its stability. The morphology change of both the binary and ternary composite cathodes during charge-discharge could be schematically represented as in **Fig. 5.8**. In the binary composite, sulfur does not remain fixed in its original position and its distribution cannot remain homogeneous upon cycling as reported by Jeon *et al* **[6]**. By adding $Mg_{0.6}Ni_{0.4}O$, the as-prepared ternary composite was enabled to maintain the homogeneous distribution of its components and unchanged morphology during charge-discharge cycling, and retain reactive sites in its nanosized structure.

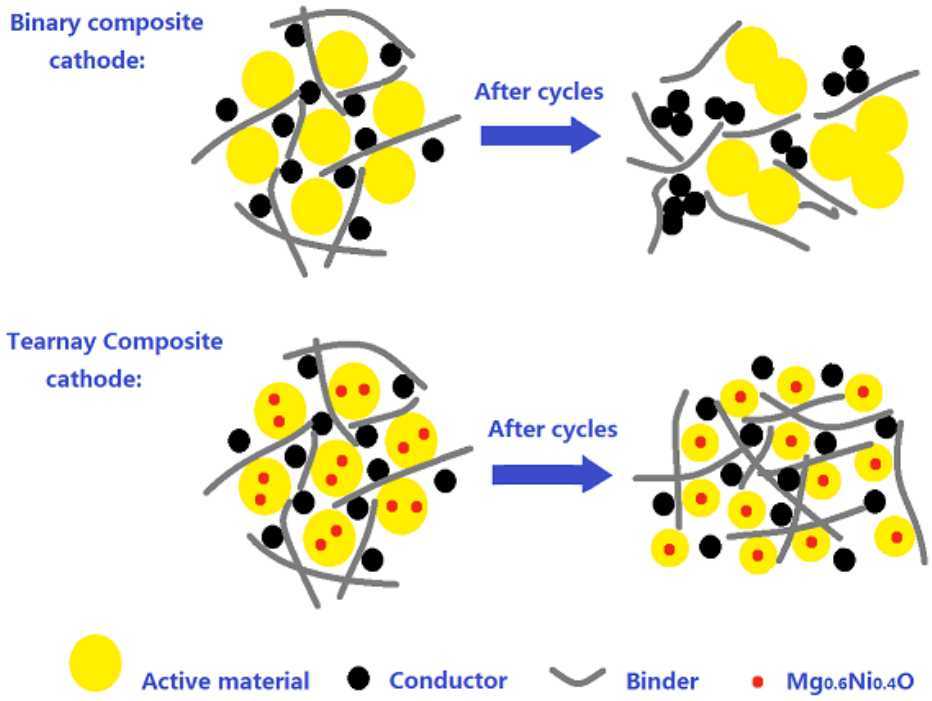

Fig 5.8 Schematic model of morphology change in composite cathode during charge-discharge cycling.

The CV curves of Li/S cells with the S/PAN and S/PAN/$Mg_{0.6}Ni_{0.4}O$ composite cathodes are shown in **Fig. 5.9**. The CV data of both the binary and ternary composite evidenced two major stage redox processes in the system which agreed well with the literature data **[7,8]**, and could be attributed to the transition of S to polysulfides (Li_2S_8, Li_2S_6, Li_2S_4, Li_2S_2), and their further transformation to lithium sulfide Li_2S, respectively. It confirmed that the $Mg_{0.6}Ni_{0.4}O$ additive was not electrochemically active in the selected voltage region. Furthermore, it can be seen that as-prepared $Mg_{0.6}Ni_{0.4}O$ as an additive leaded to the enhanced electrochemical response of the cathode. The ternary composite S/PAN/$Mg_{0.6}Ni_{0.4}O$ had a pair of well distinguished redox peaks separated by about 0.67 V. The corresponding peaks of the binary S/PAN composite are weaker and broader, and the

voltage gap between them is about 1.04 V. These observations allow us to suggest that the addition of $Mg_{0.6}Ni_{0.4}O$ leads to the enhanced electrochemical kinetics of sulfur cathode resulted in the reduced polarization of the electrodic processes on the S/PAN/$Mg_{0.6}Ni_{0.4}O$ composite cathode. This performance enhancement could be attributed to the enhanced charge transfer of the material due to the addition of $Mg_{0.6}Ni_{0.4}O$. The observed morphology advantages and stability of the ternary composite could provide a larger electrode/electrolyte interface, reducing the charge transfer resistance at this boundary.

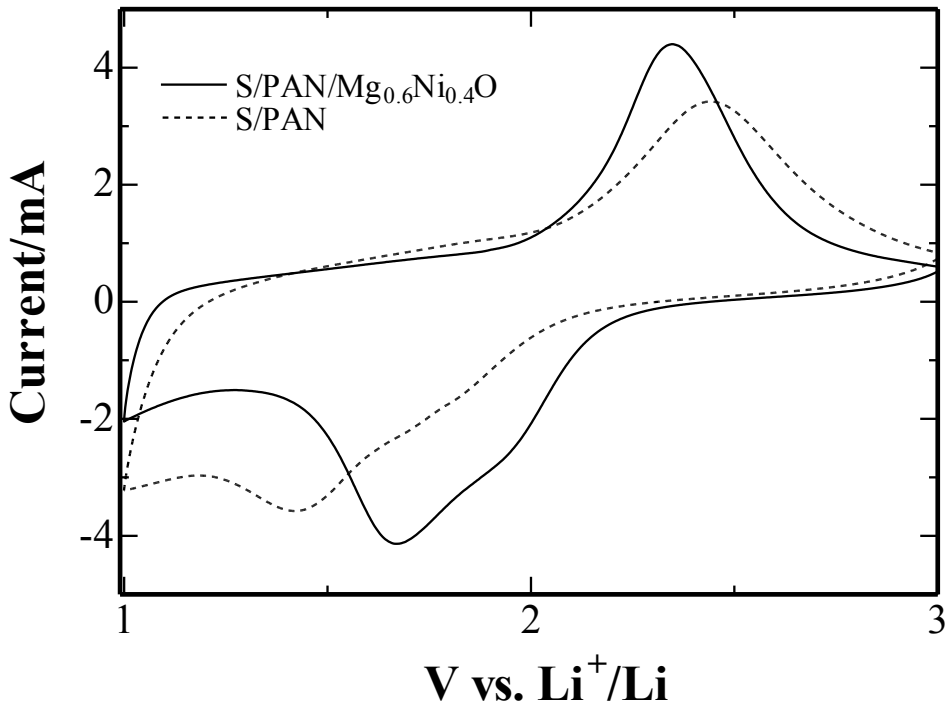

Fig 5.9 CV profiles for lithium cells with the binary and ternary composite cathodes. Scan rate 0.1 mV s^{-1}.

EIS is a powerful tool to study such interfacial effects. The EIS measurements of the

lithium half-cells with S/PAN and S/PAN/$Mg_{0.6}Ni_{0.4}O$ composite cathodes were carried out before and after the galvanostatic charge-discharge cycles. Although the direct and precise quantitative comparison of the EIS data may not be correct enough, the above mentioned measures to keep the geometry and weight of the electrodes very close to each other could allow for the quantitative comparison **[9,10]**. **Figure 5.10** presents the typical Nyquist plots for these systems illustrating their impedance trends upon cycling. The Nyquist plots of both cathodes consist of compressed semicircles in the high (HF) to medium (MF) frequency range, which could be related to the interfacial charge transfer impedance **[9-11]**. It can be seen (**Fig. 5.10a** and **inset**) that the EIS spectra of the ternary composite cathode consist of two compressed semicircles at the high to medium frequency part of EIS, and its total impedance much smaller (three times for the fresh cells and more than ten times for the cycled) than the impedance of a single semicircle of the binary composite (**Fig. 5.10b**), i.e. the addition of $Mg_{0.6}Ni_{0.4}O$ into the S composite significantly reduces its charge transfer resistance. This observation agrees well with the CV data above showing the electrochemical response improvement in the case of the ternary composite. The appearance of an additional semicircle in the ternary composite Nyquist plot could be due to the effect of charge transfer through new boundaries formed by the introduction of $Mg_{0.6}Ni_{0.4}O$.

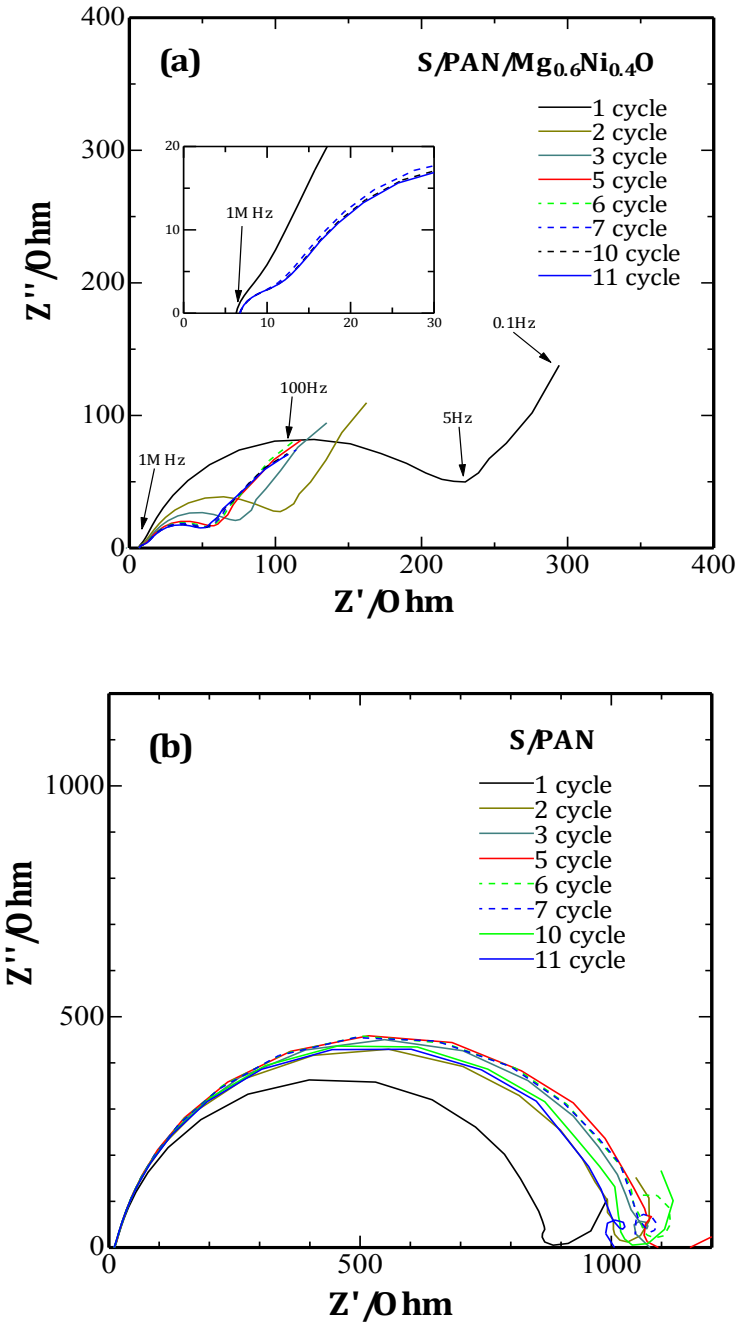

Fig 5.10 EIS data for fresh and cycled lithium cells with **(a)** ternary S/PAN/$Mg_{0.6}Ni_{0.4}O$ (Inset: Enlarged image of the high frequency part of EIS for S/PAN/$Mg_{0.6}Ni_{0.4}O$), and **(b)** binary S/PAN composite cathodes.

In the EIS spectra of the S/PAN/$Mg_{0.6}Ni_{0.4}O$ composite cathode, the semicircles part is followed by a declined line of the Warburg impedance attributed to the bulk diffusion resistance of the composite cathode **[9-13]**. The Nyquist plot of the binary S/PAN composite (**Fig. 5.10b**) has been developed differently, and the lower frequency part of the spectra is represented by a complex curve, which could be due to the high bulk impedance of S/PAN. The EIS development upon cycling for the binary and ternary composite cathodes could be compared from the **Fig. 5.10** data. The binary composite (**Fig. 5.10b**) exhibits a high charge transfer resistivity, which remarkably increases upon initial cycling and further slightly reduces and stabilizes at the values much higher than that for the fresh cell. This behavior could be explained by the active material agglomeration observed by SEM (**Fig. 5.7**), when the system resistivity drastically increases due to the separation of S/PAN composite owning very low conductivity from other cathode components, and especially from the conductive carbon. In contrast, the charge transfer impedance of the ternary composite (**Fig. 5.10a**) rapidly reduces within a few initial cycles and stabilizes at the values much lower than that of the fresh battery. The EIS data shows that the $Mg_{0.6}Ni_{0.4}O$ additive significantly improves the charge transfer properties of the composite cathode, which leads to its electrochemical performance enhancement.

The experimental EIS data for the S/PAN/$Mg_{0.6}Ni_{0.4}O$ composite were used for the equivalent circuit analysis. The studied system consisted of multiple interfacial borders and its quantitative analysis could be complicated. However, the EIS spectra analysis could provide valuable information on the additives and surface treatment effects on the interfacial stability of an electrochemical system, their charge transfer properties and electrochemical

performance [**9-13**]. As it can be seen from **Fig. 5.10a** and its inset the EIS spectra of a fresh cell with the S/PAN/$Mg_{0.6}Ni_{0.4}O$ cathode is represented by two semicircles in the high and medium frequency range, respectively, followed be a declined line of the Warburg impedance in low frequency part of EIS. The total impedance of the high to medium frequency range of EIS reduces upon a few initial cycles, which could be attributed to the development of conductive solid electrolyte interface (SEI). One can see from the inset in **Fig. 5.10a** that the high frequency semicircle becomes more distinguished and separated from the medium frequency semicircle, and both HF and MF semicircles sizes stabilize within a few initial cycles. **Fig. 5.11** shows the best fitting equivalent circuit along with the fitting results.

The fitting equivalent circuit could be considered as a derivative of the Randles circuit with an additional 'interface element' *Q/R* and it is represented as follows

$$R_1 + Q_1/R_2 + Q_2/R_3 + W \qquad (1)$$

where R_1, R_2, R_3 are the ohmic resistances at the interfaces, Q_1 and Q_2 are the constant phase elements (CPE) responsible for the double layer capacitance components of the system impedance, and W is the Warburg impedance. It can be seen that the chosen multi component equivalent circuit fits well with the experimental data (fitting goodness close to 1) and could be used for the qualitative characterization of the studied system. The changes in the circuit components parameters are monitored upon cycling. It is found that while the component R_1 has not been remarkably charged upon the battery operation, the resistance R_2 is gradually increasing (within 10% of its initial value) and the impedance represented by R_3 is remarkably reducing during a few initial cycles. Upon further cycling, the R_1 and R_3

components are stabilized and have not been changing noticeably. The constant phase elements values slightly change during the first cycle, and are not influenced by the following cycle. The changes in the Warburg impedance were not remarkable. The comparative analysis of the experimental EIS data and the equivalent circuit fitting results allow us to assign the element Q_1/R_2 to the small high frequency (HF) semicircle responsible for the electrode/electrolyte interface impedance **[10,14],** and the Q_2/R_2 element of the equivalent circuit is assigned to the following medium frequency (MF) semicircle responsible for the charge transfer resistance [**14**]. It could be suggested that the interfaces in the system are stabilized upon a few initial discharge-charge cycles, and stable and conductive layers are formed at the electrode/electrolyte interface, favouring the electrochemical stability of the system, and easier charge transfer. This could be considered as one of the reasons of the electrochemical performance stabilization and improved cyclability of the cathode.

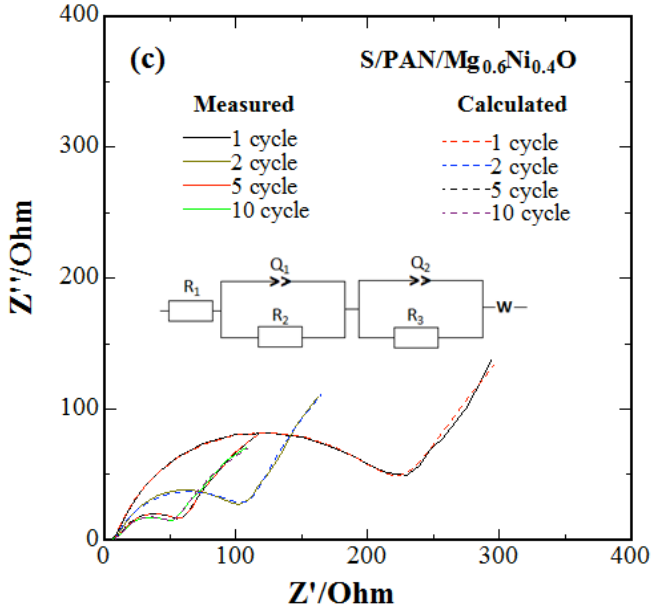

Fig 5.11 Equivalent circuit used for fitting the EIS data for the ternary composite.

The effect of the $Mg_{0.6}Ni_{0.4}O$ addition on the electrochemical performance of the composite cathode can be seen from the charge-discharge profiles, the cyclability and capacity retention data presented in **Fig. 5.12**. It can be seen that the charge-discharge polarization of the ternary composite (**Fig. 5.12c**) has been reduced compared with that of the binary cathode (**Fig. 5.12a**), which is indicated by a decrease of the voltage gap between charge and discharge processes, which is observed in the CV data in **Fig. 5.9** as well. The kinetics improvement and the polarization decrease achieved in the system by the $Mg_{0.6}Ni_{0.4}O$ addition could be very beneficial for the utilization of low-conductive sulfur active material in the composite cathode, and consequently improve the energy and power density of the battery. The ternary S/PAN/$Mg_{0.6}Ni_{0.4}O$ cathode exhibits enhanced

electrochemical performance. A specific capacity of 1545 mAh g^{-1} is delivered in the first discharge, and a reversible capacity of 1223 mAh g^{-1} is obtained for a lithium cell with this cathode in the second cycle, and the cell retains about 100% of its initial reversible discharge capacity after 100 cycles.

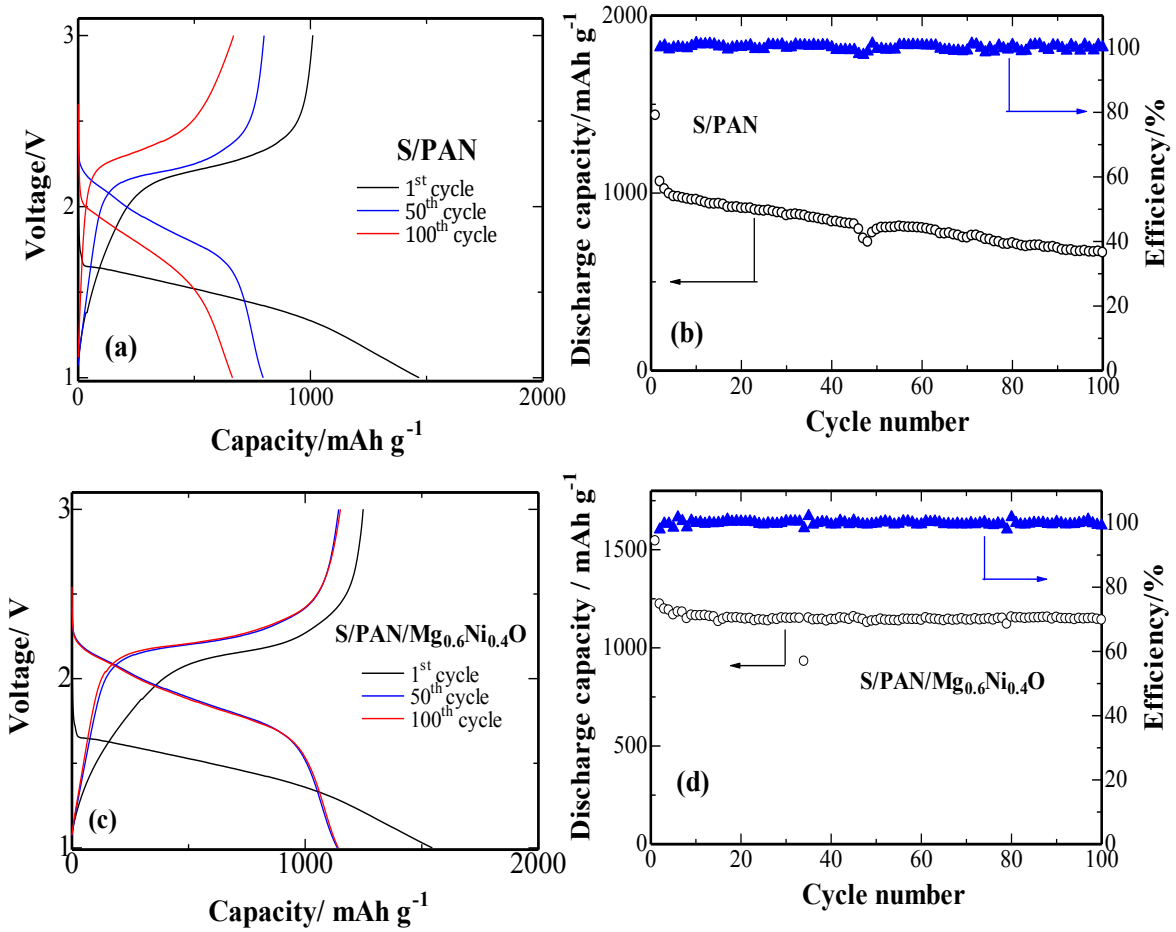

Fig 5.12 Charge-discharge profiles, cyclability and capacity retention of the cells with **(a, b)** binary and **(c, d)** ternary composite cathodes at 0.1 C.

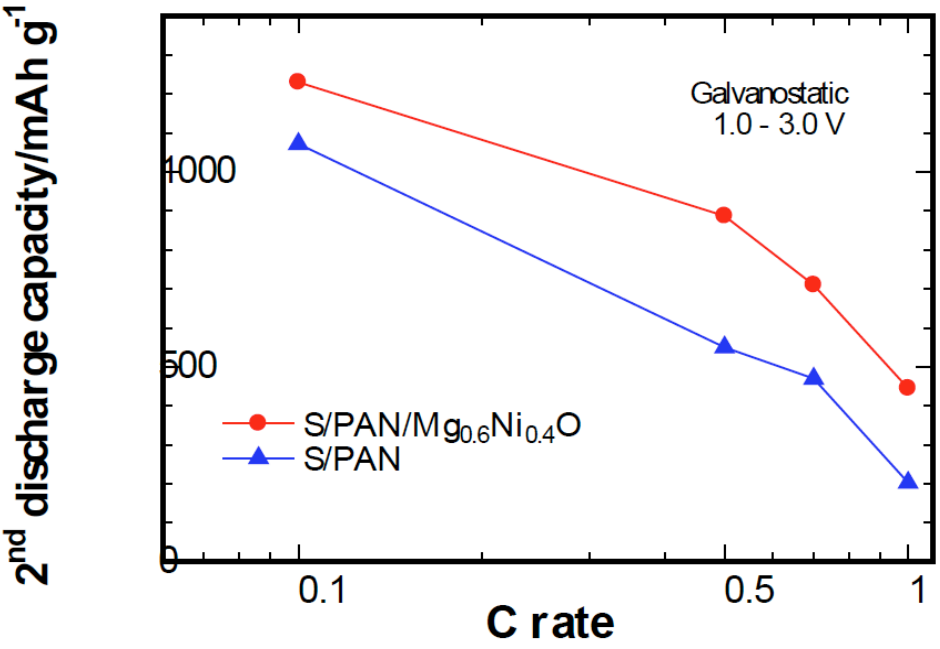

Fig 5.13 Rate capability of lithium cells with the S/PAN binary and the S/PAN/$Mg_{0.6}Ni_{0.4}O$ ternary composite cathodes at 0.1, 0.5 C, 0.7C and 1 C.

Although both cathodes exhibits high Coulombic efficiency (about 100%) over 100 cycles, which can be attributed to the shuttle effect suppression in S/PAN composite **[1]**, the binary composite suffers from very quick capacity fading and the cell with S/PAN electrode lost about 40% of its initial capacity after 100 cycles of charge-discharge. The kinetic behavior of the S/PAN/$Mg_{0.6}Ni_{0.4}O$ composite is further evaluated. The rate capability of the cells with S/PAN composite and S/PAN/$Mg_{0.6}Ni_{0.4}O$ composite was examined, respectively. The results of different C rates, namely 0.1, 0.5, 0.7 and 1 C are shown in **Fig. 5.13**. With both types of the cell, the capacity was found to decrease gradually with increasing the charge-discharge current. It is obvious that the cell with S/PAN/$Mg_{0.6}Ni_{0.4}O$ composite

cathode showed an enhanced rate capability. This was, again, due to that the $Mg_{0.6}Ni_{0.4}O$ additive significantly improved the charge transfer properties of the composite cathode, which was confirmed by the EIS studies above.

5.4 Summary

$Mg_{0.6}Ni_{0.4}O$ powders were successfully synthesized via the SHS method followed by a heat treatment. The prepared $Mg_{0.6}Ni_{0.4}O$ powder was used as an additive in the S/PAN composite to improve the composite morphology stability, chemical uniformity and the electrochemical performance. This additive led to the formation of a nanostructured composite and prevented sulfur agglomeration upon cycling allowing a high sulfur utilization. The CV data showed a noticeable polarization reduction in S/PAN/$Mg_{0.6}Ni_{0.4}O$ compared with the parent (non-additive) S/PAN cathode indicating the electrochemical kinetics improvement. The EIS experiments and analysis have confirmed these results and revealed remarkable charge transfer impedance reduction by the $Mg_{0.6}Ni_{0.4}O$ additive. These physical and electrochemical properties enhancements allowed achieving an initial reversible discharge capacity of 1223 mAh g^{-1}, the retention of this capacity over 100 cycles at 0.1 C rate along with about 100% of Coulombic efficiency. Furthermore, the cathode rate capability has been remarkably improved by the addition of $Mg_{0.6}Ni_{0.4}O$. $Mg_{0.6}Ni_{0.4}O$ synthesized via the SHS method is a very effective additive to prepare the high performance cathodes for Li/S batteries.

Chapter 6

Effect of Graphene on Sulfur/Polyacrylonitrile Nanocomposite Operation as a Cathode for High Performance Li/S Batteries

6.1 Introduction

Sulfur/polyacrylonitrile (S/PAN) composite cathode has demonstrated high sulfur utilization and relatively stable cycling behavior. However, the conductivity limitation of the S/PAN composite does not allow its use at high current operations. Graphene, with an extraordinary electronic transport property, chemical tolerance, and broad electrochemical window, is regarded as an ideal conductive carbon matrix to improve conductivity of electrode materials for lithium-ion batteries **[1-8]**.

In this part, we report on the preparation of a S/PAN/Graphene composite via simple ball milling followed by low temperature heat treatment as a novel cathode material for Li/S batteries. Graphene is chosen as a conductive additive to form a well-connected conductive network and reduce the difference between charge and discharge plateau potentials at all rates. It is found that the hybrid material exhibits significantly improved rate capability and cycling performance.

6.2 Experimental

Sulfur, PAN and graphene were mixed in the weight ratio of 4:1:0.25 and ball milled at 800 rpm for 3 h with NMP as dispersant. The mixture (precursor) was further dried in a vacuum oven at 60 °C for 12 h to remove the solvent and then heat treated at 350 °C for 6 h in a tubular furnace in Ar gas to melt sulfur and react it with PAN. For comparison with the ternary composite, the S/PAN binary composite cathode was prepared by the same route

without adding graphene.

The crystalline phases of the samples were determined by XRD analysis equipped with Cu-Kα radiation. The sample surface morphology was examined by FESEM. The S content of the samples was determined by chemical analysis (CHNS, Vario Micro Cube, Elementar). The interior structure of samples was observed using HRTEM equipped with EDS.

CR2032 coin-type cells were assembled inside a glove box filled with argon by sandwiching a polypropylene separator between the composite cathode and lithium anode, and using 1 mol dm^{-3} $LiPF_6$ in EC:DMC:DEC=1:1:1 as electrolyte. The cathode was comprised of 80 wt% binary or ternary composite, 10 wt% acetylene black as a conductive agent and 10 wt% PVdF as a binder. These materials were dispersed in NMP. The resultant slurry was spread onto an Al foil with 1 cm in diameter and then dried in vacuum oven for 12 h at 60 °C. Finally, the electrode was pressed at 8 MPa by a hydraulic press in order to achieve good contacting between the active material and current collector. The cells were tested galvanostatically between 1 and 3 V *vs.* Li^+/Li at different current densities.

The EIS measurements were carried out by applying an ac voltage of 10 mV over the frequency range from 0.1 Hz to 1 MHz.

6.3 Results and Discussion

The XRD patterns of sulfur, S/PAN and S/PAN/Graphene composite are shown in **Fig. 6.1**. The characteristic *Fddd* orthorhombic crystal structure peaks of elemental sulfur disappeared from the XRD patterns of S/PAN/Graphene composite, which indicates that embedded sulfur exists in fine particles and a highly dispersed state, with the crystalline sulfur most likely converted to amorphous sulfur by heat treatment. The XRD data did not

show appearance of any new phases in the final product, which could be an indication of absence of chemical reaction between sulfur, PAN and graphene during the nanocomposite preparation. The characteristic bands of the S/PAN composite are consistent with that of the S/PAN/Graphene composite, which indicate that the addition of graphene has no effect on the crystal structure of S/PAN composite.

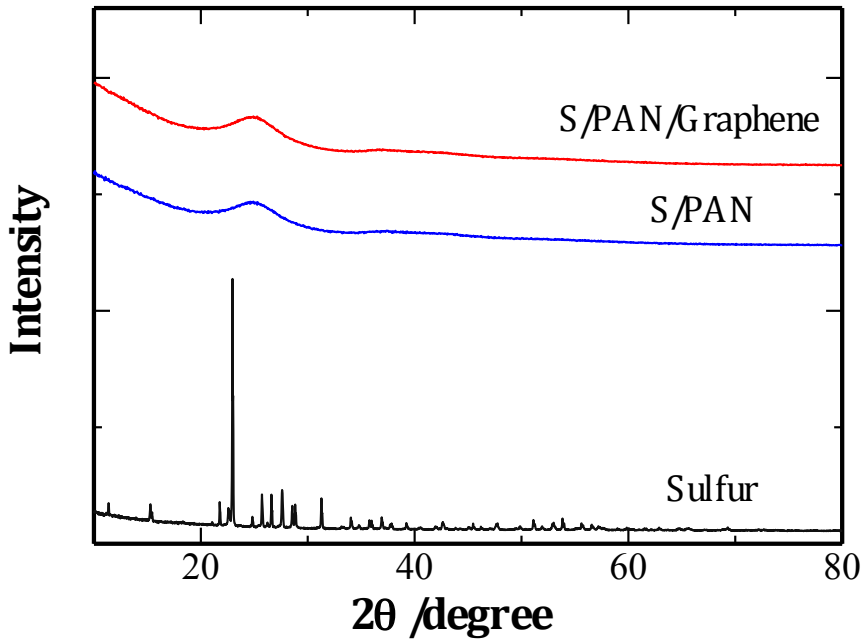

Fig 6.1 XRD patterns of S, S/PAN and S/PAN/Graphene composite samples.

The surface morphology of the S/PAN/Graphene composite is imaged by SEM, as depicted in **Fig. 6.2a.** It can be seen that the interlaced nanosheets of the S/PAN/Graphene composite irregularly stack together, forming a rough and highly developed surface. The

TEM results (**Fig. 6.2b**) show that after the high speed ball milling the composite contains the graphene nanoflakes significantly reduced in size compared with the initial graphene used for the composite synthesis. It could be suggested that the graphene nanoflakes act as nano-currentcollectors of the S/PAN particles enhancing the conductivity of the composite. On the other hand, the size reduction of graphene and formation of disordered and hollow structure of the composite agglomerates create Li^+ and electrolyte pathways providing enhanced activity of the composite. These structure specifics of the composite could positively affect the cathode rate capability, which was observed in the following electrochemical studies. The EDS mapping of S, C and N (**Fig. 6.2c**) confirms that sulfur and PAN are distributed homogeneously on the graphene surface.

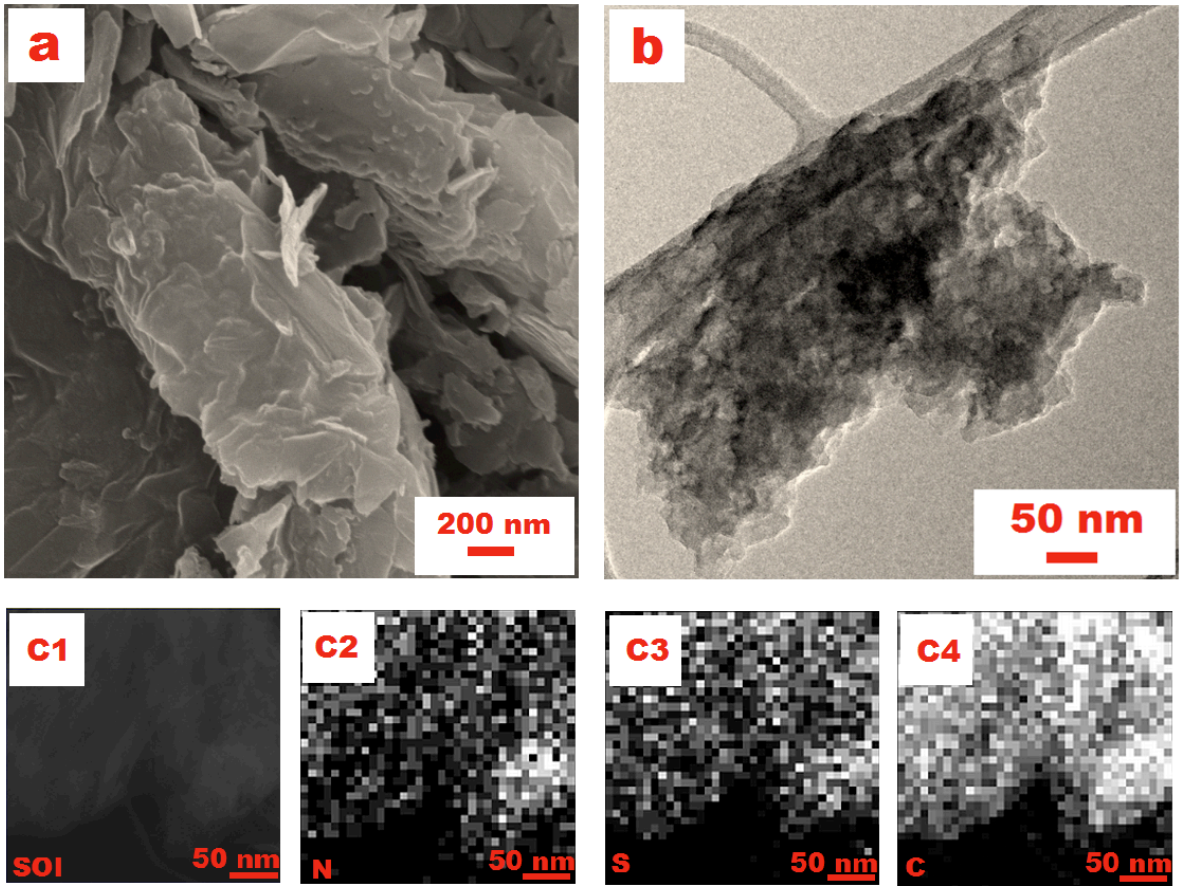

Fig 6.2 (a) SEM image of S/PAN/Graphene composite samples; **(b)** HRTEM images of S/PAN/Graphene composite； **(c)** EDS mapping showing distribution of N, S and C.

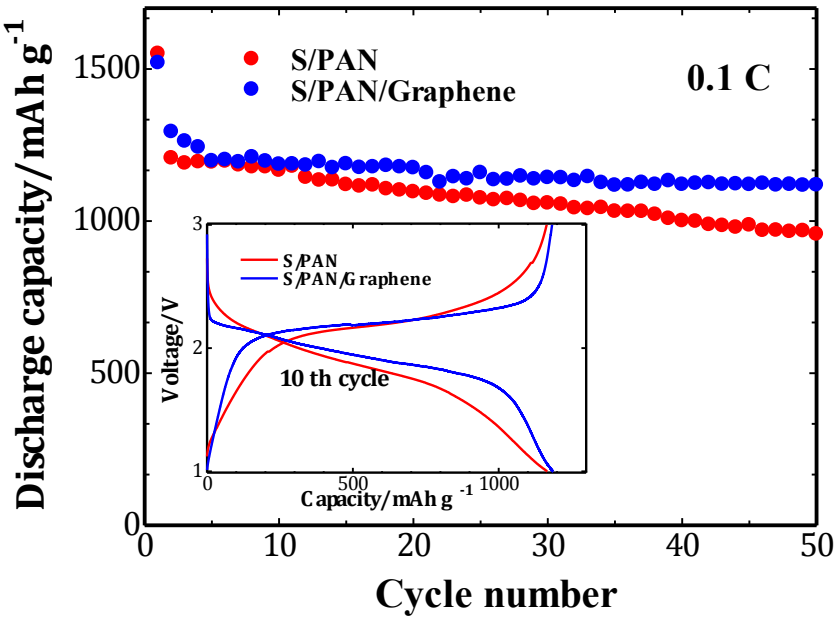

Fig 6.3 Comparative data on cyclability of lithium cells with S/PAN and S/PAN/Graphene composite cathodes at 0.1 C. Inset: 10th cycle potential profiles for these cells.

Figure 6.3 shows cycle performances of the S/PAN and S/PAN/graphene composites at 0.1 C, respectively. One can clearly see that the addition of graphene affects positively the cell reversibility as well. The lithium cell with S/PAN/graphene composite cathode delivers an initial specific capacity of 1520 mAh g^{-1} with following reversible capacity of 1293 mAh g^{-1}. Although both graphene doped and pristine composite cathodes exhibited a high Coulombic efficiency of about 100% over 50 cycles, which could be attributed to the shuttle effect suppression by PAN in the composition, the ternary composite cathode exhibits improved cyclability compared with the binary composite, which suffers from much abrupt capacity decay and the cell with S/PAN electrode loses about 38% of its initial capacity after

50 cycles of charge/discharge. The charge/discharge profiles at the 10^{th} cycle of S/PAN/graphene composite and S/PAN composite presented in the inset of **Fig. 6.3** confirm that the graphene additive reduces the charge-discharge polarization of the nanocomposite, leading to the voltage gap decrease between charge and discharge processes. This electrochemical kinetics improvement could be beneficial for the enhanced sulfur utilization compared with the low-conductive binary S/PAN composite cathode, leading to the larger energy and power density of the battery.

The results of the rate performance of a lithium cell with the S/PAN/Graphene composite cathode, shown in **Fig. 6.4**, clearly show the advantages of the graphene additive especially for the high rate operations. In the experiments presented in **Fig. 6.4a**, the cell was charged at 0.5 C and discharged at various C rates from 0.5 to 4 C. **Fig. 6.4b** represents the discharge profiles of the cell during these experiments. As expected, the cell capacity reduces upon increasing the discharge rates. However, the cell achieves a high reversible discharge capacity of 762 mAh g^{-1} even at 4 C, and the further decrease of the discharge rate to 0.5 C fully recovers the cell capacity. In these conditions, the cell delivers a reversible capacity of 1088 mAh g^{-1}, confirming a high reversibility and rate capability of the S/PAN/Graphene composite cathode.

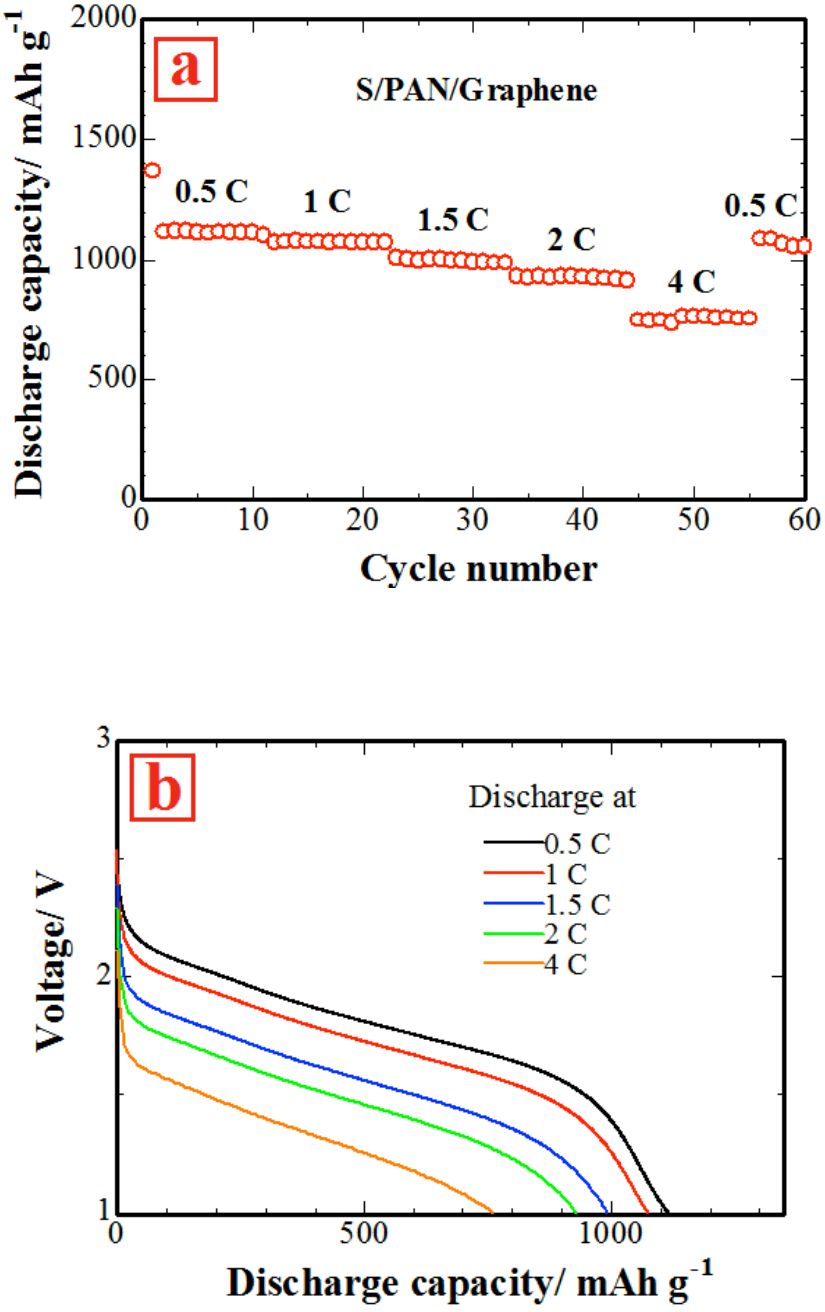

Fig 6.4 (a) Electrochemical performance of the cell with the S/PAN/Graphene ternary composite cathode at variable discharge current density tests between 0.5 to 4 C (charge at 0.5 C). **(b)** Discharge profiles of the ternary composite at different discharge rates.

Figure 6.5 represents the cyclability data for the composite cathode at 2 C. The cell exhibits very stable cyclability with a capacity retention of 100% over 100 cycles. The Coulombic efficiency of the cell was very high achieving 100% during these experiments. A discharge capacity of 603 mAh g^{-1} has been delivered at 100^{th} cycle. It can be seen that the cell performance at 2 C is superior to that of 0.1 C (**Fig. 6.5**), i.e. the graphene additive to the cathode is especially effective for the high current density operations. The exceptional high-rate performance of the S/PAN/Graphene composite is attributed to the conductivity enhancements by the highly conductive graphene additive. It could be suggested that the graphene additive significantly improves the charge transfer properties of the composite cathode. This suggestion has been confirmed by the following EIS studies.

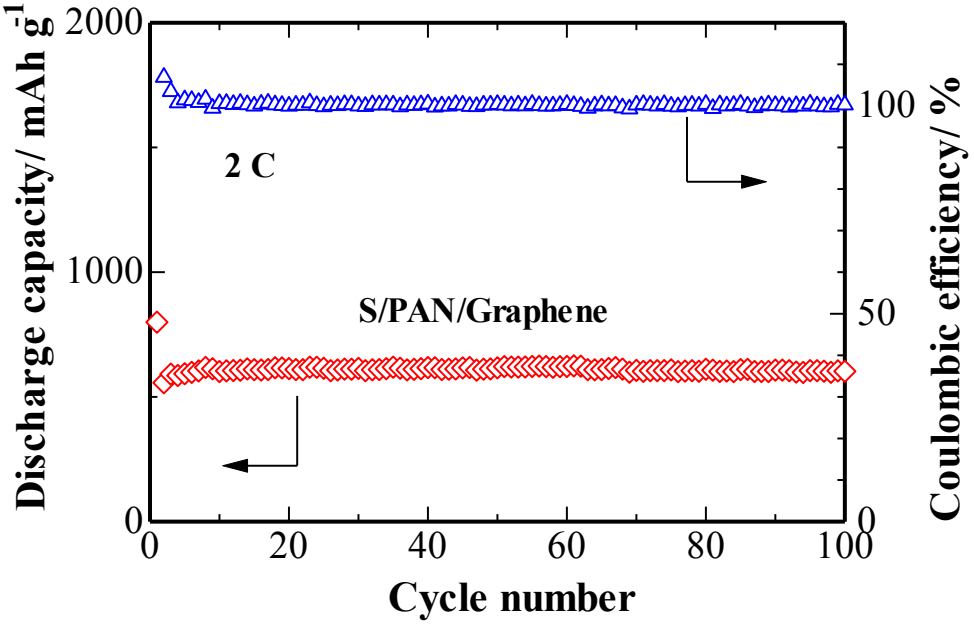

Fig 6.5 Cycle performance of the cell with the S/PAN/Graphene ternary composite cathode at 2 C.

EIS is a powerful tool to study the effect of various additives on the conductivity and charge transfer behavior in the composite cathode materials [**9**]. The comparative EIS data for the binary S/PAN and ternary S/PAN/Graphene composites measured after the first charge/discharge cycle are shown in **Fig. 6.6a**. It can be seen that for both composite cathodes the Nyquist plots are represented by a semicircle in the high-to-medium frequency range, related to the interfacial charge transfer impedance, followed by a declined line of the Warburg impedance in low frequency part attributed to the bulk diffusion resistance of the composite cathode **[9]**.

It can be seen that the charge transfer resistance of the graphene-added composite is more than 7 times lower than that of the binary composite without graphene, which supports our suggestion on the conducting property enhancement of the composite cathode by the graphene additive made above based on the charge-discharge tests results. Considering excellent conductivity of graphene [**10, 11**], this charge transfer enhancement effect by graphene could be considered as one of the main reasons of the electrochemical performance enhancement of the ternary composite compared with its binary counterpart.

The EIS equivalent circuit fitting conducted for the fresh and cycled cell with the ternary composite (similar data has been obtained for the binary composite), has shown that the EIS data before cycling is best fitted (fitting good ness close to 1) with the equivalent circuit represented by a sequence of the elements $R_1 + Q_1/R_2 + Q_2/R_3 + W$ (**Fig. 6.6b**), i.e. as one consisting of two high-to-medium circuit components [**12**]. In this circuit, the element Q_1/R_2 is attributed to the electrode/electrolyte interface impedance and the Q_2/R_3 component is related to the charge transfer resistance **[12, 13]**. The best fitting equivalent circuit has been

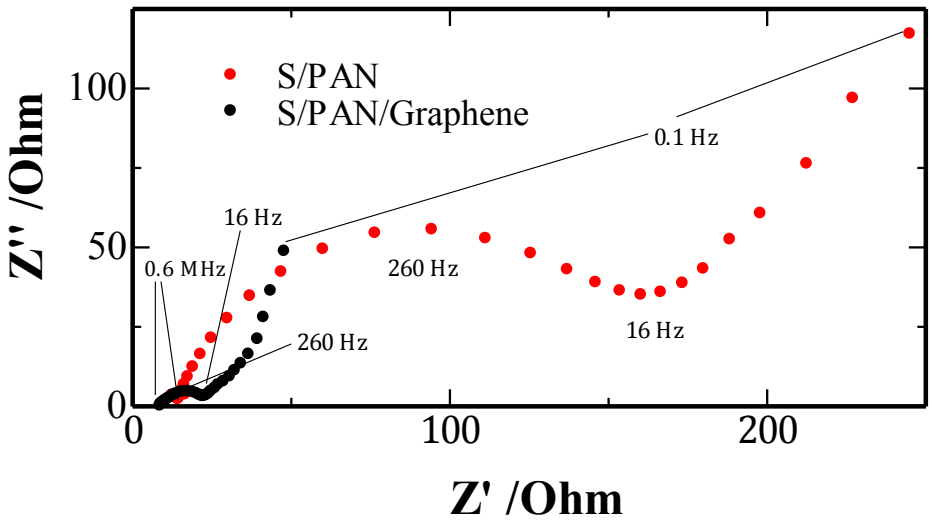

(a)

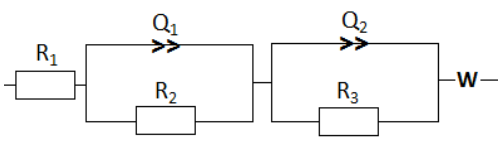

(b)

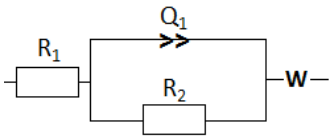

(c)

Fig 6.6 (a) Nyquist plots of the cell with the S/PAN and S/PAN/Graphene composite cathodes. The equivalent circuits for **(b)** fresh and **(c)** cycled S/PAN/Graphene composite cathode.

changed after the initial cycle to a simple Randles circuit $R_1 + Q_2/R_3 + W$ (**Fig. 6.6c**) and kept its configuration upon following cycling. This transformation could be due to the inclusion of the Q_1/R_2 component into the relatively bigger Q_2/R_3 component due to the formation of the surface conductive layer (SEI).

The EIS equivalent circuit fitting data has been used to analyze the effect of the graphene additive to the composite cathode on the cathode performance. **Figure 6.7** shows the trends in the charge transfer impedance change upon cycling in both the graphene added

(**Fig. 6.7**) and the pristine composite cathodes (inset of **Fig. 6.7**). As it was mentioned above, the charge transfer resistance (CTR) of the ternary composite cathode is much lower than that of the binary counterpart, and for the ternary composite cathode CTR is stabilized upon several initial cycles and does not change remarkably upon following cycling. In contrast, the charge transfer impedance of the binary composite cathode grows with the cycle number close to linearly. These results allow us to suggest that the graphene addition to the composite cathode remarkably enhances and stabilizes the charge transfer conditions in the system, which results in the cell performance improvement.

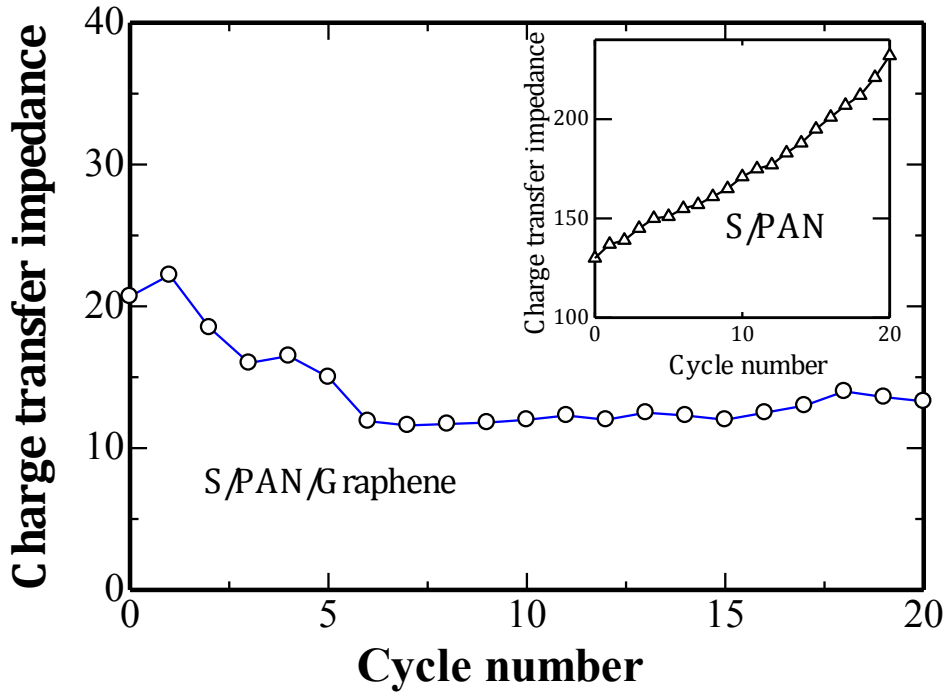

Fig 6.7 Charge transfer impedance change trends for the S/PAN/Graphene ternary composite cathode. Inset: Charge transfer impedance change for the S/PAN binary composite cathode.

6.4 Summary

A novel sulfur/polyacrylonitrile/graphene nanocomposite has been successfully synthesized via a simple combination of ballmilling with low temperature heat treatment. The composite particles were homogeneously distributed over the graphene nanoflakes serving as nano-current collectors for the S/PAN composite particles. The graphene has remarkably enhanced its conductivity, which resulted in a drastic improvement of the electrochemical performance of the resulting ternary S/PAN/Graphene nanocomposite. The cell demonstrated very stable cycling and high reversibility upon variable current density tests between 0.5 to 4 C, fully recovering its capacity upon reducing the C rate back to 0.5 C after cycling at the higher current densities. The cell exhibited about 100% capacity retention upon prolonged cycling at 2 C, delivering a reversible capacity of 603 mAh g^{-1}. It was shown that the graphene additive is especially effective for high current operations when the ternary composite exhibited better cyclability compared with the low current tests. This enhancement was attributed to the graphene additive effect on the charge transfer properties of the composite, and the EIS equivalent circuit fitting and data analysis has confirmed this suggestion.

A simple synthetic route of the sulfur based composite with the graphene additive was shown to be a versatile technique to prepare cathodes for high performance lithium/sulfur rechargeable batteries.

Chapter 7
Final Conclusions and Future Directions

Sulfur cathode have advantages over conventional cathodes for lithium batteries, but significant challenges need to be overcome before it can be employed in commercial lithium batteries. Different approaches for the preparation of improved sulfur-based composite cathodes were described in this thesis. **Table 7.1** shows a list of all composites prepared with indication of respective reference when applicable.

The experimental results indicate that the proposed methods constitute an important contribution in the development of the high capacity cathode for rechargeable Li/S battery technology. Furthermore, the innovative concept of sulfur/conductive polymer/conductive carbon ternary composites developed in this work may be used to prepare akin composites, such as sulfur/polyaniline/carbon nanotube and sulfur/polythiophene/graphene, which could lead to the development of new sulfur-based composites for high energy density applications. In particular, exploration of alternative polymeric matrices with high sulfur absorption ability is of importance for the attainment of composites that possess higher loading of sulfur, to increase the specific energy density of the cathode. Noteworthy, the techniques described here have the advantage of being reproducible, simple and inexpensive, compared with most procedures reported in the literature.

Table 7.1 The list of the sulfur composite from our work and recent publications.

NO. ★	Composite	NO. ●	Reference Journal
1	S/PPy on Ni foam	**1**	ACS Nano 2011, 5, 9187-9193
2	S/PPy on carbon foil	**2**	Chem. Mater. 2012, 24, 3081-3087
3	PPy@S	**3**	J. Phys. Chem. C 2011, 115, 24411-24417
4	S/PPy/MWNT	**4**	Nano Lett. 2011, 11, 2644-2647
5	S/PPy/GNS	**5**	J. Power Sources 2011, 196, 6951-6955
6	S/PAN/$Mg_{0.6}Ni_{0.4}O$	**6**	Solid State Ionics 2011, 192, 347-350
7	S/PAN/Graphene	**7**	J. Power Sources 2012, 206, 409-413
		8	RSC Adv. 2012, 2, 5927-5929
		9	J. Electrochem. Soc. 2013, 160, A805-A810
		10	Solid State Ionics 2013, 238, 44-49
		11	J. Power Sources, 2013, 241, 61-69

As shown in **Fig. 7.1**, after 40 cycles, the cell containing S/PAN/Graphene composite still delivers discharge capacities of 1200 mAh g^{-1}. This development represents a promising step towards viable Li/S batteries. However, many issues remain unsolved and intensive research efforts are needed to address them, for example:

- Sulfur loading should be significantly increased to improve overall specific energy of the composite while maintaining good cycle life and cathode utilization. The typical

sulfur content, both in this study and in the majority of literature reports, is 40-65 wt% while traditional battery materials require much less than 20 wt% additives. A high cell specific energy can be obtained only at elevated sulfur loadings and when good utilization is obtained. Novel approaches, leading to sulfur contents above 75%, are needed to realize a Li/S battery with volumetric energy density well beyond the limit of conventional Li-ion batteries.

- The current Li/S batteries have been limited to a conventional cell configuration consisting of sulfur as the positive electrode, lithium metal as the negative electrode and a solution of a lithium salt in aprotic organic solvents as the electrolyte. A lithium metal-free anode should be developed to avoid the safety concerns and low Coulombic efficiency of the lithium metal anode.
- Along with safety enhancement, replacement of the conventional, liquid-based electrolyte with a polymer membrane offers the advantage of much simplified fabrication and modularity in design.
- Since polysulfides are soluble in the electrolyte, more issues may arise related to self-discharge and degradation at high or low temperature. These effects should be considered in future studies.

Although many obstacles still need to be overcome before the commercialization of lithium/sulfur batteries, its high theoretical energy density far exceeds other conventional rechargeable battery systems and justifies present and future research and development efforts. Major advances in both performance enhancement and mechanism elucidation of

lithium/sulfur batteries have been reported. It is believed that further investigation will eventually lead to the practical application of Li/S batteries in the near future.

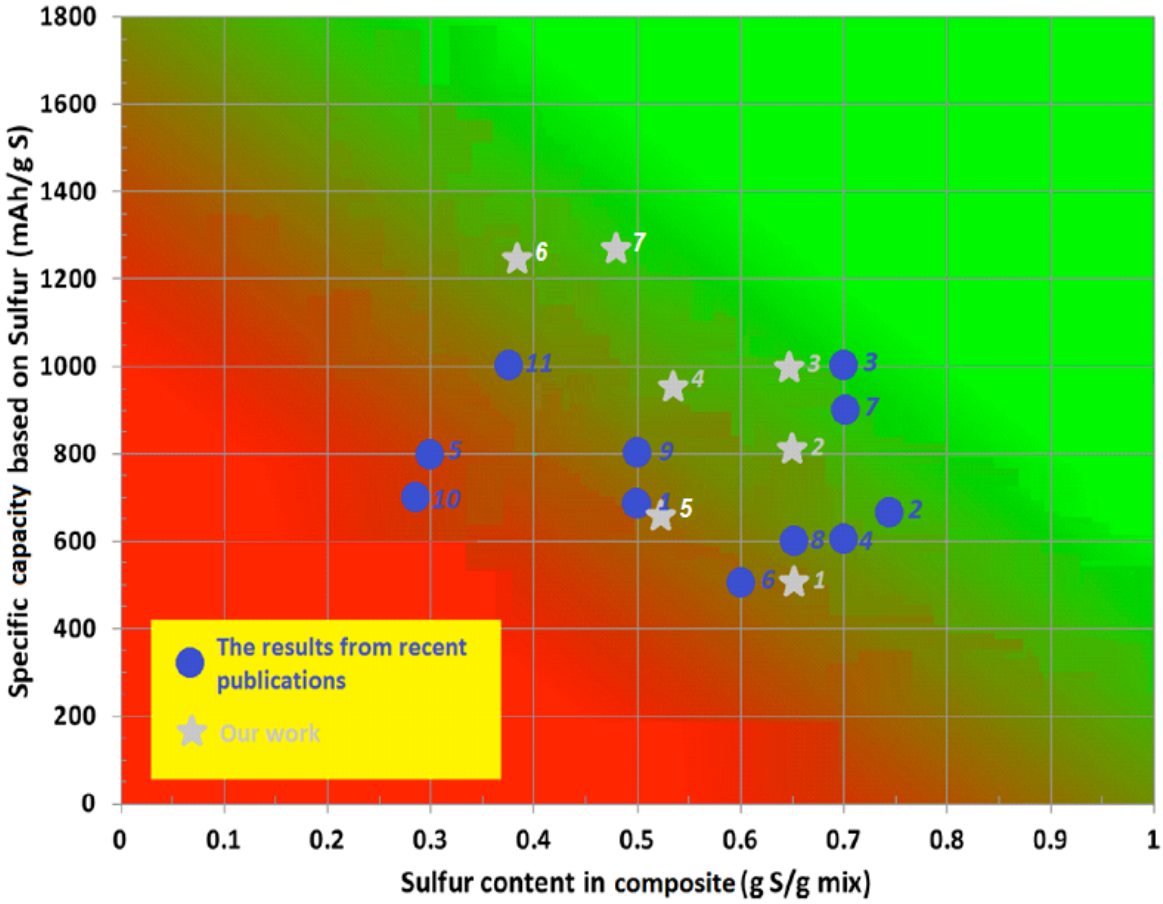

Fig 7.1 The electrochemical performance of the Li/S cells from our work and recent publications are shown in the Figure for comparison purposes, where the 40th cycle discharge capacity at 0.1 C and content of Sulfur in the cathode are reported.

Contributions to the research field

1. Y. Zhang, Y. Zhao, A. Konarov, D. Gosselink, H. G. Soboleski, P. Chen, Journal of Power Sources, 2013 (241) 517-521.
2. Y. Zhang, Y. Zhao, Z. Bakenov, M. R. Babaa, A. Konarov, C. Ding, P. Chen, Journal of The Electrochemical Society, 2013 (160) A1194-A1198.
3. Y. Zhang, Y. Zhao, A. Yermukhambetova, Z. Bakenov, P. Chen, Journal of Material Chemistry A, 2013 (1) 295-301.
4. Y. Zhang, Y. Zhao, A. Konarov, D. Gosselink, H. G. Soboleski, P. Chen, Solid State Ionics, 2013 (238) 30-35.
5. Y. Zhang, Y. Zhao, K. E. K. Sun, P. Chen, The Open Materials Science Journal, 2011 (5) 215-221.
6. Y. Zhang, Z. Bakenov, Y. Zhao, A. Konarov, T. N. L. Doan, K. E. K. Sun, A. Yermukhambetova, P. Chen, Powder Technology, 2013 (235) 248-255.
7. Y. Zhang, Z. Bakenov, Y. Zhao, A. Konarov, T. N. L. Doan, M. Malik, T. Paron, P. Chen, Journal of Power Sources, 2012 (208) 1-8.
8. Y. Zhang, Z. Bakenov, Y. Zhao, A. Konarov, Q. Wang, P. Chen, Ionics, submitted.
9. Y. Zhang, Y. Zhao, A. Konarov, D. Gosselink, Z. Li, P. Chen, Journal of Nanoparticle Research, in revision.
10. Y. Zhao, Y. Zhang, Z. Bakenov, P. Chen, Solid State Ionics, 2013 (234) 40-45.
11. Y. Zhao, Y. Zhang, D. Gosselink, T. N. L. Doan, M. Sadhu , H. J. Cheang, P. Chen, Membranes, 2012 (2) 553-564.

12. K. Jeddi, Y. Zhao, Y. Zhang, A. Konarov, P. Chen, Journal of The Electrochemical Society, 2013 (160) A1052-1060.
13. T. N. L. Doan, M. Ghaznavi, Y. Zhao, Y. Zhang, A. Konarov, M. Sadhu, R. Tangirala, P. Chen, Journal of Power Sources, 2013 (241) 61-69.
14. T. N. L. Doan, M. Ghaznavi, A. Konarov, Y. Zhang, P. Chen, Journal of Solid State Electrochemistry, accepted.
15. M. Li, J. Li, K. Li, Y. Zhao, Y. Zhang, D. Gosselink, P. Chen, Journal of Power Sources, 2013 (240) 659-666.

Copyright Permissions

Title: One-step synthesis of branched sulfur/polypyrrole nanocomposite cathode for lithium rechargeable batteries

Author: Yongguang Zhang,Zhumabay Bakenov,Yan Zhao,Aishuak Konarov,The Nam Long Doan,Muhammad Malik,Todd Paron,P. Chen

Publication: Journal of Power Sources

Publisher: Elsevier

Date: 15 June 2012

Order Completed

Thank you very much for your order.

This is a License Agreement between Yongguang Zhang ("You") and Elsevier ("Elsevier"). The license consists of your order details, the terms and conditions provided by Elsevier, and the payment terms and conditions.

Get the printable license.

License date	Jun 17, 2013
Licensed content publisher	Elsevier
Licensed content publication	Journal of Power Sources
Licensed content title	One-step synthesis of branched sulfur/polypyrrole nanocomposite cathode for lithium rechargeable batteries
Licensed content author	Yongguang Zhang,Zhumabay Bakenov,Yan Zhao,Aishuak Konarov,The Nam Long Doan,Muhammad Malik,Todd Paron,P. Chen
Licensed content date	15 June 2012
Licensed content volume number	208
Number of pages	8
Type of Use	reuse in a thesis/dissertation
Portion	full article
Format	both print and electronic
Are you the author of this Elsevier article?	Yes
Will you be translating?	No
Order reference number	
Title of your thesis/dissertation	Sulfur based Composite Cathode Materials for Rechargeable Lithium Batteries
Expected completion date	Aug 2013
Elsevier VAT number	GB 494 6272 12
Permissions price	0.00 USD
VAT/Local Sales Tax	0.00 USD
Total	0.00 USD

ORDER MORE... CLOSE WINDOW

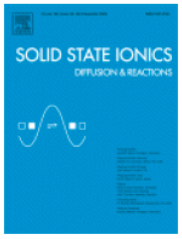

Title: A novel sulfur/polypyrrole/multi-walled carbon nanotube nanocomposite cathode with core–shell tubular structure for lithium rechargeable batteries

Author: Yongguang Zhang,Yan Zhao,The Nam Long Doan,Aishuak Konarov,Denise Gosselink,Hayden Greentree Soboleski,P. Chen

Publication: Solid State Ionics

Publisher: Elsevier

Date: 1 May 2013

Order Completed

Thank you very much for your order.

This is a License Agreement between Yongguang Zhang ("You") and Elsevier ("Elsevier"). The license consists of your order details, the terms and conditions provided by Elsevier, and the payment terms and conditions.

Get the printable license.

License date	Jun 17, 2013
Licensed content publisher	Elsevier
Licensed content publication	Solid State Ionics
Licensed content title	A novel sulfur/polypyrrole/multi-walled carbon nanotube nanocomposite cathode with core–shell tubular structure for lithium rechargeable batteries
Licensed content author	Yongguang Zhang,Yan Zhao,The Nam Long Doan,Aishuak Konarov,Denise Gosselink,Hayden Greentree Soboleski,P. Chen
Licensed content date	1 May 2013
Licensed content volume number	238
Number of pages	6
Type of Use	reuse in a thesis/dissertation
Portion	full article
Format	both print and electronic
Are you the author of this Elsevier article?	Yes
Will you be translating?	No
Order reference number	
Title of your thesis/dissertation	Sulfur based Composite Cathode Materials for Rechargeable Lithium Batteries
Expected completion date	Aug 2013
Elsevier VAT number	GB 494 6272 12
Permissions price	0.00 USD
VAT/Local Sales Tax	0.00 USD
Total	0.00 USD

ORDER MORE... CLOSE WINDOW

Title: A novel nano-sulfur/polypyrrole/graphene nanocomposite cathode with a dual-layered structure for lithium rechargeable batteries

Author: Yongguang Zhang,Yan Zhao,Aishuak Konarov,Denise Gosselink,Hayden Greentree Soboleski,P. Chen

Publication: Journal of Power Sources

Publisher: Elsevier

Date: 1 November 2013

Order Completed

Thank you very much for your order.

This is a License Agreement between Yongguang Zhang ("You") and Elsevier ("Elsevier"). The license consists of your order details, the terms and conditions provided by Elsevier, and the payment terms and conditions.

Get the printable license.

License date	Jun 17, 2013
Licensed content publisher	Elsevier
Licensed content publication	Journal of Power Sources
Licensed content title	A novel nano-sulfur/polypyrrole/graphene nanocomposite cathode with a dual-layered structure for lithium rechargeable batteries
Licensed content author	Yongguang Zhang,Yan Zhao,Aishuak Konarov,Denise Gosselink,Hayden Greentree Soboleski,P. Chen
Licensed content date	1 November 2013
Licensed content volume number	241
Number of pages	5
Type of Use	reuse in a thesis/dissertation
Portion	full article
Format	both print and electronic
Are you the author of this Elsevier article?	Yes
Will you be translating?	No
Order reference number	
Title of your thesis/dissertation	Sulfur based Composite Cathode Materials for Rechargeable Lithium Batteries
Expected completion date	Aug 2013
Elsevier VAT number	GB 494 6272 12
Permissions price	0.00 USD
VAT/Local Sales Tax	0.00 USD
Total	0.00 USD

RSC | Advancing the Chemical Sciences

Royal Society of Chemistry
Thomas Graham House
Science Park
Milton Road
Cambridge
CB4 0WF

Tel: +44 (0)1223 420 066
Fax: +44 (0)1223 423 623
Email: contracts-copyright@rsc.org

www.rsc.org

Acknowledgements to be used by RSC authors

Authors of RSC books and journal articles can reproduce material (for example a figure) from the RSC publication in a non-RSC publication, including theses, without formally requesting permission providing that the correct acknowledgement is given to the RSC publication. This permission extends to reproduction of large portions of text or the whole article or book chapter when being reproduced in a thesis.

The acknowledgement to be used depends on the RSC publication in which the material was published and the form of the acknowledgements is as follows:

- For material being reproduced from an article in *New Journal of Chemistry* the acknowledgement should be in the form:
    - [Original citation] - Reproduced by permission of The Royal Society of Chemistry (RSC) on behalf of the Centre National de la Recherche Scientifique (CNRS) and the RSC
- For material being reproduced from an article *Photochemical & Photobiological Sciences* the acknowledgement should be in the form:
    - [Original citation] - Reproduced by permission of The Royal Society of Chemistry (RSC) on behalf of the European Society for Photobiology, the European Photochemistry Association, and RSC
- For material being reproduced from an article in *Physical Chemistry Chemical Physics* the acknowledgement should be in the form:
    - [Original citation] - Reproduced by permission of the PCCP Owner Societies
- For material reproduced from books and any other journal the acknowledgement should be in the form:
    - [Original citation] - Reproduced by permission of The Royal Society of Chemistry

The acknowledgement should also include a hyperlink to the article on the RSC website.

The form of the acknowledgement is also specified in the RSC agreement/licence signed by the corresponding author.

Except in cases of republication in a thesis, this express permission does not cover the reproduction of large portions of text from the RSC publication or reproduction of the whole article or book chapter.

A publisher of a non-RSC publication can use this document as proof that permission is granted to use the material in the non-RSC publication.

VAT Registration Number: GB 342 1764 71 Registered Charity Number: 207890

References

Chapter 1

[1]Winter M, Brodd RJ. What are batteries, fuel cells and supercapacitors. Chemical Reviews 2004; 104: 4245-69.

[2]Bruce PG. Energy storage beyond the horizon: rechargeable lithium batteries. Solid State Ionics 2008; 179: 752-60.

[3]Tarascon JM, Armand M. Issues and challenges facing rechargeable lithium batteries. Nature 2001; 414: 359-67.

[4]Armand M, Tarascon JM. Building better batteries. Nature 2008; 451: 652-7.

[5]Whittingham MS. Lithium batteries and cathode materials. Chemical Reviews 2004; 104: 4271-302.

[6]Ji XL, Lee KT, Nazar LF. A highly ordered nanostructured carbon-sulphur cathode for lithium-sulphur batteries. Nature Materials 2009; 8: 500-6.

[7]Sun YK, Myung ST, Park BC, Prakash J, Belharoua I, Amine K. High-energy cathode material for long-life and safe lithium batteries. Nature Materials 2009; 8: 320-4.

[8]Yang Y, McDowell MT, Jackson A, Cha JJ, Hong SS, Cui Y. New nanostructured Li_2S/silicon rechargeable battery with high specific energy. Nano Letters 2010; 10: 1486-91.

[9]Tischer RP. The Sulfur Electrode. Academic Press, New York, 1983.

[10]Song MK, Cairns EJ, Zhang Y. Lithium/sulfur batteries with high specific energy: old challenges and new opportunities. Nanoscale 2013; 5: 2186-204.

[11]Kumaresan K, Mikhaylik Y, Whitea RE. A mathematical model for a lithium-sulfur cell. J Electrochem Soc 2008; 155: A576-82.

[12]Yang Y, Zheng G, Cui Y. Nanostructured sulfur cathodes. Chem Soc Rev 2013; 42: 3018-32.

[13]Manthiram A, Fu Y, Su YS. Challenges and prospects of lithium-sulfur batteries. Account Chem Res 2013; 46: 1125-34.

[14]Zhang B, Qin X, Li GR, Gao XP. Enhancement of long stability of sulfur cathode by encapsulating sulfur into micropores of carbon spheres. Energy Environ Sci 2010; 3: 1531-7.

[15]Schuster J, He G, Mandlmeier B, Yim T, Lee KT, Bein T, Nazar LF. Spherical ordered mesoporous carbon nanoparticles with high porosity for lithium-sulfur batteries. Angew Chem Int Ed 2012; 51: 3591-5.

[16]Jayaprakash N, Shen J, Moganty SS, Corona A, Archer LA. Porous hollow carbon@sulfur composites for high-power lithium-sulfur batteries. Angew Chem Int Ed 2011; 50: 5904-8.

[17]Ji L, Rao M, Zheng H, Zhang L, Li Y, Duan W, Guo J, Cairns EJ, Zhang Y. Graphene oxide as a sulfur immobilizer in high performance lithium/sulfur cells. J Am Chem Soc 2011; 133: 18522-5.

[18]Ji L, Rao M, Aloni S, Wang L, Cairns EJ, Zhang Y. Porous carbon nanofiber-sulfur composite electrodes for lithium/sulfur cells. Energy Environ Sci 2011; 4: 5053-9.

[19]Zheng G, Yang Y, Cha JJ, Hong SS, Cui Y. Hollow carbon nanofiber-encapsulated sulfur cathodes for high specific capacity rechargeable lithium batteries. Nano Lett 2011; 11: 4462-7.

Chapter 2

[1]Zhang Y, Wang LZ, Zhang A, Song Y, Li X, Feng H, Wu X, Du P. Novel V_2O_5/S composite cathode material for the advanced secondary lithium batteries. Solid State Ionics 2010; 181: 835-8.

[2]Zhang Y, Zhang AQ, Gui YH, Wang LZ, Wu XB, Zhang CF, Zhang P. Application of biphenyl additive in electrolyte for liquid state Al-plastic film lithium-ion batteries. J Power Sources 2008; 185: 492-500.

[3]Xiang JF, Chang CX, Zhang F, Sun JT. Effects of Mg doping on the electrochemical properties of $LiNi_{0.8}Co_{0.2}O_2$ cathode material. J Alloys Compd 2009; 475: 483-7.

[4]Chen XJ, Cao GS, Zhao XB, Tu JP, Zhu TJ. Electrochemical performance of $LiFe_{1-x}V_xPO_4$/carbon composites prepared by solid-state reaction. J Alloys Compd 2008; 463: 385-9.

[5]Kolosnitsyn VS, Karaseva EV. Lithium-Sulfur Batteries: Problems and Solutions. Russ J Electrochem 2008; 44: 506-9.

[6]Besenhard JO. Handbook of Battery Materials. Wiley: New York; 1998.

[7]Jin B, Kim JU, Gu HB. Electrochemical properties of lithium-sulfur batteries. J Power Sources 2003; 117: 148-52.

[8]Kobayashi T, Imade Y, Shishihara D et al. All solid-state battery with sulfur electrode and thio-LISICON electrolyte. J Power Sources 2008; 182: 621-5.

[9]Ji XL, Lee KT, Nazar LF. A highly ordered nanostructured carbon-sulphur cathode for lithium-sulphur batteries. Nat Mater 2009; 8: 500-6.

[10]Song MS, Han SC, Kim HS, Kim JH, Kim KT, Kang YM, Ahn HJ, Dou SX, Lee JY. Effects of nano-sized adsorbing material on electrochemical properties of sulfur cathodes for Li/S secondary batteries. J Electrochem Soc 2004; 151: A791-5.

[11]Yamin H, Gorenshtein A, Penciner J, Sternberg Y, Peled E. Lithium Sulfur Battery Oxidation/Reduction Mechanisms of Polysulfides in THF Solutions. J Electrochem Soc 1988; 135: 1045-8.

[12]Yamin H, Penciner J, Gorenshtain A, Elam M, Peled E. The electrochemical behavior of polysulfides in tetrahydrofuran. J Power Sources 1985; 14: 129 -34.

[13]Marmorstein D, Yu TH, Striebel KA, Mclamon FR, Hou J, Cairns EJ. Electrochemical performance of lithium/sulfur cells with three different polymer electrolytes. J Power Sources 2000; 89: 219-26.

[14]Degott P, Ph.D. Thesis, l'Institut National Polytechnique de Grenoble, France; 1986.

[15]Chu MY. Rechargeable positive electrode. US5523179, June 4, 1996.

[16]Eichinger G, Besenhard J. High energy density lithium cells. Part II. Cathodes and complete cells. J Electroanal Chem 1976; 72: 1-31.

[17]Murphy DW, Carides JN. Low Voltage Behavior of Lithium/Metal Dichalcogenide Topochemical Cells. J Electrochem Soc 1979; 126: 349-51.

[18]Ho CB, Ph.D. Thesis, Korea Advance Institute of Science and Technology; 2001.

[19]Nimon ES, Sukeshini M, Visco SJ: The 11th International Meeting on Lithium Batteries; June 2002; Monterey, California, US; 2002.

[20]Yin L, Wang JL, Lin F, Yang J, Nuli Y. Polyacrylonitrile/graphene omposite as a precursor to a sulfur-based cathode material for high-rate rechargeable Li-S batteries. Energy Environ Sci 2012; 5: 6966-72.

[21]Wang JL, Yang J, Xie JY, Xu NX, Li Y. Sulfur-carbon nano-composite as cathode for rechargeable lithium battery based on gel electrolyte. Electrochem Commun 2002; 4: 499-502.

[22]Bonhote P, Dias AP, Papageorgiou N, Kalyanasundaram K, Gratzel M. Hydrophobic, highly conductive ambienttemperature molten salts. Inorg Chem 1996; 35: 1168-78.

[23]Liang CD, Dudney NJ, Howe JY. Hierarchically Structured Sulfur/Carbon Nanocomposite Material for High-Energy Lithium Battery. Chem Mater 2009; 21: 4724-30.

[24]Wang XQ, Liang CD, Dai S. Facile synthesis of ordered mesoporous carbons with high thermal stability by self-assembly of resorcinol-formaldehyde and block copolymers under highly acidic conditions. Langmuir 2008; 24: 7500-5.

[25]Liang CD, Hong KL, Guiochon GA, Guiochon GA, Mays JW, Dai S. Synthesis of a large-scale highly ordered porous carbon film by self-assembly of block copolymers. Chem Int Ed 2004; 43: 5785-9.

[26]Steinhart M, Liang CD, Lynn GW, Gosele U, Dai S. Direct Synthesis of Mesoporous Carbon Microwires and Nanowires. Chem Mater 2007; 19: 2383-5.

[27]Liang CD, Dai S. Synthesis of mesoporous carbon materials via enhanced hydrogen-bonding interaction. J Am Chem Soc 2006; 128: 5316-7.

[28]Wang J, Chew SY, Zhao ZW, Ashraf S, Wexler D, Chen J, Ng SH, Chou SL, Liu HK. Sulfur-mesoporous carbon composites in conjunction with a novel ionic liquid electrolyte for lithium rechargeable batteries. Carbon 2008; 46: 229-35.

[28]Wang JL, Yang J, Wan CR, Du K, Xie J, Xu N. Sulfur composite cathode materials for rechargeable Lithium batteries. Adv Funct Mater 2003; 13: 487-92.

[29]Choi YJ, Kim KW, Ahn HJ, Ahn HJ, Ahn JH. Improvement of cycle property of sulfur electrode for lithium/sulfur battery. J Alloys Compd 2008; 449: 313-6.

[30]Ji LW, Rao M, Aloni S, Wang L, Cairns EJ, Zhang Y. Porous carbon nanofiber-sulfur composite electrodes for lithium/sulfur cells. Energy Environ Sci 2011; 4: 5053-9.

[31]Han SC, Song MS, Lee H, Kim HS, Ahn HJ, Lee JY. Effect of multiwalled carbon nanotubes on electrochemical properties of Lithium/Sulfur rechargeable batteries. J Electrochem Soc 2003; 150: A889-93.

[32]Chen JJ, Zhang Q, Shi YN, Qin LL, Cao Y, Zheng MS, Dong QF. A hierarchical architecture S/MWCNT nanomicrosphere with large pores for lithium sulfur batteries. Phys Chem Chem Phys 2012; 14: 5376-82.

[33]Zhang B, Qin X, Li GR, Gao XP. Enhancement of long stability of sulfur cathode by encapsulating sulfur into micropores of carbon spheres. Energy Environ Sci 2010; 3: 1531-7.

[34]Evers S, Nazar LF. Graphene-Enveloped Sulfur in a One Pot Reaction: a Cathode with Good Coulombic Efficiency and High Practical Sulfur Content. Chem Commun 2012; 48: 1233-5.

[35]Li NW, Zheng M, Lu HL, Hu Z, Shen C, Chang X, Ji G, Cao J, Shi Y. High-rate lithium-sulfur batteries promoted by reduced graphene oxide coating. Chem Commun 2012; 48: 4106-8.

[36]Wang J, Chen J, Konstantinov K, Zhao L, Ng SH, Wang GX, Guo ZP, Liu HK. Sulphur-polypyrrole composite positive electrode materials for rechargeable lithium batteries. Electrochim Acta 2006; 51: 4634-8.

[37]Zhang XT, Zhang J, Song WH, Liu Z. Controllable Synthesis of Conducting Polypyrrole Nanostructures. J Phys Chem B 2006; 110: 1158-65.

[38]Sun MM, Zhang SC, Jiang T, Zhang L, Yu J. Nano-wire networks of sulfur-polypyrrole composite cathode materials for rechargeable lithium batteries. Electrochem Commun 2008; 10: 1819-22.

[39]Liang X, Liu Y, Wen ZY, Huang L, Wang X, Zhang H. A nano-structured and highly ordered polypyrrole-sulfur cathode for lithium-sulfur batteries. J Power Sources 2011; 196: 6951-5.

[40]Wei W, Wang JL, Zhou LJ, Yang J, Schumann B, Nuli Y. CNT enhanced sulfur composite cathode material for high rate lithium battery. Electrochem Commun 2011; 13: 399-402.

[41]Cheon SE, Ko KS, Cho JH, Kim SW, Chin EY, Kim HT. Rechargeable Lithium Sulfur Battery. J Electrochem Soc 2003; 150: A796-9.

[42]Liang X, Wen Z, Liu Y, .Wu M, Jin J, Zhang H, Wu X. Improved cycling performances of lithium sulfur batteries with $LiNO_3$-modified electrolyte. J Power Sources 2011; 196: 9839-43.

[43]Choi JW, Kim JK, Cheruvally G, Ahn JH, Ahn HJ, Kim KW. Rechargeable lithium/sulfur battery with suitable mixed liquid electrolytes. Electrochimica Acta 2007; 52: 2075-82.

[44]Chang DR, Lee SH, Kim SW, Kim HT. Binary electrolyte based on tetra(ethylene glycol) dimethyl ether and 1,3-dioxolane for lithium-sulfur battery. J Power Sources 2002; 112: 452-60.

[45]Kim S, Jung Y, Park SJ. Effects of imidazolium salts on discharge performance of rechargeable lithium-sulfur cells containing organic solvent electrolytes. J Power Sources 2005; 152: 272-7.

[46]Choi JW, Cheruvally G, Kim DS, Ahn JH, Kim KW, Ahn HJ. Rechargeable lithium/sulfur battery with liquid electrolytes containing toluene as additive. J Power Sources 2008; 183: 441-5.

[47]Song JY, Wang YY, Wan CC. Review of gel-type polymer electrolytes for lithium-ion batteries. J Power Sources 1999; 77: 183-97.

[48]Gray FM. Solid polymer electrolytes-fundamentals and technological applications, VCH: New York, United States, 1991.

[49]Scrosati B. Applications of electroactive polymers, Chapman Hall: London, UK, 1993.

[50]Gray FM. Polymer electrolytes, The Royal Society of Chemistry: Canterbury, UK, 1997.

[51]MacCallum JR, Vincent CA. Polymer electrolytes reviews-I, Elsevier: London, UK, 1987.

[52]Idris NH, Rahman MM, Wang JZ, Liu HK. Microporous gel polymer electrolytes for lithium rechargeable battery application. J Power Sources 2012; 201: 294-300.

[53]Scrosati B. Applications of electroactive polymers, Chapman Hall: London, UK, 1993.

[54]Gray FM. Polymer electrolytes, The Royal Society of Chemistry: Canterbury, UK, 1997.

[55]MacCallum JR, Vincent CA. Polymer electrolytes reviews-II, Elsevier: London, UK, 1989.

[56]Kim KM, Park NG, Ryu KS, Chang SH. Characteristics of PVdF-HFP/TiO_2 composite membrane electrolytes prepared by phase inversion and conventional casting methods. Electrochim Acta 2006; 51: 5636-44.

[57]Weston JE, Steele BCH. Effects of inert fillers on the mechanical and electrochemical properties of lithium salt-poly(ethylene oxide) polymer electrolytes. Solid State Ionics 1982; 7: 75-9.

[58]Jeon BH, Yeon JH, Kim KM, Chung IJ. Preparation and electrochemical properties of lithium-sulfur polymer batteries. J Power Sources 2002; 109: 89-97.

[59]Croce F, Persi L, Scrosati B, Serraino-Fiory F, Plichta E, Hendrickson MA. Role of the ceramic fillers in enhancing the transport properties of composite polymer electrolytes. Electrochim Acta 2001; 46: 2457-61.

[60]Dissanayake MAKL, Jayathilake PARD, Bokalawela RSP, Albinsson I, Mellander BE. Effect of concentration and grain size of alumina filler on the ionic conductivity enhancement of the $(PEO)_9LiCF_3SO_3$:Al_2O_3 composite polymer electrolyte. J Power Sources 2003; 119-121: 409-14.

[61]Ahn JH, Wang GX, Liu HK, Dou SX. Nanoparticle-dispersed PEO polymer electrolytes for Li batteries. J Power Sources 2003; 119-121: 422-6.

[62]Appetecchi GB, Croce F, Persi L, Ronci F, Scrosati B. Transport and interfacial properties of composite polymer electrolyte. Electrochim Acta 2000; 45: 1481-90.

[63]Jayathilake PARD, Dissanayake MAKL, Albinsson I, Mellander BE. Effect of nano-porous Al_2O_3 on thermal, dielectric and transport properties of the $(PEO)_9LiTFSI$ polymer electrolyte system. Electrochim Acta 2002; 47: 3257-68.

[64]Lin CW, Hung CL, Venkateswarlu M, Hwang BJ. Influence of TiO_2 nano-particles on the transport properties of composite polymer electrolyte for lithium-ion batteries. J Power Sources 2005; 146: 397-401.

[65]Xi J, Qiu X, Ma X, Cui M, yang J, Tang X, Zhu W, Chen L. Composite polymer electrolyte doped with mesoporous silica SBA-15 for lithium polymer battery. Solid State Ionics 2005; 176: 1249-60.

[66]Chung SH, Wang Y, Persi L, Croce F, Greenbaum SG, Scrosati B, Plichta E. Enhancement of ion transport in polymer electrolytes by addition of nanoscale inorganic oxides. J Power Sources 2001; 97-98: 644-8.

[67]Croce F, Settimi L, Scrosati B. Superacid ZrO_2-added, composite polymer electrolytes with improved transport properties. Electrochem Commun 2006; 8: 364-8.

[68]Shin JH, Kim KW, Ahn HJ, Ahn JH. Electrochemical properties and interfacial stability of $(PEO)_{10}LiCF_3SO_3$-Ti_nO_{2n-1} composite polymer electrolytes for lithium/sulfur battery. Mater Sci Eng B 2002; 95: 148-56.

[69]Jeong SS, Lim YT, Choi YJ, Cho GB, Kim KW, Ahn HJ, Cho KK. Electrochemical properties of lithium sulfur cells using PEO polymer electrolytes prepared under three different mixing conditions. J Power Sources 2007; 174: 745-50.

[70]Zhu X, Wen Z, Gu Z, Lin Z. Electrochemical characterization and performance improvement of lithium/sulfur polymer batteries. J Power Sources 2005; 139: 269-73.

[71]Liang X, Wen Z, Liu Y, Zhang H, Huang L, Jin J. Highly dispersed sulfur in ordered mesoporous carbon sphere as a composite cathode for rechargeable polymer Li/S battery. J Power Sources 2011; 196: 3655-8.

[72]Wu YP, Zhang HP, Wu F, Li Z. Polymer Lithium-Ion Batteries, Chemical Industry Press: Beijing, China, 2007.

[73]Xu JJ, Ye H. Polymer gel electrolytes based on oligomeric polyether/cross-linked PMMA blends prepared via in situ polymerization. Electrochem Commun 2005; 7: 829-35.

[74]Oliver M. US Patent, 1997, 5658685.

[75]Hassoun J, Scrosati B. A High-Performance Polymer Tin Sulfur Lithium Ion Battery. Angew Chem Int Ed 2010; 49: 2371-4.

[76]Scrosati B. Lithium Polymer Electrolytes. In Advances in Lithium Ion Batteries, Schalkwijk, Scrosati, Eds.; Kluwer Academic/Plenum Publishers: New York, United States, 2002; 251-266.

[77]Appetecchi GB, Romagnoli P, Scrosati B. Composite gel membranes: a new class of improved polymer electrolytes for lithium batteries. Electrochem Commun 2001; 3: 281-4.

[78]MacDonald J, Barsoukov JR. Impedance Spectroscopy, Theory, Experiment and Application. Wiley Interscience, 2nd ed., 2005.

[79]Liu F, Hashim NA, Liu Y, Abed MRM, Li K. Progress in the production and modification of PVDF membranes. J Membrane Sci 2011; 375: 1-27.

[80]Song JY, Wang YY, Wan CC. Review of gel-type polymer electrolytes for lithium-ion batteries. J Power Sources 1999; 77: 183-97.

[81]Watanabe M, Kanba M, Matsuda H, Tsunemi K, Mizoguchi K, Tsuchida E, Shinohara I. High lithium ionic conductivity of polymeric solid electrolytes. Makromol Chem-Rapid 1981; 2: 741-4.

[82]Ryu HS, Ahn HJ, Kim KW. Discharge process of Li/PVdF/S cells at room temperature. J Power Sources 2006; 153: 360-4.

[83]Stephan AM, Nahm KS, Kulandainathan MA, Ravi G, Wilson J. Poly(vinylidene fluoride-hexafluoropropylene) (PVdF-HFP) based composite electrolytes for lithium batteries. Eur Polym J 2006; 42: 1728-34.

[84]Stephan MA, Dale T. Charge-discharge studies on a lithium cell composed of PVdF-HFP polymer membranes prepared by phase inversion technique with a nanocomposite cathode. J Power Sources 2003; 119-121: 460-7.

[85]Stephan MA, Dale T. Characterization of PVdF-HFP polymer membranes prepared by phase inversion technique I. Morphology and charge discharge studies. Electrochim Acta 2003; 48: 2143-8.

[86]Shin JH, Jung SS, Kim KW, Ahn HJ, Ahn JH. Preparation and characterization of plasticized polymer electrolytes based on the PVdF-HFP copolymer for lithium/sulfur battery. J Mater Sci-Mater El 2002; 13: 727-33.

Chapter 3

[1]Liang X, Liu Y, Wen ZY, Huang LZ, Wang XY, Zhang H. A nano-structured and highly ordered polypyrrole-sulfur cathode for lithium-sulfur batteries. J Power Sources 2011; 196: 6951-5.

[2]Wu A, Kolla H, Manohar SK. Chemical synthesis of highly conducting polypyrrole nanofiber film. Macromolecules 2005; 38: 7873-5.

[3]Sun MM, Zhang SC, Jiang T, Zhang L, Yu JH. Nano-wire networks of sulfur polypyrrole composite cathode materials for rechargeable lithium batteries. Electrochem Commun 2008; 10: 1819-22.

[4]Lei JT, Liang WB, Martin CR. Infrared investigations of pristine, doped and partially doped polypyrrole. Synth Met 1992; 48: 301-12.

[5]Cheah K, Forsyth M, Truong VT. Ordering and stability in conducting polypyrrole. Synth Met 1998; 94: 215-9.

[6]Fu HB, Xiao DB, Yao JN, Yang GQ. Nanofibers of 1,3-Diphenyl-2-pyrazoline Induced by Cetyltrimethylammonium Bromide Micelles. Angew Chem Int Edit 2003; 42: 2883-6.

[7]Taniguchi I. Powder properties of partially substituted $LiM_xMn_{2-x}O_4$ (M = Al, Cr, Fe and Co) synthesized by ultrasonic spray pyrolysis. Mater Chem Phys 2005; 92: 172-9.

[8]He X, Ren J, Wang L, Pu W, Jiang C, Wan C. Expansion and shrinkage of the sulfur composite electrode in rechargeable lithium batteries. J Power Sources 2009; 190: 154-6.

[9]Marmorstein D, Yu TH, Striebel KA, Mclarnon FR, Hou J, Cairns EJ. Electrochemical performance of lithium/sulfur cells with three different polymer electrolytes. J Power Sources 2000; 89: 219-26.

[10]Han DH, Kim BS, Choi SJ, Jung Y, Kwak J, Park SM. Time-Resolved In Situ Spectroelectrochemical Study on Reduction of Sulfur in N,N′-Dimethylformamide. J Electrochem Soc 2004; 151: E283-90.

[11]Yamin H, Gorenshtain A, Penciner J, Sternberg Y, Peled E. Lithium Sulfur Battery: Oxidation/Reduction Mechanisms of Polysulfides in THF Solutions. J Electrochem Soc 1988; 135: 1045-8.

[12]Kolosnitsyn VS, Karaseva EV. Lithium-Sulfur Batteries: Problems and Solutions. Russ J Electrochem 2008; 44: 506-9.

[13]Choi YJ, Chung YD, Baek CY, Kim KW, Ahn HJ, Ahn JH. Effects of carbon coating on the electrochemical properties of sulfur cathode for lithium/sulfur cell. J Power Sources 2008; 184: 548-52.

[14]Wang JL, Yang J, Xie JY, Xu NX, Li Y. Sulfur-carbon nano-composite as cathode for rechargeable lithium battery based on gel electrolyte. Electrochem Commun 2002; 4: 499-502.

[15]Ji XL, Lee KT, Nazar LF. A highly ordered nanostructured carbon-sulphur cathode for lithium-sulphur batteries. Nat Mater 2009; 8: 500-6.

[16]Wang J, Chew SY, Zhao ZW, Ashraf S, Wexler D, Chen J, Ng SH, Chou SL, Liu HK. Sulfur-mesoporous carbon composites in conjunction with a novel ionic liquid electrolyte for lithium rechargeable batteries. Carbon 2008; 46: 229-35.

[17]Armand M, Tarascon JM. Building better batteries. Nature 2008; 451: 652-7.

[18]Hassoun J, Scrosati B. A High-Performance Polymer Tin Sulfur Lithium Ion Battery. Angew Chem Int Ed 2010; 49: 2371-4.

[19]Ding B, Yuan C, Shen L, Xu G, Nie P, Zhang X. Encapsulating Sulfur into Hierarchically Ordered Porous Carbon as a High-Performance Cathode for Lithium-Sulfur Batteries. Chem Eur J 2013; 19: 1013-9.

[20]Zhang Y, Zhao Y, Doan TNL, Konarov A, Gosselink D, Soboleski HG, Chen P. A novel sulfur/polypyrrole/multi-walled carbon nanotube nanocomposite cathode with core-shell tubular structure for lithium rechargeable batteries. Solid State Ionics 2013; 238: 30-35.

[21]Choi YJ, Kim KW, Ahn HJ, Ahn JH. Improvement of cycle property of sulfur electrode for lithium/sulfur battery. J Alloy Compd 2008; 449: 313-6.

[22]Zhang Y, Zhao Y, Yermukhambetova A, Bakenov Z, Chen P. Ternary sulfur/polyacrylonitrile/ $Mg_{0.6}Ni_{0.4}O$ composite cathodes for high performance lithium/sulfur batteries. J Mater Chem A 2013; 1: 295-301.

[23]Fu Y, Manthiram A. Orthorhombic Bipyramidal Sulfur Coated with Polypyrrole Nanolayers As a Cathode Material for Lithium-Sulfur Batteries. J Phys Chem C 2012; 116: 8910-5.

[24]Fu Y, Manthiram A. Core-shell structured sulfur-polypyrrole composite cathodes for lithium-sulfur batteries. RSC Adv 2012; 2: 5927-9.

[25]Zhang Y, Bakenov Z, Zhao Y, Konarov A, Doan TNL, Malik M, Paron T, Chen P. One-step synthesis of branched sulfur/polypyrrole nanocomposite cathode for lithium rechargeable batteries. J Power Sources 2012; 208: 1-8.

[26]Wei W, Wang J, Zhou L, Yang J, Schumann B, Li YN. CNT enhanced sulfur composite cathode material for high rate lithium battery. Electrochem Commun 2011; 13: 399-402.

[27]Barchasz C, Mesguich F, Dijon J, Lepretre JC, Patoux S, Alloin F. Novel positive electrode architecture for rechargeable lithium/sulfur batteries. J Power Sources 2012; 211: 19-26.

[28]Wang L, He X, Li J, Gao J, Fang M, Tian G, Wang J, Fan S. J Power Sources 2013; 239: 623-7.

[29]Kim H, Lee JT, Yushin G. High temperature stabilization of lithium-sulfur cells with carbon nanotube current collector. J Power Sources 2013; 226: 256-65.

[30]Kim TK, Chen W, Wang C. Heat treatment effect of the Ni foam current collector in lithium ion batteries. J Power Sources 2011; 196: 8742-6.

[31]Sa Q, Wang Y. Ni foam as the current collector for high capacity C-Si composite electrode. J Power Sources 2012; 208: 46-51.

[32]Yao M, Okuno K, Iwaki T, Awazu T, Sakai T. Long cycle-life $LiFePO_4$/Cu-Sn lithium ion battery using foam-type three-dimensional current collector. J Power Sources 2010; 195: 2077.

[33]Ji X, Liu DY, Prendiville DG, Zhang Y, Liu X, Stucky GD. Spatially heterogeneous carbon-fiber papers as surface dendrite-free current collectors for lithium deposition. Nano Today 2012; 7: 10-20.

[34]Yu Y, Chen CH, Shui JL, Xie S. Nickel-Foam-Supported Reticular CoO-Li_2O Composite Anode Materials for Lithium Ion Batteries. Angew Chem Int Ed 2005; 44: 7085-9.

[35]Yu Y, Shi Y, Chen CH, Wang C. Facile Electrochemical Synthesis of Single-Crystalline Copper Nanospheres, Pyramids, and Truncated Pyramidal Nanoparticles from Lithia/Cuprous Oxide Composite Thin Films. J Phys Chem 2008; 112: 4176-9.

[36]Shafiei M, Alpas AT. Electrochemical performance of a tin-coated carbon fibre electrode for rechargeable lithium-ion batteries. J Power Sources 2011; 196: 7771-8.

[37]Bakenov Z, Taniguchi I. Physical and electrochemical properties of LiMnPO4/C composite cathode prepared with different conductive carbons. J Power Sources 2010; 195: 7445-51.

[38]Osaka T, Momma T, Mukoyama D, Nara H. Proposal of novel equivalent circuit for electrochemical impedance analysis of commercially available lithium ion battery. J Power Sources 2012; 205: 483-6.

[39]Hang T, Mukoyama D, Nara H, Takami N, Momma T, Osaka T. Electrochemical impedance spectroscopy analysis for lithium-ion battery using $Li_4Ti_5O_{12}$ anode. J Power Sources 2013; 222: 442-7.

[40]Xu G, Ding B, Shen L, Nie P, Han J, Zhang X. Sulfur embedded in metal organic framework-derived hierarchically porous carbon nanoplates for high performance lithium-sulfur battery. J Mater Chem A 2013; 1: 4490-6.

[41]Wu F, Wu S, Chen R, Chen J, Chen S. Sulfur-polythiophene composite cathode materials for rechargeable lithium batteries. Electrochem Solid St 2010; 13: A29-31.

[42]Boyano I, Bengoechea M, Meatza ID, Miguel O, Cantero I, Ochoteco E, Rodriguez J, Lira-Cantu M, Gomez-Romero P. Improvement in the Ppy/V_2O_5 hybrid as a cathode material for Li ion batteries using PSA as an organic additive. J Power Sources 2007; 166: 471-7.

[43]Huang YH, Goodenough JB. High-Rate LiFePO4 Lithium Rechargeable Battery Promoted by Electrochemically Active Polymers. Chem Mater 2008; 20: 7237-41.

[44]Zhang Y, Bakenov Z, Zhao Y, Konarov A, Doan TNL, Sun KEK, Yermukhambetova A,

Chen P. Effect of nanosized $Mg_{0.6}Ni_{0.4}O$ prepared by self-propagating high temperature synthesis on sulfur cathode performance in Li/S batteries. Powder Technol 2013; 235: 248-55.

[45]Li GC, Li GR, Ye SH, Gao XP. A polyaniline-coated sulfur/carbon composite with an enhanced high-rate capability as a cathode material for lithium/sulfur batteries. Adv Energy Mater 2012; 2: 1238-45.

[46]Zhao MQ, Liu XF, Zhang Q, Tian GL, Huang JQ, Zhu W, Wei F. Graphene/single-walled carbon nanotube hybrids: one-step catalytic growth and applications for high-rate Li-S batteries. ACS Nano 2012; 6: 10759-69.

Chapter 4

[1]Ruckenstein E, Sun Y. Synthesis of surface conductive polyurethane films. Synth Met 1995; 75: 79-84.

[2]Chehimi MM, Abdeljalil E. A study of the degradation and stability of polypyrrole by inverse gas chromatography, X-ray photoelectron spectroscopy, and conductivity measurements. Synth Met 2004; 145: 15-22.

[3]Wang J, Chen J, Konstantinov K, Zhao L, Ng SH, Wang GX, Guo ZP, Liu HK. Sulphur-polypyrrole composite positive electrode materials for rechargeable lithium batteries. Electrochim Acta 2006; 51: 4634-8.

[4]Liang X, Liu Y, Wen ZY, Huang LZ, Wang XY, Zhang H. A nano-structured and highly ordered polypyrrole-sulfur cathode for lithium-sulfur batteries. J Power Sources 2011; 196: 6951-5.

[5]Zhang YG, Bakenov Z, Zhao Y, Konarov A, Doan TNL, Malik M, Paron T, Chen P. One-step synthesis of branched sulfur/polypyrrole nanocomposite cathode for lithium rechargeable batteries. J Power Sources 2012; 208: 1-8.

[6]Fan J, Wan M, Zhu D, Chang B, Pan Z, Xie S. Synthesis, Characterizations, and Physical Properties of Carbon Nanotubes Coated by Conducting Polypyrrole. J Appl Poly Sci 1999; 74: 2605-10.

[7]Sahoo NG, Jung YC, So HH, Cho JW. Polypyrrole coated carbon nanotubes: Synthesis, characterization, and enhanced electrical properties. Synth Met 2007; 157: 374-9.

[8]Sun MM, Zhang SC, Jiang T, Zhang L, Yu JH. Nano-wire networks of sulfur polypyrrole composite cathode materials for rechargeable lithium batteries. Electrochem Commun 2008;

10: 1819-22.

[9]Lei JT, Liang WB, Martin CR. Infrared investigations of pristine, doped and partially doped polypyrrole. Synth Met 1992; 48: 301-12.

[10]Cheah K, Forsyth M, Truong VT. Ordering and stability in conducting polypyrrole. Synth Met 1998; 94: 215-9.

[11]Vishnuvardhan TK, Kulkarni VR, Basavaraja C, Raghavendra SC. Synthesis, characterization and a.c. conductivity of polypyrrole/Y_2O_3 composites. Bull Mater Sci 2006; 29: 77-83.

[12]Pirlot C, Willems I, Fonseca A, Nagy JB, Delhalle J. Preparation and Characterization of Carbon Nanotube/Polyacrylonitrile Composites. Adv Eng Mater 2002; 4:109-14.

[13]Endo M, Takeuchi K, Hiroka T, Furuta T, Kasai T, Sun X, Kiang CH, Dresselhaus MS. Stacking nature of graphene layers in carbon nanotubes and nanofibres. J Phys Chem Solids 1997; 58: 1707-12.

[14]Marmorstein D, Yu TH, Striebel KA, Mclarnon FR, Hou J, Cairns EJ. Electrochemical performance of lithium/sulfur cells with three different polymer electrolytes. J Power Sources 2000; 89: 219-26.

[15]Han DH, Kim BS, Choi SJ, Jung Y, Kwak J, Park SM. Time-Resolved In Situ Spectroelectrochemical Study on Reduction of Sulfur in N,N'-Dimethylformamide. J Electrochem Soc 2004; 151: E283-90.

[16]Yamin H, Gorenshtein A, Penciner J, Sternberg Y, Peled E. Lithium Sulfur Battery. J Electrochem Soc 1988; 135: 1045-8.

[17]Kolosnitsyn VS, Karaseva EV. Lithium-Sulfur Batteries: Problems and Solutions. Russ J

Electrochem 2008; 44: 506-9.

[18]Jiang Y, Xu Y, Yuan T, Yan M. Phase-tailored synthesis of tin oxide-graphene nanocomposites for anodes and their enhanced lithium-ion battery performance. Mater Lett 2013; 91: 16-9.

[19]Novoselov KS, Geim AK, Morozov SV, Jiang D, Zhang Y, Dubonos SV, Grigorieva IV, Firsov AA. Electric field effect in atomically thin carbon films. Science 2004; 306: 666-9.

[20]Miao F, Wijeratne S, Zhang Y, Coskun UC, Bao W, Lau CN. Phase-Coherent Transport in Graphene Quantum Billiards. Science 2007; 317: 1530-3.

[21]Zhang S, Shao Y, Liu J, Aksay IA, Lin Y. Graphene-polypyrrole nanocomposite as a highly efficient and low cost electrically switched ion exchanger for removing ClO_4^- from wastewater. Appl Mater Interfaces 2011; 3: 3633-7.

[22]Lu XJ, Zhang F, Dou H, Yuan CZ, Yang SD, Hao L, Shen L, Zhang LJ, Zhang XG. Preparation and electrochemical capacitance of hierarchical graphene/polypyrrole/carbon nanotube ternary composites. Electrochim Acta 2012; 69: 160-6.

[23]Chang HH, Chang CK, Tsai YC, Liao CS. Electrochemically synthesized graphene/polypyrrole composites and their use in supercapacitor. Carbon 2012; 50: 2331-6.

[24]Zhang D, Zhang X, Chen Y, Yu P, Wang CH, Ma Y. Enhanced capacitance and rate capability of graphene/polypyrrole composite as electrode material for supercapacitors. J Power Sources 2011; 196: 5990-6.

[25]Xu CH, Sun J, Gao L. Synthesis of novel hierarchical graphene /polypyrrole nanosheetcomposites and their superior electrochemical performance. J Mater Chem 2011; 21: 11253-8.

[26]Sahoo S, Karthikeyan G, Nayak GC, Das CK. Electrochemical characterization of in situ polypyrrole coated graphene nanocomposites. Synthetic Metals 2011; 161: 1713-9.

[27]Chandra V, Kim KS. Highly selective adsorption of Hg^{2+} by a polypyrrole-reduced grapheneoxide composite. Chem Commun 2011; 47: 3942-4.

[28]Biswas S, Drzal LT. Multilayered Nanoarchitecture of Graphene Nanosheets and Polypyrrole Nanowires for High Performance Supercapacitor Electrodes. Chem Mater 2010; 22: 5667-71.

[29]Chen JJ, Zhang Q, Shi YN, Qin LL, Cao Y, Zheng MS, Dong QF. A hierarchical architecture S/MWCNT nanomicrosphere with large pores for lithium sulfur batteries. Phys Chem Chem Phys 2012; 14: 5376-82.

[30]Zhang Y, Zhao Y, Doan TNL, Konarov A, Gosselink D, Soboleski HG, Chen P. A novel sulfur/polypyrrole/multi-walled carbon nanotube nanocomposite cathode with core–shell tubular structure for lithium rechargeable batteries. Solid State Ionics 2013; 238: 30-5.

[31]Liang X, Liu Y, Wen ZY, Huang LZ, Wang XY, Zhang H. A nano-structured and highly ordered polypyrrole-sulfur cathode for lithium-sulfur batteries. J Power Sources 2011; 196: 6951-5.

Chapter 5

[1]Wang J, Yang J, Wan CR, Du K, Xie JY, Xu NX. Sulfur Composite Cathode Materials for Rechargeable Lithium Batteries. Adv Funct Mater 2003; 13: 487-92.

[2]Han SC, Song MS, Lee H, Kim HS, Ahn HJ, Lee JY. Effect of Multiwalled Carbon Nanotubes on Electrochemical Properties of Lithium/Sulfur Rechargeable Batteries. J Electrochem Soc 2003; 150: A889-93.

[3]Choi YJ, Kim KW, Ahn HJ, Ahn JH. Improvement of cycle property of sulfur electrode for lithium/sulfur battery. J Alloys Compd 2008; 449: 313-6.

[4]Song MS, Han SC, Kim HS, Kim JH, Kim KT, Kang YM. Effects of Nanosized Adsorbing Material on Electrochemical Properties of Sulfur Cathodes for Li/S Secondary Batteries. J Electrochem Soc 2004; 151: A791-5.

[5]Zhang Y, Wu XB, Feng H, Wang LZ, Zhang AQ, Xia TC, Dong HC. Effect of nanosized $Mg_{0.8}Cu_{0.2}O$ on electrochemical properties of Li/S rechargeable batteries. Int J Hydrogen Energy 2009; 34: 1556-9.

[6]Jeon BH, Yeon JH, Kim KM, Chung IJ. Preparation and electrochemical properties of lithium-sulfur polymer batteries. J Power Sources 2002; 109: 89-97.

[7]Jeon BH, Yeon JH, Chung IJ. Preparation and electrical properties of lithium-sulfur-composite polymer batteries. J Mater Process Technol 2003; 143-144, 93-7.

[8]Evans A, Montenegro MI, Pletcher D. The mechanism for the cathodic reduction of sulphur in dimethylformamide: low temperature voltammetry. Electrochem Commun 2001; 3: 514-8.

[9]Bakenov Z, Taniguchi I. $LiMg_xMn_{1-x}PO_4/C$ cathodes for lithium batteries prepared by a combination of spray pyrolysis with wet ballmilling. J Electrochem Soc 2010; 157: A430-6.

[10]Bakenov Z, Taniguchi I. Physical and electrochemical properties of LiMnPO4/C composite cathode prepared with different conductive carbons. J Power Sources 2010; 195: 7445-51.

[11]Choi JW, Kim JK, Cheruvally G, Ahn JH, Ahn HJ, Kim KW. Rechargeable lithium/sulfur battery with suitable mixed liquid electrolytes. Electrochim Acta 2007; 52: 2075-82.

[12]Choi YJ, Chung YD, Baek CY, Kim KW, Ahn HJ, Ahn JH. Effects of carbon coating on the electrochemical properties of sulfur cathode for lithium/sulfur cell. J Power Sources 2008; 184: 548-52.

[13]Martha SK, Markovsky B, Grinblat J, GoferY, Haik O, Zinigrad E, Aurbach D, Drezen T, Wang D, Deghenghi G, Exnar I. $LiMnPO_4$ as an Advanced Cathode Material for Rechargeable Lithium Batteries. J Electrochem Soc 2009; 156: A541-52.

[14] Bakenov Z, Wakihara M, Taniguchi I. Battery performance of nanostructured lithium manganese oxide synthesized by ultrasonic spray pyrolysis at elevated temperature. J Solid State Electrochem 2008; 12: 57-62.

Chapter 6

[1]Geim Ak, Novoselov KS. The rise of graphene. Nat Mater 2007; 6: 183-91.

[2]Stankovich S, Dikin DA, Dommett GHB, Kohlhaas KM, Zimney EJ, Stach EA, Piner RD, Nguyen ST, Ruoff RS. Graphene-based composite materials. Nature 2006; 442: 282-6.

[3]Yoon S, Jung KN, Yeon SH, Jin CS, Shin KH. Electrochemical properties of $LiNi_{0.8}Co_{0.15}Al_{0.05}O_2$-graphene composite as cathode materials for lithium-ion batteries. J Electroanal Chem 2012; 683: 88-93.

[4]Zhou GM, Wang DW, Li F, Zhang LL, Li N, Wu ZS, Wen L, Lu GQ, Cheng HM. Graphene-Wrapped Fe_3O_4 Anode Material with Improved Reversible Capacity and Cyclic Stability for Lithium Ion Batteries. Chem Mater 2010; 22: 5306-13.

[5]Shi Y, Wen L, Li F, Cheng HM. Nanosized $Li_4Ti_5O_{12}$/graphene hybrid materials with low polarization for high rate lithium ion batteries. J Power Sources 2011; 196: 8610-7.

[6]Wu ZS, Ren WC, Wen L, Gao LB, Zhao JP, Chen ZP, Zhou GM, Li F, Cheng HM. Graphene Anchored with Co_3O_4 Nanoparticles as Anode of Lithium Ion Batteries with Enhanced Reversible Capacity and Cyclic Performance. ACS Nano 2010; 4: 3187-94.

[7]Evers S, Nazar LF. Graphene-enveloped sulfur in a one pot reaction: a cathode with good coulombic efficiency and high practical sulfur content. Chem Commun 2012; 48: 1233-5.

[8]Geim AK. Graphene: Status and Prospects. Science 2009; 324: 1530-4.

[9]Bakenov Z, Taniguchi I. Physical and electrochemical properties of $LiMnPO_4$/C composite cathode prepared with different conductive carbons. J Power Sources 2010; 195: 7445-51.

[10]Yoon S, Jung KN, Yeon SH, Jin CS, Shin KH. Electrochemical properties of $LiNi_{0.8}Co_{0.15}Al_{0.05}O_2$-graphene composite as cathode materials for lithium-ion batteries. J Electroanal Chem 2012; 683: 88-93.

[11Zhou GM, Wang DW, Li F, Zhang LL, Li N, Wu ZS, Wen L, Lu GQ, Cheng HM. Graphene-Wrapped Fe_3O_4 Anode Material with Improved Reversible Capacity and Cyclic Stability for Lithium Ion Batteries. Chem Mater 2010; 22: 5306-13.

[12]Zhang Y, Zhao Y, Yermukhambetova A, Bakenov Z, Chen P. Ternary sulfur/polyacrylonitrile /$Mg_{0.6}Ni_{0.4}O$ composite cathodes for high performance lithium/sulfur batteries. J Mater Chem A 2013; 1: 295-301.

[13]Bakenov Z, Taniguchi I. $LiMg_xMn_{1-x}PO_4$/C Cathodes for Lithium Batteries Prepared by a Combination of Spray Pyrolysis with Wet Ballmilling. J Electrochem Soc 2010; 157: A430-6.